UNIVERSITE DE LILLE-NORD DE FRANCE

Faculté de médecine

Année 2021 N° _____

THESE

POUR L'OBTENTION DU GRADE DE

DOCTEUR de L'UNIVERSITE de LILLE-NORD DE FRANCE

Spécialité : Neurosciences

Présentée par

Laurent Puy

Mécanismes et Conséquences de l'Oedème Cérébral sur le Pronostic des Hémorragies IntraCérébrales Spontanées

---

Co-Directeurs de Thèse : Pr. Charlotte Cordonnier & Pr. Vincent Bérézowski

Soutenue le 17 Decembre 2021

JURY

Pr. Isabelle Margaill	Rapportrice
Pr. Mikael Mazighi	Rapporteur
Pr. Sophie Susen	Examinatrice
Pr Rustam Al-Shahi Salman	Examinateur
Pr. Vincent Bérézowski	Co-directeur de thèse
Pr. Charlotte Cordonnier	Co-directrice de thèse

Thèse réalisée au sein du laboratoire de recherche Inserm U1172 « LilNCog »

Remerciements

Je tiens à remercier l'ensemble des membres composant le jury de cette thèse qui me font le grand honneur d'avoir accepté de juger ce travail.

Madame le Professeur Charlotte Cordonnier,

Charlotte, sans vous, rien de tout ceci n'aurait été possible. Vous êtes, pour beaucoup, mais pour moi particulièrement une source d'inspiration, d'admiration. Je mesure la chance que j'ai de pouvoir apprendre chaque jour à vos côtés. Je veux aussi vous transmettre ici mon amitié.

Monsieur le Professeur Vincent Bérézowski,

Vincent, je te remercie de m'avoir encadré et soutenu tout au long de ce travail. Merci pour ta confiance, ton enthousiasme, tes encouragements et tes conseils. Tu es, à mes yeux, un peu plus qu'un directeur de thèse. Tu as tout mon respect et toute mon amitié.

Madame le Professeur Isabelle Margaill,

Je tiens à vous exprimer mes sincères remerciements pour votre participation à ce jury de thèse en tant que rapportrice ainsi que pour l'intérêt que vous portez à mes travaux depuis leurs débuts, je vous remercie et vous témoigne ma reconnaissance.

Monsieur le Professeur Mikael Mazighi,

Je souhaite te témoigner ici ma reconnaissance pour la bienveillance que tu as toujours eu à mon égard, dès mes premiers pas en Master 2. J'admire tes qualités humaines et professionnelles. Merci pour ton soutien et pour avoir accepté d'être rapporteur de ce travail.

Madame le Professeur Sophie Susen

Vous me faites l'honneur d'avoir accepté de participer à ce jury de thèse en examinant et jugeant ce travail. Soyez assurée de ma reconnaissance et de mes sincères remerciements. L'éclairage que vous porterez sur ce travail me sera riche d'enseignements.

Professor Rustam Al-Shahi Salman

I am really honored and grateful that you have accepted to review this thesis. Your precious advices will substantially strengthen this work.

Je tiens aussi à remercier:

Juliette, toujours sur le qui-vive de l'Amour, mais à trois cette fois.
Margaux, lorsque tu liras ces lignes tu auras drôlement grandi. Je veux que tu saches que ton père t'aime.

A ma famille à laquelle je tiens tant : mes parents, mon frère et pauline, ma sœur et Thibault, mon neveu Georges et ma future nièce. Je pense également à ma tante et à mes grands-parents dont ma chère mamie Monique. Je pense aussi à ceux de Catalogne.

A ma belle-famille toujours aussi gentille et bienveillante à mon égard.

A mes amis, d'enfance et d'Amiens que j'aimerais voir plus souvent. Merci pour votre amitié, qui dure malgré le temps.

Je remercie également le Professeur Régis Bordet et l'ensemble de l'équipe U1172 ainsi que la team d'imagerie. Grâce à vous j'ai pu m'essayer et prendre gout à la vie de scientifique dans la bonne humeur et la convivialité. Plus qu'un simple travail, j'ai vécu une expérience de vie que je n'oublierai jamais. J'ai une pensée particulière pour Romain et Laura mes co-thésards ☺ et à la Deguil Scale.
Je remercie également Bélinda Duchêne et Marie-Hélène Gevaert pour leur aide précieuse dans ce travail.

Je remercie également le formidable service de neurologie vasculaire dans laquelle je m'épanouis actuellement. Francois, Nelly, Lucie, Marco, Marie, Hilde, Arnaud : c'est un honneur pour moi d'être membre de votre équipe, je continuerai d'apprendre de chacun d'entre vous. Merci également à toute l'équipe paramédicale qui me permet de travailler dans la bonne humeur.

Je remercie aussi ici, chacune des personnes que j'ai eu l'occasion de rencontrer dans mon parcours de médecin et de chercheur.

Encore une fois à toi Juliette parce que, vraiment, tu le mérites.

Table des matières

Table des figures

Résumé

L'hémorragie intracérébrale spontanée (HIC) est associée à un pronostic dramatique et reste dépourvue de traitement spécifique. Par conséquent, une meilleure compréhension de ses mécanismes physiopathologiques et de ses conséquences est impérative. La zone péri-hémorragique, communément appelée "œdème péri-hémorragique" (OPH), pourrait faire l'objet de thérapies ciblées. Cependant, ses mécanismes, son évolution naturelle et sa valeur pronostique restent encore à préciser. Cette thèse avait pour but d'étudier les mécanismes et les conséquences de cet OPH. Pour ce faire, nous avons combiné une approche expérimentale (modèle animal d'HIC) et une approche neuropathologique (étude post-mortem sur tissu humain). Nous avons utilisé le modèle de double injection de sang autologue pour reproduire une HIC chez une large cohorte de rats mâles et femelles. Dans une première étude, nous avons montré à quel point l'IRM multimodale est un outil fiable pour suivre la progression dynamique des lésions péri-hémorragiques et nous avons caractérisé la cinétique des différents composants de l'OPH (densité en eau, atteinte [micro-]vasculaire, neuro-inflammation et dépôts de fer). Dans une deuxième étude, nous avons examiné les conséquences à court et à long terme de l'HIC. Nous avons montré qu'une HIC profonde provoque une atteinte cognitive hippocampique et non hippocampique à long terme, contrastant avec une récupération locomotrice spontanée précoce. Nous avons par ailleurs montré qu'une HIC striatale focale induit une atrophie et un hypométabolisme cérébral à distance, impliquant les structures du système limbique et les zones corticales. Nous avons mené une étude post-mortem sur 19 cas de patients décédés d'HIC. Nous avons prouvé l'infiltration de *Neutrophil extracellular Traps* (NETs) dans le cœur de l'HIC mais également dans l'OPH. Nous avons également étudié la cinétique naturelle du processus de résorption du sang après une HIC, en nous concentrant sur la voie du récepteur scavenger des monocytes-macrophages (CD163) / hème oxygénase-1 (HO-1).

Nos résultats contribuent à affiner notre perception de l'OPH, à renforcer les liens entre recherche clinique et pré-clinique, et, nous l'espérons, à identifier des stratégies thérapeutiques innovantes pour l'HIC.

Mots clefs : hémorragie intracérébrale spontanée ; œdème cérébral ; IRM ; cognition ; modèle expérimental ; post-mortem.

Abstract

Spontaneous intracerebral haemorrhage (ICH) is associated with a dramatic prognosis and remains devoid of specific treatment. Therefore, understanding the mechanisms of ICH pathology and repair is a matter of high priority. The peri-haemorrhagic zone, commonly called "peri-haematomal oedema" (PHE), might be a promising candidate for therapeutic interventions. However, its underlying mechanisms, natural evolution and prognostic value remain to date unclear. This thesis aimed at studying the mechanisms and consequences of this PHE. To do so, we combined an experimental (animal model of ICH) and a neuropathological (post-mortem study on human tissue) approach.

We used the double autologous blood injection model to reproduce ICH in a large cohort of male and female rats. In a first study, we showed how multimodal MRI is a reliable tool to track the dynamic progression of peri-haematomal injuries and we characterized the kinetics of different PHE components (water content, [micro]-vessel injuries, neuro-inflammation and iron deposits). In a second study, we investigated the short and long-term consequences of ICH. We reported that a deep ICH provokes long term cognitive impairments in rats that affects both hippocampal and non hippocampal aspects of cognition contrasting with early spontaneous locomotor recovery. We also showed that focal striatal ICH induces distant brain atrophy and hypometabolism involving limbic system structures and cortical areas. We included 19 cases of patients who died from ICH in a post-mortem study. We provided evidence for *Neutrophil extracellular Traps* (NETs) infiltration within the haematoma core but also and within the PHE. We also investigated the natural kinetic of natural blood clearance process after ICH in human brain tissue with a focus on the monocyte-macrophage scavenger receptor (CD163)/hemoxygenase-1 (HO-1) pathway. Our findings contribute to refine our perception of PHE, to optimize the translational pipeline and, hopefully, to identify innovative therapeutic strategies for ICH.

Key words: intracerebral haemorrhage; cerebral edema; MRI; cognition; experimental model; post-mortem.

INTRODUCTION GENERALE

1. Hémorragies intracérébrales spontanées

1.1 Définition

Les accidents vasculaires cérébraux (AVC) occupent une place importante en matière de santé publique. Ils représentent la première cause de handicap physique acquis de l'adulte, la deuxième cause de troubles cognitifs majeurs et la troisième cause de mortalité (Puy et Cordonnier 2019). Parmi eux, les AVC hémorragiques ou hémorragies intracérébrales (HIC) représentent 15 à 20% de tous les AVC en Europe et ont une part bien plus importante en Asie et en Afrique. Ces hémorragies résultent d'un saignement cérébral intra-parenchymateux en lien avec la rupture de petits vaisseaux généralement touchés par une microangiopathie dont l'origine est intimement liée à la localisation du saignement (Figure 1). (1) Les HIC localisées dans les régions profondes du cerveau (dites HIC profondes) sont le résultat de la rupture des petites artères touchant préférentiellement le putamen et le thalamus et sont sous-tendues par une angiopathie des artères perforantes profondes favorisée par l'âge et l'hypertension artérielle (Qureshi et al. 2001). (2) Les HIC de localisation lobaire (dites HIC lobaires) proviennent de la rupture des artères de petit et moyen calibre perforant le cortex et la substance blanche sous-corticale dont la cause principale est l'angiopathie amyloïde cérébrale. Cette angiopathie amyloïde cérébrale provient de l'accumulation progressive de dépôts de peptide amyloïde β dans les petits vaisseaux corticaux et leptomeninges (Puy et Cordonnier 2019).

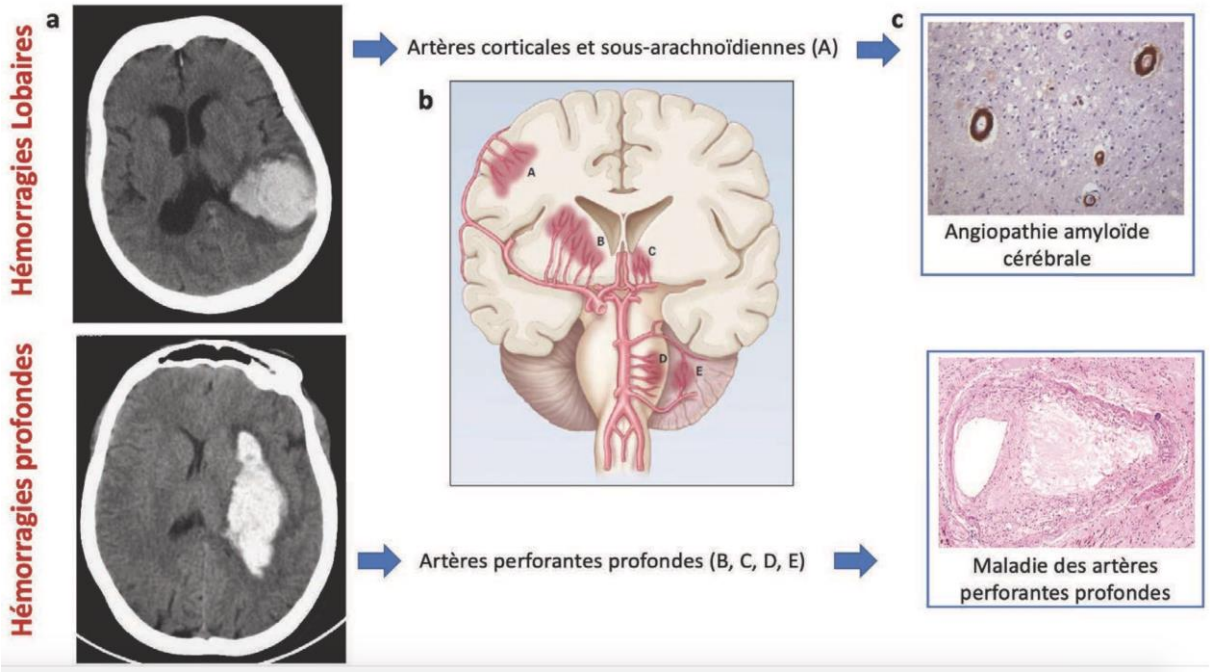

Figure 1. Localisation de l'hémorragie et microangiopathie cérébrale sous-jacente. Figure adaptée de (Qureshi et al. 2001).

1.2 Une maladie grave

Malgré l'optimisation des traitements de prévention primaire, l'incidence des HIC n'a pas diminué depuis les années 80. Contrairement aux AVC ischémiques, les HIC n'ont pas vu de progrès majeur dans leur prise en charge depuis plus de 25 ans ce qui explique qu'elles gardent un pronostic sombre avec une mortalité précoce (<48 heures) demeurant importante et stable (Béjot et al. 2017). La survie à 1 an après une HIC est évaluée à 46% et seulement à 29% à 5 ans (Poon, Fonville, et Al-Shahi Salman 2014). Le pronostic à long terme est également sombre : parmi les patients ayant survécu au moins 30 jours après l'HIC, le taux cumulé de survie à 10 ans était de 38% (Pasi et al. 2021).

Au-delà de la mortalité, l'HIC induit un handicap fonctionnel majeur. Une méta-analyse évaluant le pronostic fonctionnel des patients présentant une HIC, révèle seulement 12 à 39% d'indépendance fonctionnelle à long terme (van Asch et al. 2010). Ce handicap n'est pas exclusivement moteur puisque le pronostic cognitif des HIC est également mauvais. En effet, parmi les survivants sans trouble cognitif préexistant, l'incidence de la démence est estimée à 14% à 1 an et à 28% à 4 ans (Moulin et al. 2016).

1.3 Une maladie dépourvue de traitement spécifique

Toutes les stratégies thérapeutiques (médicaments hémostatiques, évacuation chirurgicale), ayant pour objectif la lutte contre l'expansion de l'hémorragie, ont échoué (Steiner et al. 2014). Seule la baisse rapide de la pression artérielle < 140/90 mmHg a montré un bénéfice fonctionnel modeste avec cependant la perte de ce bénéfice et la survenue d'effets indésirables si cette baisse descend en dessous des 120 mmHg de pression artérielle systolique (Moullaali et al. 2019).

Ce constat d'échec nous oblige à une meilleure compréhension de la cinétique évolutive de l'HIC et de ses conséquences afin d'envisager d'autres cibles thérapeutiques. C'est dans ce contexte que notre attention s'est portée sur la zone péri-hémorragique, communément appelée « œdème péri-hémorragique » (OPH), qui pourrait avoir une implication pronostique donc être une cible thérapeutique. Cependant, peu de données sont disponibles concernant sa physiopathologie, son évolution naturelle et sa valeur pronostique. Nous proposons ici un état des lieux des connaissances actuelles sur l'OPH.

2. L'œdème péri-hémorragique (OPH)

Le tissu cérébral, siège de la rupture d'un vaisseau et de l'hémorragie initiale, s'expose secondairement à des réactions cytotoxiques et inflammatoires en réponse à l'effet de masse initial ainsi qu'aux composants toxiques des produits de dégradation du sang.

2.1 Physiopathologie de la formation de l'OPH

De nombreux acteurs semblent contribuer à la formation de l'OPH. Mais sa physiopathologie ne reste que partiellement comprise. En 2021, trois phases sont décrites (**Figure 2**) :

(1) *Phase précoce (première heure), une composante « mécanique »*. L'entrée massive de sang dans le parenchyme cérébral provoque, de manière précoce, une diffusion rapide de plasma dans les tissus environnants (Zazulia et al. 1999). L'accumulation de ce plasma élève la pression osmotique interstitielle et favorise le mouvement des fluides des capillaires vers la zone péri-hémorragique. Enfin, en coagulant, le sang forme un caillot dont la rétraction va également induire une libération de protéines plasmatiques (Xi et al. 1998; G. Y. Yang, Betz, et Hoff 1994). Ces mécanismes ont été observés dans des modèles d'HIC chez les gros animaux qui présentaient une barrière hémato-encéphalique (BHE) intacte, soulignant le

rôle d'un gradient osmotique dans la formation précoce de l'OPH (Richard F. Keep, Hua, et Xi 2012).

(2) *Phase intermédiaire (premiers jours), le rôle de la thrombine*. La cascade de coagulation s'active dès que le sang pénètre dans le tissu cérébral, et la thrombine joue un rôle identifié (Ye et al. 2021; Negrier, Shima, et Hoffman 2019). D'une part, en convertissant le fibrinogène en fibrine, elle participe à la coagulation du sang et à la rétraction du caillot formé. Par ailleurs, la présence de thrombine génère deux effets majeurs : (1) un effet pro-inflammatoire et (2) une participation à la rupture de la BHE. Elle agit en induisant la libération de divers médiateurs de la réaction inflammatoire (facteur de nécrose tumoral kappa B (NFκB), interleukine 1β, chimiokines), et diverses enzymes protéolytiques qui dégradent l'interstitium et la matrice extracellulaire : les métalloprotéinases matricielles (MMP). Elle stimule également la voie du complément. Elle active le récepteur PAR-1 (Protease Activated Receptor-1) dont la surexpression est associée à une neurotoxicité et une activation microgliale exacerbée (Zheng et al. 2016). Sous l'effet des PAR et MMP, la thrombine participe à la rupture de la BHE en modifiant les interactions entre cellules endothéliales et matrice extracellulaire (Guan et al. 2004; Liu et al. 2010; Bodmer et al. 2012). Tous ces mécanismes thrombine-dépendant amplifient la réponse inflammatoire s'opérant dans la zone autour de l'HIC ce qui contribue au développement de l'OPH (López et al. 2014; Keep et al. 2008).

(3) *Phase tardive (au-delà du 3ème jour), le rôle des produits de dégradation du sang.* Après hémolyse et libération de l'hémoglobine (Hb) dans l'espace extra-cellulaire, cette dernière est prise en charge par l'haptoglobine et l'hème libre par l'hémopexine. Cet thème, tout comme le fer à l'état libre, sont de puissants pro-oxydants. Par la réaction de Fenton, le fer héminique s'oxyde, passant de l'état ferreux (2^+) à l'état ferrique (3^+), générant la formation d'espèces réactives de l'oxygène (ROS). Les ROS comprennent l'anion radical superoxyde ($O_2^{\cdot -}$), le peroxyde d'hydrogène (H_2O_2) qui interagit avec les ions ferreux (réaction de Fenton) pour produire le radical hydroxyl ($\cdot OH$), l'espèce radicalaire la plus délétère du stress oxydant (Dixon et Stockwell 2014). Ces réactions d'oxydation concernent principalement les lipides et les lipoprotéines des composants membranaires occasionnant la lyse et la mort cellulaire par cytotoxicité (peroxydation lipidique). Les ROS contribuent aussi à la rupture de la BHE et au développement de l'œdème péri-hémorragique (Pun, Lu,

et Moochhala 2009). Par ailleurs, l'hème libre joue un rôle capital au cours de la réponse inflammatoire en stimulant l'expression endothéliale des molécules d'adhésion ICAM-1, VCAM-1 et sélectine E qui permettent l'extravasation des leucocytes. Enfin, les dépôts de fer exacerbent l'expression de l'Aquaporine-4 (AQP4), hautement impliquée dans l'homéostasie hydrique du tissu cérébral. Ils activent aussi la microglie par la voie du récepteur TLR4 (Toll-like receptor-4) (Zheng et al. 2016). L'organisme dispose de moyens d'élimination de l'hème par le système CD163 / hème oxygénase 1 (HO-1) (Garton et al. 2017, 163; Thomsen et al. 2013; Q.-Q. Li et al. 2018). Le récepteur CD163 permet la capture du complexe hémoglobine/haptoglobine par la microglie et les macrophages recrutés. Puis, après son incorporation, l'Hb est décomposée en Fe2+, CO et biliverdine sous l'action de l'hème oxygénase-1 (HO-1). L'HO-1 a des capacités antioxydantes, anti-inflammatoires et anti-apoptotiques (Campbell, Fitzgerald, et Dunne 2021). Cependant, lorsqu'une hémolyse importante survient au cours d'un état pathologique comme l'hémorragie cérébrale, les capacités d'élimination de l'hème se trouvent dépassées, ce qui conduit aux effets toxiques décrits plus haut.

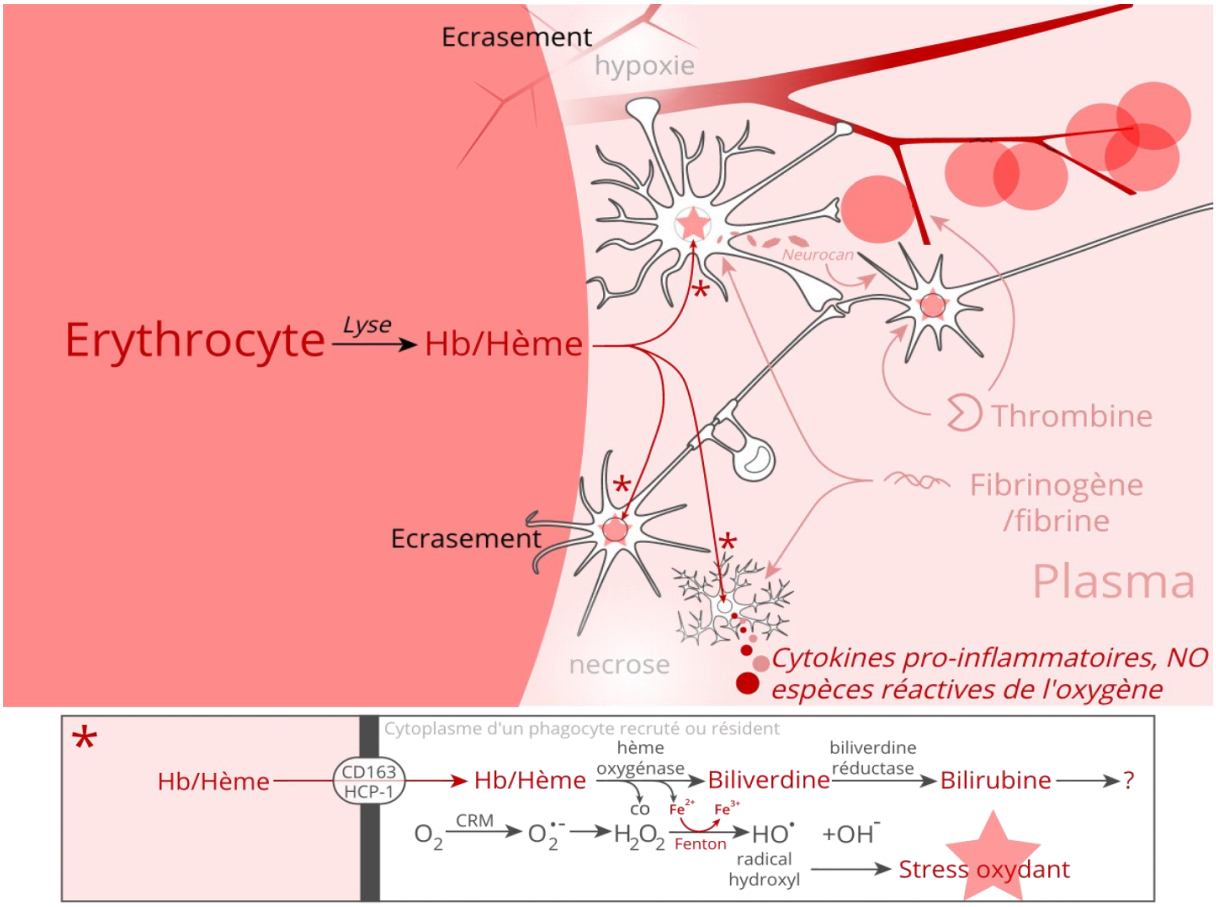

Figure 2. Hypothèses physiopathologiques des conséquences de l'Hémorragie intracérébrale sur le parenchyme cérébral. Adaptée de (Pétrault et al. 2019).

CO : monoxyde de carbone ; Hb : hémoglobine ; HCP-1 : protéine porteuse de l'hème-1 ; H2O2 : peroxyde d'hydrogène ; MRC : chaîne respiratoire mitochondriale ; NO : monoxyde d'azote ; O2 : dioxygène ; O2- : anion superoxyde ; OH· : radicaux hydroxyles ; ROS : espèces réactives de l'oxygène.

2.2 Réponse inflammatoire et mécanismes de mort cellulaire

2.2.1 La réponse inflammatoire

2.2.1.1 Le recrutement leucocytaire

Les cellules microgliales sont des cellules dérivées de monocytes sanguins qui résident dans le parenchyme cérébral et constituent 10 % des cellules du SNC (Aguzzi, Barres, et Bennett 2013). Elles surveillent constamment le microenvironnement cérébral et détectent immédiatement tout type d'agression exogène (agents infectieux) ou endogène (HIC par exemple). L'irruption de sang dans le parenchyme cérébral va induire leur activation. Bien qu'elles prolifèrent rapidement, leur capacité de phagocytose est rapidement dépassée. Elles vont donc adresser, par le biais de cytokines pro-inflammatoires, un signal aux cellules endothéliales afin de déclencher une réponse inflammatoire autorisant un recrutement de phagocytes plus nombreux et plus performants. Celui-ci s'opère au niveau des veinules post-capillaires à travers lesquelles s'infiltrent des leucocytes. Le passage d'un leucocyte à travers l'endothélium se fait en 3 étapes (Carman 2009) : le roulement, la margination et la diapédèse. Les polynucléaires neutrophiles et éosinophiles et/ou les cellules mononucléées (monocytes, lymphocytes) affluent alors sur le site inflammatoire. Les neutrophiles sont les premiers leucocytes recrutés, suivi par les monocytes qui s'activent en macrophages une fois dans le tissu. Ces cellules vont phagocyter les hématies libres ainsi que les débris cellulaires. Enfin, l'infiltrat lymphocytaire va induire la mort par apoptose des cellules en souffrance avant qu'elles ne propagent la nécrose. Pour permettre le recrutement de ces cellules, les cellules endothéliales augmentent leur perméabilité capillaire ce qui autorise l'extravasation (Maślińska et Gajewski 1998). Le plasma et ses constituants vont aussi traverser les parois vasculaires. Ce liquide, nommé « exsudat », contient de nombreuses enzymes, anticorps et diverses molécules qui perturbent l'homéostasie ionique et le fonctionnement cellulaire local, amplifiant également la réponse inflammatoire. L'ensemble du processus de recrutement cellulaire est résumé dans la **Figure 3**.

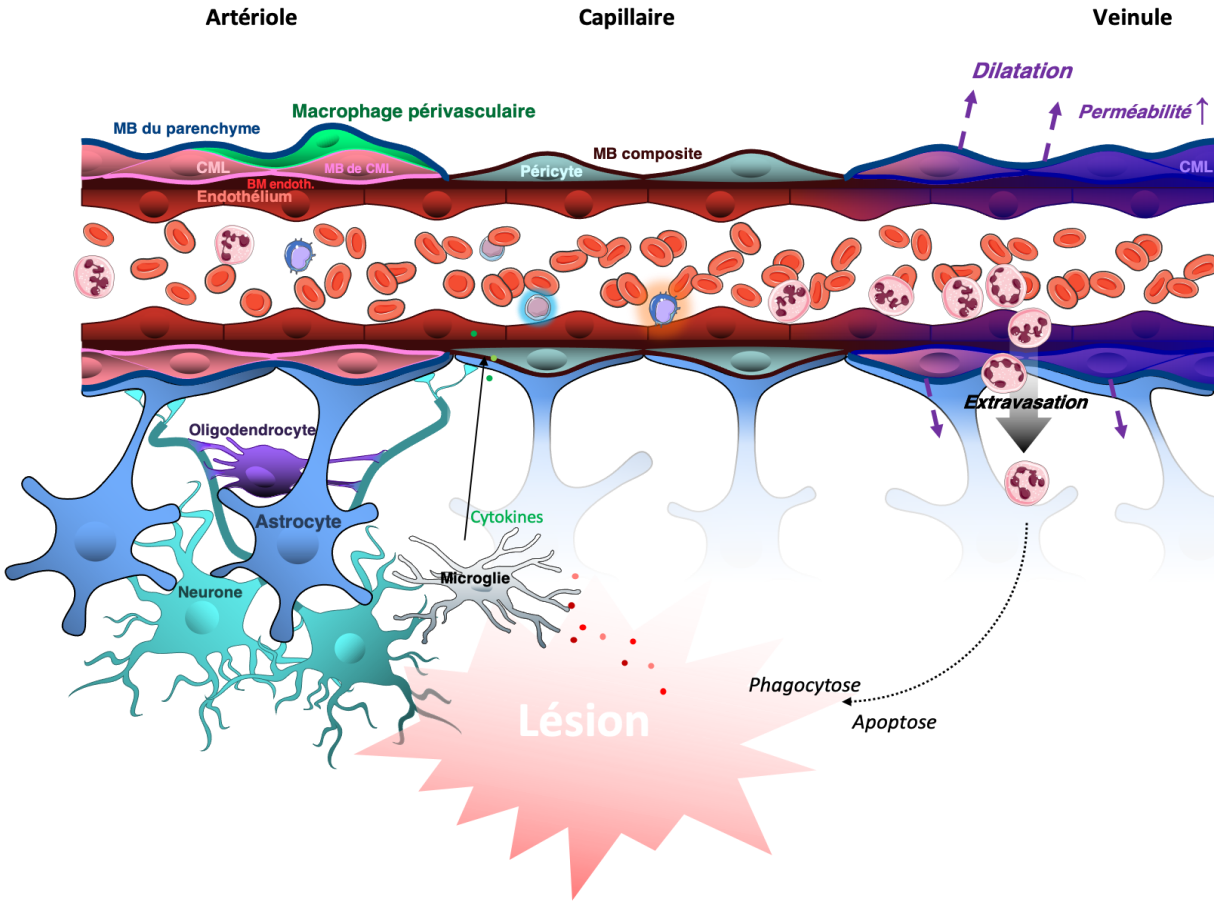

Figure 3. Mécanismes impliqués dans la neuro-inflammation. Figure adaptée de (Endres et al. 2008).

CML : cellules musculaires lisses ; MB : membrane basale

2.2.1.2 La rupture de la barrière hémato-encéphalique (BHE)

La BHE est une interface, un lieu d'échange, entre les capillaires sanguins et le cerveau. Elle comporte des propriétés restrictives exerçant un contrôle strict du passage des nutriments et des éléments passant du sang au cerveau (**Figure 4**). Il s'agit d'une barrière sélective empêchant le passage non-spécifique de la plupart des molécules hydrophiles par la présence de jonctions serrées intercellulaires (Daneman et Prat 2015). Les molécules issues du sang ne peuvent donc la traverser qu'en empruntant les voies transcellulaires spécifiques, c'est-à-dire exigeant une reconnaissance préalable des molécules par les systèmes de transport. De plus, des propriétés de barrière métabolique (enzymes, pompes d'efflux) limitent encore le passage d'un large spectre de molécules hydrophiles comme lipophiles. Ces propriétés de barrière sont entretenues par l'influence des pieds astrocytaires. La persistance de la lésion hémorragique, tout comme l'inflammation prolongée, endommage les astrocytes et donc altère les propriétés sélectives des

cellules endothéliales. La perte de sélectivité de cette BHE génère des fuites vers le tissu cérébral avec exsudation du plasma, provoquant un œdème dit vasogénique qui amplifie l'effet indésirable œdémateux de la réponse inflammatoire (Beaumont et al. 2000).

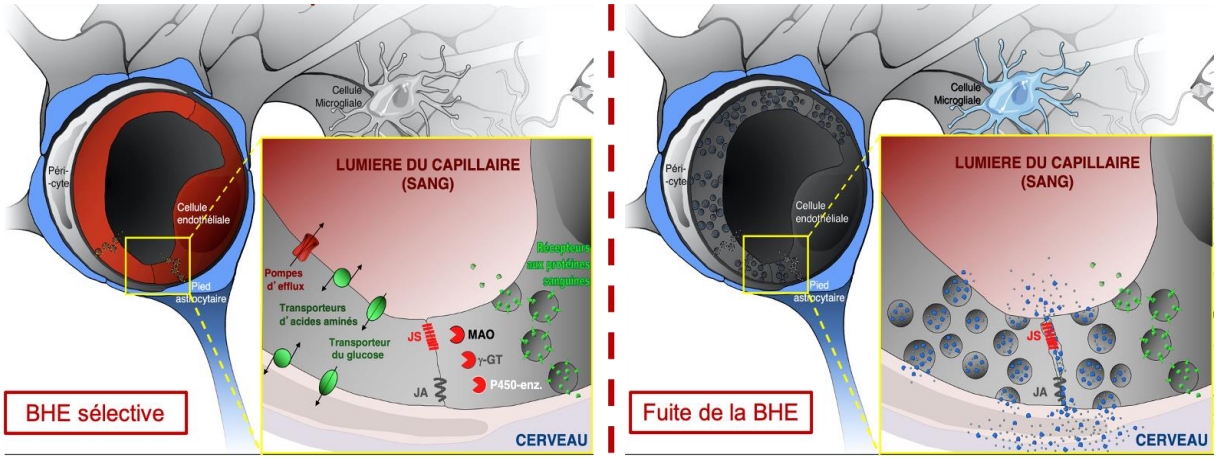

Figure 4. Représentation schématique de la barrière hémato-encéphalique et conséquences de sa rupture. Figure modifiée de (Bérézowski et al. 2012).

MAO : monoamine oxydase ; P450 : cytochromes P450 ; γ -GT : gamma-glutamyltranspeptidase ; JS : jonction serrée ; JA : jonction adhérente.

2.2.2 La mort cellulaire dans l'HIC : nécrose, apoptose et ferroptose

L'HIC induit une mort cellulaire par des mécanismes différents et des temps pouvant varier de quelques secondes à plusieurs jours.

2.2.2.1 La nécrose

Bien qu'il ne représente que 2 % de la masse du corps humain, le cerveau consomme prés de 20% de l'énergie de l'organisme (Raichle et Gusnard 2002). Cette forte consommation, ajoutée à l'absence de réserves, rend le cerveau extrêmement sensible aux variations d'approvisionnement en dioxygène et en substrat énergétique par le sang. La nécrose est une mort cellulaire non programmée, survenant en réponse à une agression exogène, et se manifestant par une perte d'intégrité de la membrane plasmique et un déversement du contenu cellulaire (Vanden Berghe et al. 2014). Dans les secondes suivant l'hémorragie, la pression intracranienne va subitement augmenter. Cela a pour conséquence une compression mécanique

(i) du tissu neuroglial et son altération physique comprenant de la nécrose cellulaire, et (ii) des microvaisseaux adjacents, réduisant localement la perfusion sanguine et entrainant ainsi une réduction des apports sanguins. Le dioxygène étant l'accepteur final des électrons de la chaîne respiratoire mitochondriale, la diminution de sa concentration réduit les phosphorylations oxydatives, ne permettant plus une production suffisante d'adénosine triphosphate (ATP) au sein des cellules cérébrales. Ce déficit énergétique constitue l'élément déclencheur de multiples réactions cellulaires qui vont conduire à la mort des cellules cérébrales. La glycolyse anaérobie compensatrice mise en place s'accompagne d'une acidification du tissu cérébral par accumulation d'acide lactique et de protons. Cette acidose loco-régionale est à l'origine de nombreuses perturbations comme la formation accrue de radicaux libres à l'origine d'un stress oxydant participant à la mort cellulaire, mais également à la perturbation du fonctionnement de nombreux transporteurs ioniques transmembranaires. La déplétion en ATP compromet l'activité de l'échangeur membranaire Na/K -ATPase, ce qui conduit à une augmentation de la concentration intracellulaire en Na^+ et à une libération accrue de K^+. Cette perte de l'homéostasie ionique entraine un gonflement cellulaire qui affecte aussi bien les neurones que les cellules gliales et conduit à la lyse cellulaire (Eguchi, Shimizu, et Tsujimoto 1997). Suite au déficit énergétique et à l'altération de l'homéostasie ionique, les neurones et les cellules gliales vont perdre leur potentiel membranaire. Cette dépolarisation, dans le cas des neurones, s'accompagne du relargage de nombreux neuromédiateurs, en particulier le glutamate. Cette libération massive de glutamate au niveau synaptique et extra-synaptique participe à la mort neuronale par "excitotoxicité" (Kroemer et al. 2009). Cette mort nécrotique libère des contenus cellulaires toxiques pour les cellules voisines, ce qui propage la nécrose. Enfin, les cellules nécrosantes relarguent des protéases et des DAMPs (Damage/Danger-Associated Molecular Patterns) qui vont être repérés par les cellules microgliales. Ces dernières vont activer *in fine* la réponse inflammatoire qui vise à éliminer les cellules mortes et leurs débris pour stopper la propagation de la nécrose (Roh et Sohn 2018).

2.2.2.2 L'apoptose

A contrario de la nécrose, l'apoptose est un mécanisme de mort cellulaire programmée et finement régulé. Outre son rôle dans différents contextes pathologiques (notamment en oncologie), l'apoptose est essentielle au cours du développement (Meier, Finch, et Evan 2000). Son déclenchement repose sur l'activation de protéases spécifiques appelées caspases, qui se chargent de dégrader de façon coordonnée les différentes structures cellulaires (condensation

du cytoplasme, condensation de la chromatine, fragmentation de l'ADN...). Cette dégradation progressive en cascade aboutit à la formation de corps apoptotiques constitués de débris des différents organites enveloppés d'une membrane. Ces corps apoptotiques permettent une élimination « propre » des cellules, sans déversement du contenu cellulaire à l'extérieur, et donc sans inflammation majeur. Ces corps apoptotiques seront ensuite éliminés par les macrophages (Elmore 2007). Dans le cadre de l'HIC, cette mort cellulaire est plus tardive que la nécrose et survient dans des zones plus éloignées de l'hématome, et s'applique aux cellules en souffrance afin de prévenir leur nécrose (Dirnagl, Iadecola, et Moskowitz 1999).

2.2.2.3 La Ferroptose

En 2012, Dixon *et al.* proposent un nouveau concept de mort cellulaire dépendante du fer, la ferroptose (Dixon et al. 2014). Cette dernière correspond à une mort cellulaire programmée non-apoptotique, déclenchée par le fer, et caractérisée par une accumulation de ROS. Ces ROS sont dérivées du métabolisme du fer, induisant une peroxydation lipidique (Mahoney-Sánchez et al. 2021). Une quantité excessive de fer intracellulaire libre contribue à la ferroptose en produisant des ROS par la réaction de Fenton couplée à la réaction d'Haber-Weiss. Morphologiquement, la ferroptose est caractérisée par la présence de mitochondries plus petites que la normale avec une condensation des membranes mitochondriales, une réduction ou une disparition des crêtes mitochondriales et une rupture de la membrane mitochondriale externe. Toutefois, la membrane cellulaire reste intacte, le noyau est de taille normale et il n'y a pas de condensation de la chromatine. Des données *in vitro* et *in vivo* confirment l'implication de la ferroptose dans l'HIC (Bai, Liu, et Wang 2020). La ferroptose semble plus tardive que la nécrose et l'apoptose puisque qu'elle survient après la lyse des érythrocytes et la dégradation de l'hémoglobine dont le produit peptidique s'accumule *in fine* en un complexe d'hémosidérine, qui stocke le fer sous forme d'hydroxyde ferrique.

La plupart des mécanismes physiopathologiques abordés dans cette section ont fait l'objet de pharmaco-modulations, prometteuses en science expérimentale mais non efficaces chez l'Homme. Cela montre que notre compréhension de la physiopathologie de l'ICH est limitée. Plusieurs raisons sont envisageables dont par exemple, une méconnaissance de la contribution respective et de la cinétique précise de chacun des mécanismes évoqués, un mécanisme prépondérant restant à découvrir, sans oublier les variations interindividuelles liées au terrain des patients victimes d'AVC. Toutes ces incertitudes ont des conséquences pharmacologiques sur le choix de la molécule à cibler, la dose précise à délivrer ainsi que sur le délai, la durée et la biodisponibilité du traitement employé. Avant de concevoir une nouvelle molécule, il semble donc nécessaire de mieux caractériser, *ex vivo* et *in vivo*, la chronologie de l'intervention des différents acteurs responsables de l'OPH que ce soit dans les modèles expérimentaux mais également chez l'Homme.

2.3 *Apport de l'imagerie cérébrale dans l'étude de l'OPH*

En préambule de ce travail de thèse, nous avons réalisé une revue systématique de la littérature qui a permis de sélectionner 24 articles pertinents, traitant de la thématique de l'OPH et de son impact pronostic (**Table 1**).

2.3.1 Des méthodes d'évaluation hétérogènes

En comparant ces différents articles, nous avons mis en évidence une grande hétérogénéité dans les méthodes de mesure de l'OPH :

(1) Le type d'imagerie utilisée (**Table 1**). En raison de son accessibilité et de sa rapidité d'acquisition, la tomodensitométrie (TDM), où scanner cérébral, est la modalité de neuro-imagerie privilégiée pour la quantification de l'OPH. Sur le scanner (**Figure 5A**), l'OPH se manifeste par une hypodensité dont la densité de signal (en unités de Hounsfield) est similaire au liquide céphalo-rachidien et à certains marqueurs de maladie des petites artères cérébrales (lacune, hypersignaux de substance blanche évolués) ce qui complique la segmentation et le recours aux algorithmes de détection des seuils ou des bords de la lésion (Ironside et al. 2020). Pourtant, l'imagerie par résonnance magnétique (IRM) apparait être un outil plus performant pour la segmentation de l'OPH. Par exemple, la séquence T2 FLAIR permet de délimiter l'OPH, bien visible en hypersignal (**Figure 5B**). Les études ayant utilisé uniquement l'IRM sont peu nombreuses et ont des effectifs faibles (moins de 60 patients).

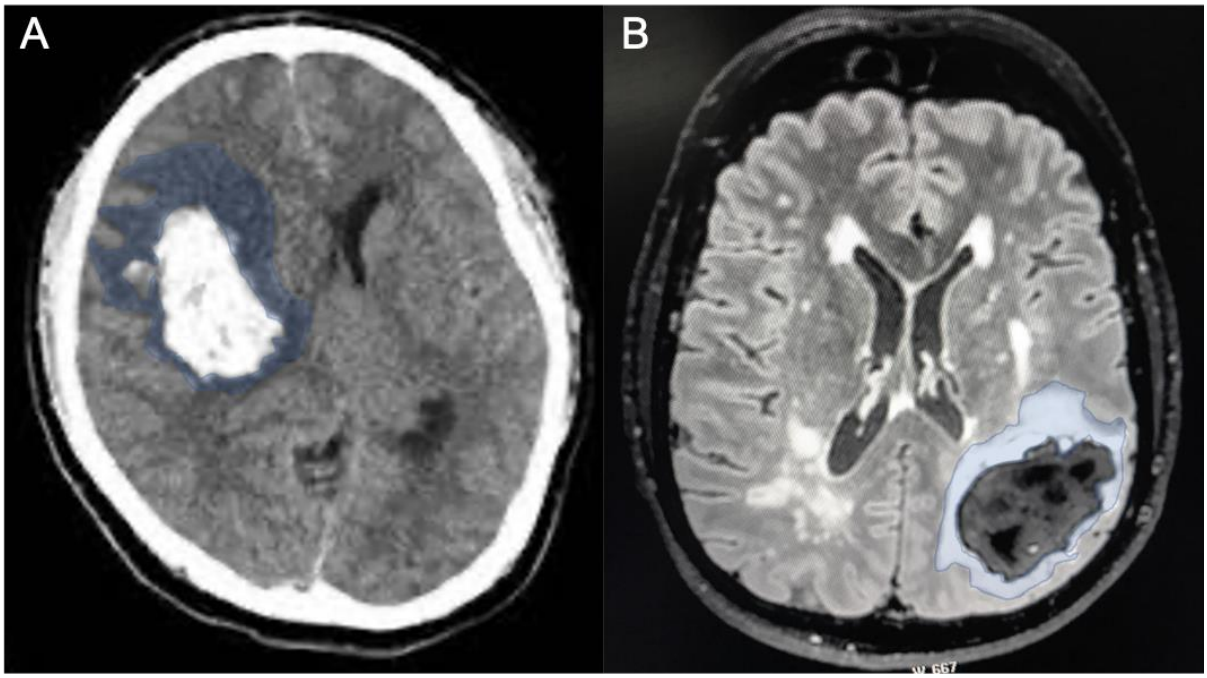

Figure 5. Différentes modalités d'imagerie cérébrale pour évaluer l'œdème péri-hémorragique.

(A) Scanner cérébral en coupe axiale. L'hémorragie intracérébrale (HIC) se traduit par une hyperdensité spontanée entourée d'une zone hypodense : l'œdème péri-hémorragique (OPH, surligné en bleu. (B) IRM cérébrale en séquence T2-FLAIR, coupe axiale. HIC lobaire pariéto-occipital gauche visible en hyposignal, entouré d'un hypersignal correspondant à l'OPH (surligné en bleu).

(2) *Des méthodes de mesures variables* (**Table 1**). Certains auteurs étudient le volume absolu de l'OPH, tandis que d'autres utilisent le volume relatif (avec ratio du volume d'OPH sur le volume de l'HIC). Les temps d'analyse varient également d'une étude à l'autre mais se concentrent généralement sur la phase aiguë : nous n'avons identifié que 4 articles ayant étudié le volume d'OPH au-delà du septième jour. Enfin, à l'heure actuelle la segmentation de l'OPH repose essentiellement sur des méthodes manuelles, longues et fastidieuses et qui présentent des taux de variabilité intra et inter-observateurs élevés. Par conséquent, l'optimisation et la normalisation de l'analyse volumétrique de l'OPH sont nécessaires. Certaines équipes ont mis au point des méthodes de segmentation semi-automatiques sur scanner et IRM (Ironside et al. 2020; Pszczolkowski et al. 2019). Cependant, ces méthodes sont limitées par le manque de validation externe ainsi que par la petite taille des échantillons étudiés. Il n'existe à ce jour aucune méthode de segmentation de l'OPH et de l'HIC pleinement automatisée. Le développement d'une telle technologie est un enjeu de taille car une quantification précise et fiable de l'OPH sera cruciale pour les futurs essais cliniques de l'HIC qui utilisent l'OPH comme biomarqueur de l'efficacité d'un traitement.

Il résulte de cette variabilité méthodologique une hétérogénéité des résultats concernant la description de la cinétique de l'OPH et de son impact pronostique après une HIC.

2.3.2 Une histoire naturelle imprécise

Les études cliniques ont mis en évidence deux phases distinctes dans l'histoire naturelle de l'OPH : une phase initiale de croissance rapide dans les 24 premières heures après l'HIC et une phase de croissance lente s'étendant sur plusieurs jours à semaines. Le pic d'OPH survient classiquement entre la deuxième et la troisième semaine après l'HIC. Ainsi le volume maximal de l'OPH peut être atteint jusqu'à 21 jours suivant l'AVC (Wu et al. 2017; Venkatasubramanian et al. 2011). Néanmoins, les délais varient beaucoup d'une étude à l'autre. Cette variabilité s'explique en partie par des limites méthodologiques incluant des durées de suivi radiologique différentes d'une étude à l'autre, des méthodes de quantification de l'OPH hétérogène ainsi que des effectifs de patients limités (**Table 1**). Ainsi, d'autres études longitudinales portant sur la caractérisation de l'histoire naturelle de l'OPH sont nécessaires.

2.4 *L'OPH a une valeur pronostique incertaine*

Les données actuelles de la littérature qui ont étudié l'effet propre de l'OPH sur le pronostic des HIC sont discordantes (et sont résumées dans la **Table 1**). En effet, même si la majorité des études montrent une influence négative de l'OPH sur le pronostic fonctionnel, d'autres rapportent un effet neutre voir même une influence paradoxale positive. Du fait de l'hétérogénéité des études dans la méthode de mesure de l'OPH, seulement 2 études ont pu être incluses dans une méta-analyse récente (Yu et al. 2017). Dans cette méta-analyse, le taux de croissance de l'OPH à 72 heures était indépendamment associé à un moins bon pronostic fonctionnel à 3 mois [odd ratio : 1.62 ; IC 95% 1.27–2.06].

2.5 *Peu de marqueurs du risque d'extension de l'OPH*

Une meilleure compréhension des facteurs de risque qui précipitent l'expansion de l'OPH est très utile pour identifier les patients à risque d'aggravation. Si le volume initial de l'hématome est reconnu comme facteur de risque d'avoir un OPH plus important, nous ne disposons pas de données robustes permettant d'identifier d'autres facteurs de risque. L'hypertension artérielle a fait l'objet d'une attention particulière. Dans l'étude INTERACT (Intensive Blood Pressure

Reduction in Acute Cerebral Hemorrhage Trial), incluant 3000 patients, la pression artérielle systolique à l'admission était inversement corrélée à la croissance absolue de l'OPH à 72 heures (P=0,02). En revanche, l'étude ATACH (Antihypertensive Treatment of Acute Cerebral Hemorrhage) n'a pas permis d'établir une association entre un contrôle agressif de la pression artérielle systolique et une réduction de la croissance relative de l'OPH sur 24 heures (risque relatif, 0,74 [0,43-1,29]) (Yang et al. 2015). En conséquence, les preuves sont insuffisantes pour affirmer que la gestion intensive de la pression artérielle systolique modifie la trajectoire de l'OPH. La topographie (et donc la maladie vasculaire sous-jacente) de l'HIC a également été étudiée, toujours dans l'idée de pouvoir sélectionner des patients éligibles à des thérapeutiques ciblant le développement de l'OPH. Mais, sur les cinq articles ayant évalué l'existence d'une association entre le volume d'OPH et la topographie de l'HIC, aucun d'entre eux ne met en évidence d'association statistiquement significative (Yang et al. 2015; Arima et al. 2009; Staykov et al. 2011; Appelboom et al. 2013; Grunwald et al. 2017). Enfin, des travaux ont montré un effet de certains traitements à l'admission. La prise d'anticoagulant semble être associée à un volume relatif d'OPH plus faible à l'admission (P<0,05), ce qui est cohérent avec les effets facilitateurs de l'activation de la cascade de coagulation sur la formation de l'OPH que nous avons décrit précédemment (Levine et al. 2007). Dans une cohorte de 125 patients HIC, une exposition antérieure aux statines était indépendamment associée à une réduction des volumes absolus (P=0,035) et relatifs (P=0,021) de l'OPH à l'admission (Naval et al. 2008). Une deuxième étude prospective portant sur 176 patients, ne confirmait finalement pas cet effet (Witsch et al. 2019). Aucune étude n'a étudié l'effet des statines sur le taux de croissance de l'OPH.

Finalement, nous ne disposons à ce jour d'aucun marqueur robuste, permettant d'identifier les profils de patients à risque d'aggraver leur OPH et qui pourraient bénéficier d'une thérapie ciblée.

Table 1. Résumé des études cliniques pertinentes portant sur la relation entre l'OPH et le pronostic clinique après une HIC spontanée

Etude	Design	Nb patients	Modalité	Temps de mesure	Méthode de mesure OPH	Critère de jugement	Résultats
(McCarron et al. 1999)	Prospectif, 1 centre	102	TDM	Admission	VA	Mortalité intra-hospitalière	↓
(Gebel et al. 2002)	Prospectif, 1 centre	86	TDM	<3 h	VA + VR	Mortalité à 1 mois mRS score ≥3 à 4 mois	VR: mortalité: ↓/handicap: ↔ VA: ↔
(Lauren H. Sansing et al. 2003)	Rétrospectif, 1 centre	80	TDM	Non spécifié	VA	Mortalité intra-hospitalière, mRS score ≥3 à 3 mois	↓
(Levine et al. 2007)	Rétrospectif, 1 centre	98	TDM	Admission	VA	Mortalité à 3 mois	↑
(Zubkov et al. 2008)	Rétrospectif, 1 centre	88	TDM	Non spécifié	VA	mRS score >3 à 7 jours	↔
(Arima et al. 2009)	Rétrospectif, >1 centre	270	TDM	Admission, J1-J3	VA + VR augmentation	mRS score ≥3 à 3 mois	↔
(Venkatasubramanian et al. 2011)	Prospectif, 1 centre	27	IRM	J2-J7-J14-J21	VA + VR J2 Augmentation VA + VR Pic VR	Aggravation à J2 Handicap à 3 mois	VA à 48h: ↓ Autres paramètres: ↔
(L. H. Sansing et al. 2011)	Prospectif, 1 centre	303	IRM	J3	VA	mRS score ≥3 à 3 mois	↓
(Staykov et al. 2011)	Rétrospectif, 1 centre	219	TDM	J1, 2, 3, 4–6, 7–11, 12–16, 17–21, >22	Pic VA + VR Augmentation VA + VR J1-J3	Mortalité intra-hospitalière	Augmenation VA J1-J3: ↓ Autres paramètres: ↔
(N. Li, Worthmann, et al. 2013)	Prospectif, 1 centre	59	IRM	Admission, J3	VA Composante cytotoxique	mRS score ≤3 à 3 mois	VA à 3 jours: ↓ Autres paramètres: ↔
(N. Li, Liu, et al. 2013)	Prospectif, 1 centre	21	IRM	Admission, J3, J7	VA Composante cytotoxique		↓

(Appelboom et al. 2013)	Rétrospectif, 1 centre	133	TDM	Admission	VA + VR	Discharge mRS score ≤3	VA : ↓ uniquement ≤30 mL. VR: ↔
(Bakhshayesh et al. 2014)	Prospectif, 1 centre	63	TDM	Admission, J3	VA + VR	Mortalité intra-hospitalière mRS score ≤3 à 3 mois	VA à 3 jours: ↓ mortalité Autre paramère et handicap : ↔
(J. Yang et al. 2015)	Rétrospectif, >1 centre	1138	TDM	Admission, J1	VA	mRS score ≥3 à 3 mois	↓
(Murthy et al. 2016)	Rétrospectif, >1 centre	596	TDM	Admission, J3	VA	mRS score ≥3 à 3 mois	↓ (++ < 30 ml)
(Volbers et al. 2016)	Rétrospectif, 1 centre	220	TDM	J1, 2–3, 4–6, 7–9, 10–12	Pic VA + VR Augmentation VA + VR J1-J3	Discharge mRS score ≤3	Pic VA: ↓ Autres paramètres: ↔
(Urday et al. 2016)	Rétrospectif, 1 centre	139	TDM	Admission, J1-J3	VA	mRS score ≥3 à 3 mois	↓
(Wu et al. 2017)	Rétrospectif, 1 centre	861	TDM	Admission, J3	Augmentation distance	Mortalité à 6 mois	↓
(Grunwald et al. 2017)	Rétrospectif, 1 centre	115	TDM	Admission, J1-J3	VA	mRS score ≥3 à 3 mois	↓
(Volbers et al. 2018)	Rétrospectif, 1 centre	292	TDM	J1, 2–3, 4–6, 7– 9, 10–12	Pic VA Augmentation VA J1-J3	mRS score ≥3 à 3 mois	Pic VA: ↓ Autres paramètres: ↔
(Ozdinc et al. 2016)	Rétrospectif, 1 centre	106	TDM	Admission	VA + VR	Mortalité à 1 mois	↓
(Rodriguez-Luna et al. 2016)	Rétrospectif, 1 centre	322	TDM	Admission, J1	VA	Détérioration à 24h mRS score ≥3 à 3 mois Mortalité à 3 mois	↔
(Tsai et al. 2011)	Prospectif, 1 centre	46	IRM	< 24h	Composante cytotoxique	mRS à 6 mois	↓
(Gupta et al. 2014)	Prospectif, 1 centre	44	TDM	Admission	VA	mRS < 3 à 3 mois	↑

Légende : TDM: tomodensitométrie; IRM: imagerie par résonnance magnétique; VA: valeur absolue ; VR: valeur relative ; ↓: aggravation du pronostic ; ↑: amélioration du pronostic ; ↔: pas d'effet.

2.6 *Échec des thérapies ayant ciblées l'OPH*

En préambule de ce travail de thèse, nous avons analysé les perspectives des nouvelles thérapies ciblées sur l'inflammation et/ou l'œdème à la phase aiguë de l'HIC au travers des bases de données disponibles (Ovid MEDLINE, base de données de recherche sur les AVC [DORIS, www.askdoris.org], et la plate-forme internationale de registre des essais cliniques [ICTRP] de l'OMS). Plusieurs molécules visant l'OPH ont été expérimentées dans le cadre d'essais contrôlés et randomisés. L'antagoniste de la glycine, gavestinel^{R} ; le NXY-059 (agent neuroprotecteur antagoniste de la Citicoline, piégeur de radicaux libres) ; le Celecoxib (inhibiteur sélectif de la cyclo-oxygénase 2) (Lee et al. 2013); le mannitol et le glycérol (Y. L. Yu et al. 1992; Misra et al. 2005); un agoniste du récepteur de sphingosine-1-phosphate, le Fingolimod^{R} (Fu et al. 2014); et l'agoniste du récepteur PPAR-γ, Pioglitazone^{R} (Gonzales et al. 2013). Toutes ces molécules ont présenté une balance bénéfice/risque peu concluante. Pour résumer, aucun traitement ciblant l'installation et l'expansion de l'OPH n'est à ce jour validé en pratique courante.

Cette partie démontre nos carences en matière de compréhension des mécanismes à l'origine de l'apparition et du développement de l'OPH. Elle souligne également des faiblesses dans notre approche méthodologique pour étudier *in vivo* l'OPH et ses effets.

La recherche translationnelle offre des opportunités uniques pour pallier ces manques.

3. Hémorragie cérébrale et modèles animaux

Malgré certaines limites, les modèles expérimentaux animaux sont des outils indispensables pour appréhender les mécanismes physiopathologiques de l'œdème et établir une corrélation entre des données histologiques, biologiques et d'imagerie cérébrale. Ils sont également essentiels pour la mise au point de nouvelles stratégies thérapeutiques. Les modèles animaux s'étendent du poisson zèbre (*Zebrafish*) aux gros mammifères (Withers et al. 2020). Mais les rongeurs sont les plus couramment utilisés pour étudier l'HIC. Une de leurs limites repose sur la relative rareté de la substance blanche par rapport à l'homme, comme l'illustre la **Figure 6**. Les animaux lissencéphales comme les rongeurs ont un ratio substance grise/substance blanche plus élevé, ce qui ne représente pas le ratio chez l'homme (Krafft et al. 2012). Cette différence peut avoir un impact sur les manifestations lésionnelles et leurs conséquences fonctionnelles car la substance blanche est un constituant majeur et actif du système nerveux central, dont le

rôle ne se réduit pas à une simple structure de soutien. Elle permet de lier différentes aires cérébrales entre elles, par le biais de fibres commissurales, associatives et de projection (Filley et Fields 2016). Elle joue également un rôle dans la vitesse de conduction des messages nerveux ainsi que dans l'apprentissage et le contrôle des émotions (Y. Wang et al. 2018).

Figure 6. Volumes approximatifs des encéphales et ratio substance grise/blanche chez plusieurs espèces en comparaison avec l'homme. Figure adaptée de Krafft et al., 2012 (Krafft et al. 2012).

G (grey) : subtance grise ; W (white) : substance blanche.

3.1 Différents modèles pour induire une HIC

Il existe différents modèles permettant d'induire une HIC dont la grande majorité ne sont pas spontanés et impliquent des techniques invasives pour générer un saignement, par injection stéréotaxique de sang autologue ou de collagénase, comme décrit ci-dessous.

3.1.1 Modèle d'injection de sang autologue

Le modèle d'injection de sang autologue a été mis au point comme modèle animal contrôlable et reproductible de l'HIC et a fait l'objet de nombreux ajustements depuis sa création en 1982. Initialement, les auteurs de Ropper et al. avaient utilisé le sang artériel d'un rat donneur injecté dans le striatum droit d'un rat receveur (Ropper et Zervas 1982; Bullock et al. 1984). Du fait de la réaction immunitaire provoquée, l'utilisation de sang de donneur est rapidement devenue obsolète, et a été remplacée par l'utilisation de sang autologue. Actuellement, le modèle le plus abouti consiste en une injection stéréotaxique de sang autologue en deux temps dans le striatum (Ma et al. 2011). Cette double injection, mise en œuvre pour la première fois en 1996, a été utilisée pour permettre à une petite quantité de sang de coaguler, afin d'éviter un reflux le long du trajet de l'aiguille, permettant au volume de sang restant d'accentuer l'hématome

(Deinsberger et al. 1996). Ce modèle permet de reproduire un saignement unique, facilement reproductible. Il mime un bon nombre des caractéristiques clés observées chez l'homme, tels que l'effet de masse, la formation d'OPH et induit un déficit neurologique significatif (Manaenko et al. 2011). Cependant, le modèle de sang autologue ne reproduit pas la rupture de vaisseaux responsable du saignement et ne peut pas être utilisé pour étudier l'expansion de l'hématome, qui est présente chez un tiers des patients au cours des 24 heures suivant l'apparition de l'HIC (Schlunk et Greenberg 2015). Par conséquent, l'utilisation principale du modèle de sang autologue est d'étudier les conséquences d'une entrée massive de sang dans le cerveau.

3.1.2 Modèle d'injection de collagénase

Le modèle de collagénase est la technique la plus couramment utilisée pour induire une HIC chez les rongeurs. Il implique l'injection de collagénase, une métalloprotéinase qui dégrade la paroi des vaisseaux en digérant le collagène de leur membrane basale, induisant leur rupture (Montfort et Pérez-Tamayo 1975). Ce modèle a été réalisé pour la première fois chez le rat par Rosenberg et ses collègues en 1990 (Rosenberg et al. 1990). Le saignement est observé à partir de 10 minutes après l'injection, le volume de l'hématome étant corrélé à la concentration de collagénase utilisée. Si ce modèle reproduit bien la rupture de vaisseaux, il présente également des inconvénients. L'enzyme possède des propriétés pro-inflammatoires, ce qui induit un biais dans l'étude des réactions tissulaires autour de l'hémorragie (Andaluz, Zuccarello, et Wagner 2002). Les études comparatives entre le modèle « sang autologue » et le modèle « collagénase » ont permis de dégager plusieurs conclusions essentielles. L'injection de collagénase produit une lésion primaire plus importante, très probablement attribuable à l'expansion de l'hématome qui peut se produire dans ce modèle. Il est intéressant de noter que, bien que le sang autologue génère un volume sanguin plus concentré et un effet de masse initial plus important, le modèle à la collagénase induit toujours plus de mort cellulaire, d'œdème et d'inflammation (Manaenko et al. 2011). La littérature est contradictoire en ce qui concerne l'atteinte neurologique, qui serait plus durable dans le modèle à la collagénase, ce qui le rendrait avantageux lorsque l'observation des déficits à long terme de l'HIC est souhaitable (Manaenko et al. 2011; MacLellan et al. 2008). En définitive, le choix du modèle dépend de la question de recherche posée. Dans le cadre de notre travail, nous avons opté pour le modèle de double injection de sang autologue, limitant ainsi le risque d'inflammation induite par la collagenase.

3.1.3 Modèles d'hémorragies spontanées

Il existe des modèles de facteurs de risque modifiables et non modifiables (âge, hypertension artérielle, maladie des petits vaisseaux [AAC, COL4A1] afin de mieux comprendre comment l'HIC peut être prévenue dans ces populations (Winkler et al. 2001; Gould et al. 2006). Ces modèles sont particulièrement utiles pour mieux étudier les causes de la rupture spontanée des vaisseaux, mais ils présentent également des inconvénients : la survenue, la taille et la localisation de ces hémorragies sont aléatoires, ce qui rend plus difficile l'étude des conséquences de l'HIC (Withers et al. 2020).

3.2 Utilisation de l'imagerie cérébrale pour l'étude de l'OPH dans les modèles animaux

Dans les modèles expérimentaux d'HIC, l'OPH se développe généralement dans les 2 heures, atteint son pic le troisième jour puis diminue mais persiste jusqu'à 7 jours (Zheng et al. 2016). Ces données sont principalement issues de travaux ayant quantifié l'OPH via des méthodes *ex vivo*, nécessitant l'euthanasie des animaux. Nous avons souhaité faire un état des lieux des connaissances concernant l'utilisation de l'IRM cérébrale pour l'étude de l'OPH en recherche expérimentale. Cette revue de la littérature a constitué le mémoire de Master 1, d'Emilien Hourquet, étudiant que j'ai eu l'occasion d'encadrer. Plusieurs points ressortaient de notre stratégie de recherche systématique de la littérature : (1) une sous-utilisation de l'IRM pour quantifier l'OPH (seulement 12 articles) ; (2) des méthodes de segmentation perfectibles et hétérogènes d'une étude à l'autre ; (3) une absence d'étude de l'effet du sexe ainsi que de la corrélation aux données comportementales (notamment cognitives) à long terme. Ce dernier constat est cohérent avec une récente revue systématique sur le mode d'évaluation du comportement dans les modèles pré-cliniques d'AVC. Dans cette revue, Hietamies et al. montrent que 74% des travaux se contentent d'une évaluation motrice à court terme, à l'aide d'échelles subjectives. Par ailleurs, ils soulignent également la sous-représentation des femelles (seulement 16%) (Hietamies et al. 2018).

En conclusion, il nous semblait nécessaire de s'intéresser à l'IRM multimodale pour quantifier et caractériser l'OPH, mais également d'approfondir nos connaissances sur les conséquences comportementales motrices et cognitives, à court et à long terme d'une HIC chez le petit animal.

4. Hémorragie cérébrale et études post-mortem

Par une rapide évaluation PubMed de la littérature en utilisant les termes de recherche " intracerebral h(a)emorrhage in rats " et " intracerebral h(a)emorrhage in mice " nous avons identifié 1330 études publiées depuis 2010. Parmi elles, plusieurs centaines ont évalué des thérapies candidates prometteuses. Malgré un grand nombre de ces dernières rapportant des effets bénéfiques, aucun des traitements n'a pour l'instant été transposé avec succès en clinique. Sur la base de cette observation, il semble que la démarche translationnelle actuelle ne fonctionne pas. Une des solutions proposées est de vérifier, avant toute tentative de pharmacomodulation, que les observations tissulaires observées dans les modèles expérimentaux le soient également chez l'Homme, dans des cinétiques similaires. Les études neuropathologiques post-mortem chez l'Homme prennent alors toute leur importance. Pourtant, les études *ex vivo* ayant utilisé des cerveaux de patients décédés d'HIC sont peu fréquentes. D'après une revue exhaustive de la littérature (numéro CRD42018110204 du registre prospectif international des revues systématiques), il n'existe que 44 études post-mortem qui ont étudié les mécanismes inflammatoires survenant autour de l'hémorragie (Loan et al. 2021). Parmi elles, 21 ont utilisé des données post-mortem (rapportant un total de 373 cas). Le reste des études a utilisé des biospies réalisées en per-opératoire (rapportant un total de 730 cas). La majorité des études s'est focalisée sur la phase hyper-aigüe de l'HIC puisque seulement 14 études ont étudié les changements inflammatoires au-delà des 3 premiers jours. Ce qui est surprenant puisque, d'après les quelques données dont nous disposons, le pic de l'OPH est atteint chez l'Homme bien au-delà du troisième jour (Venkatasubramanian et al. 2011; Wu et al. 2017). Enfin, seulement 2 études ont eu recours à des méthodes permettant une analyse génétique des tissus regroupant 14 cas (Rosell et al. 2011; Carmichael et al. 2008). Les auteurs concluent que « les analyses transcriptomiques sur tissu humain sont une priorité pour identifier des cibles thérapeutiques pertinentes ».
D'autre travaux post-mortem sont donc nécessaires pour mieux comprendre la cinétique des événements s'opérant dans le tissu cérébral chez l'Homme après une HIC.

OBJECTIFS DE LA THESE

Ce travail de thèse est centré sur l'étude de l'OPH. Nos objectifs étaient de mieux comprendre son histoire naturelle, sa physiopathologie et son implication sur le pronostic fonctionnel après une hémorragie cérébrale.

Pour cela, nous avons utilisé un modèle animal d'HIC et des données post-mortem sur tissu humain.

Les méthodes et résultats de ce travail sont présentés en deux parties. La première partie rapporte les données issues du modèle animal. La deuxième partie rapporte les données issues de l'étude post-mortem.

PARTIE I

MODELE EXPERIMENTAL

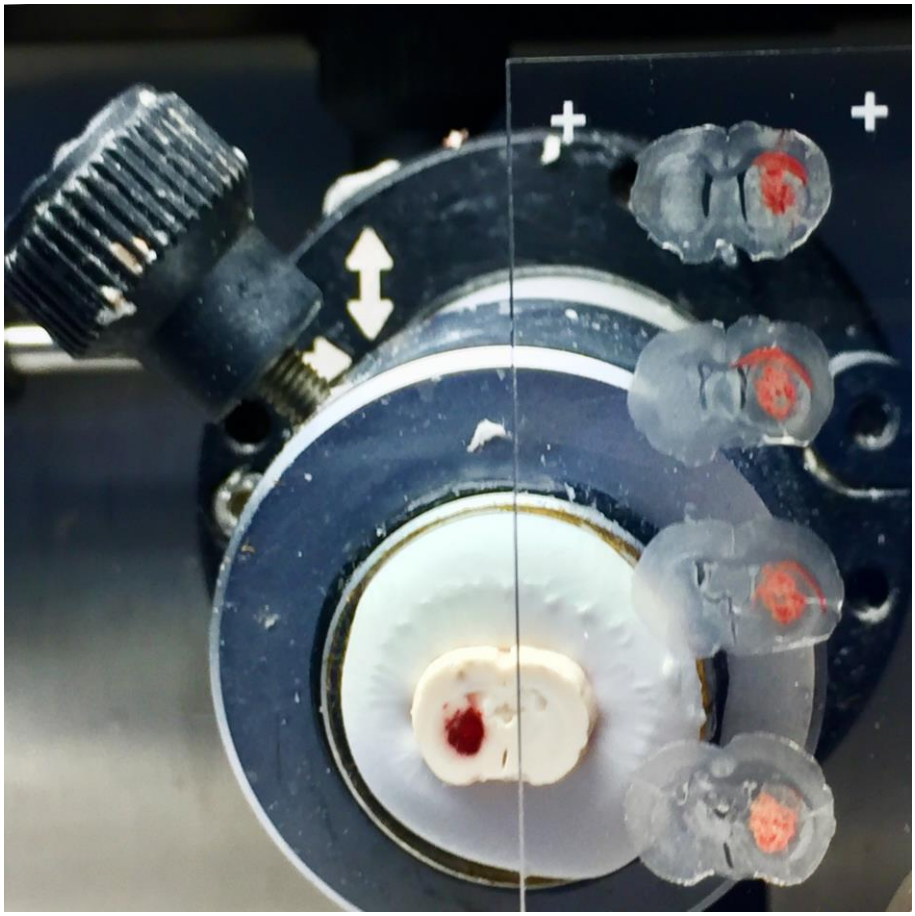

Introduction à la partie expérimentale

Nos travaux de recherche expérimentale sont nés d'un constat simple : aucune thérapie ciblée de l'HIC et de l'OPH efficace en pré-clinique n'a démontré son efficacité chez l'Homme. Nous avons relevé deux principales explications à cet échec :

(a) Premièrement, notre compréhension des mécanismes et des conséquences à court et long terme de l'HIC est insuffisante.
(b) La deuxième explication est d'ordre méthodologique. Comme décrit en introduction, la littérature pré-clinique sur l'HIC, se caractérise par une sous-utilisation de marqueurs radiologiques *in vivo* (IRM cérébrale), des tailles d'effectif généralement faibles, une sous-représentation des femelles et des effets fonctionnels pharmacologiques testés exclusivement sur des performances motrices à court terme.

A l'aide d'une méthodologie solide, nous avons mis au point un modèle animal pour mieux comprendre les conséquences tissulaires et comportementales de l'HIC. Nous avons ainsi tenté de répondre à deux problématiques :

1. Etudier de manière longitudinale la cinétique et la nature de l'OPH par de l'IRM multimodale avec corrélats histologiques.
2. Etudier les conséquences comportementales à court et à long terme après une hémorragie cérébrale, avec un accent sur les fonctions cognitives.

Travail numéro 1

Title: Natural history of peri-haematomal area after experimental haemorrhage in the rat brain: a longitudinal and multimodal MRI study.

Authors: Laurent Puy; Gregory Kuchcinski; Clémence Leboullenger; Florent Auger; Belinda Duchêne; Charlotte Cordonnier and Vincent Bérézowski.

Status: in preparation

Abstract:

Introduction: We aimed to characterize the early temporal evolution of volume and nature of peri-hematomal area (PHA) after ICH in healthy male and female rats using repeated multimodal MRI and histological and behavioral correlates.

Methods: We prospectively studied 230 male and female Wistar rats (sex ratio 1:1). ICH was induces using the double injection autologous blood model. After surgery, rats were followed-up at three time-points: day 0 (D0: 4±2 hours), day 3 (D3) and day 7 (D7). We combined behavioural (spontaneous locomotion: distance travelled, number of rearing, maximum speed recorded and resting time), radiological and histological tools. We used repeated multimodal 7T brain MRI with the assessment of following parameters: volume (T2) water density (T2 relaxometry), iron accumulation (multi-echo T2*), parenchymal water mobility (ADC map), microvascular fluid mobility (D* coefficient) and brain tissue blood perfusion (ASL) using relative values and voxel-based analysis. Histological examination included neuroinflammation, iron deposits and BBB (FITC-Dextran) evaluation. We used (semi-)automated methods for all investigated parameters and statistically tested their respective correlations.

Results: Initial ICH volume was 22.28 ± 9.4 mm^3. We observed the PHA volume peak at D3 (25.23 ± 10.1 mm^3), which was associated with locomotion performances ($p< 0.05$ for each parameter in statistical model adjusted for sex). The study of both FITC-Dextran and relative and voxel-based approach of ADC, ASL and D* values showed early hypoperfusion at the microvessel level within the PHA, followed at D3 by vasogenic and BBB leakage and a normalization of vascular integrity at D7. We observed a strong negative correlation between glial cells activation and water content within the PHA (r= -0.95 and -0.83, for GFAP and Iba1, all p-value < 0.0001). The rR2* at D7 was positively correlated to ICH and PHA volumes at D0 (r=0.66 and 0.53 respectively, all p-values < 0.001) and with irons deposits (r= 0.76, p-value < 0.0001)

Conclusion: Our current study shows that multimodal MRI is a reliable tool to track the dynamic progression of peri-haematomal injuries that should be widely uses to monitor therapeutic interventions in preclinical ICH models.

Introduction

Intracerebral haemorrhage (ICH) is associated with a dramatic prognosis and remains devoid of specific treatment. Therefore, understanding the mechanisms of ICH pathology and repair is a matter of high priority.[1] Patients who survive the initial injury experience further damage to the brain parenchyma surrounding the site of blood entry, for the ensuing days to weeks. This perihematomal area (PHA) represents a promising surrogate marker of secondary brain injury after ICH and of potential therapeutic intervention.[2] However, to date, observational clinical studies did not validate PHA as a reliable marker for prognosis after ICH.[3] This emphasizes the complexity of PHA and justifies further experimental investigation. In preclinical ICH models, PHA represents the common endpoint of several pathophysiological pathways induced by ICH. The large majority of these experimental studies uses *ex vivo* methods to investigate changes in PHA, hampering the monitoring of PHA over time in the same subject and correlation with behavioral assessment. This results in misleading interpretations when comes the time to assess treatment effect. Advances in magnetic resonance imaging (MRI) allow the *in vivo* study of PHA from animal models to humans. To date, few preclinical studies used MRI to quantify PHA volume and current methods are based on manual segmentation, with inherent bias.[4–15] Beyond quantification, multimodal MRI offers a unique opportunity to assess the nature of changes that occur within the PHA over time, but this approach has rarely been used in the pre-clinical ICH literature.[13,16–25] Because elucidating pathogenic mechanisms and testing potential therapies are the focus of current preclinical ICH research, it appears important to test clinically relevant MRI parameters to assess the evolution of ICH-induced brain damage and repair in the same subject.

In this study, we aimed at characterizing the changes in PHA status, with related-behavior impact in a rodent ICH model. Over a 7-day period, we used repeated multimodal MRI in healthy male and female ICH rats to characterize the early temporal evolution of PHA volume and components (water content, water mobility, microvascular water mobility, tissue perfusion and iron accumulation). We also investigated the correlation between these MRI features and both histological changes and neurologic deficits.

Methods

Ethical aspects

All experiments were approved by the national Ethical Committee in Animal Experimentation (CEEA, Comité d'Ethique en Experimentation Animale), from the French Ministry for Education and Research (agreement number: APAFIS#14066-2018031312529642v3) and were performed in strict compliance with the European Union Directive 2010/63/EU. Experiments were reported in accordance with the ARRIVE guidelines for reporting experiments involving animals.

Animals and Study design

We used 12-weeks-old Wistar rats and included both males (280 to 350g) and females (220 to 300 g) to adhere to the standards of good practice in experimental research. We prospectively studied 230 animals: 156 in the ICH group (sex ratio 1:1) and 74 in the sham group (sex ratio 1:1). After surgery, rats were prospectively followed-up for seven days at three time-points: day 0 (D0 = 4±2 hours post ICH), day 3 (D3) and day 7 (D7). Repeated behavioral and MRI measurements were achieved for each rat at each timepoint. A quarter of the animals was euthanized for histological purposes at the end of each time point.

Intracerebral haemorrhage induction: the double injection autologous blood model

Animals were anesthetized with isoflurane (1.5% to 2%) through spontaneous respiration and core temperature was maintained at 36°C to 37°C throughout all surgical procedures. A stereotaxic apparatus was used to position the tip of the needle (26 gauge) at coordinates 0.4 mm anterior, 3.2 mm lateral, and 5.8 mm deep relative to bregma through a 1-mm craniotomy. ICH was produced by injection of 50 μL of fresh (non heparinized) autologous whole blood into the right striatum at a constant rate of 8 μL/min. After a 10-minute break, other 50 μL of blood were infused at the same rate for a total of 100 μL. The needle was left in place for 10 minutes after the infusion and was then withdrawn and the incision closed with sutures.[26] Rats were randomly assigned to the sham or ICH group. Sham operation was restricted to needle insertion.

In vivo Brain MRI

MRI Acquisition Parameters

All rats underwent a 7-Tesla micro-MRI (7-Tesla; BioSpec 70/ 20, Bruker, Ettlingen, Germany). Animals were anesthetized with isoflurane (1.5% to 2%) through spontaneous respiration and core temperature was maintained at 36°c to 37°c throughout all MRI procedures. A cylindrical emitter antenna with an inner diameter of 72 mm and a receiving surface head coil both allow data recording. A birdcage radiofrequency coil and a surface coil were used for radiofrequency transmission and reception, respectively. A 3-plane scout imaging sequence was obtained at the start of each MRI session to reproducibly position the animal in the magnet. The following sequences were performed at each time point (D0, D3, D7) and for each rat: *Anatomic Axial and coronal T2-weighted spin-echo sequences* (repetition time/echo time [TR/TE] = 5000/77 ms, field of view [FOV] = 4×4 cm, matrix = 256×256, slice thickness = 1 mm, no gap, 20 slices) ; *Multiecho T2 spin-echo relaxometry* (TR/TE = 5000/7, 21, 35, 49 and 63 ms, FOV = 4× cm, matrix = 256×256, slice thickness = 1 mm, no gap, 20 slices) ; *Multiecho T2 gradient-echo (*TR/TE = 800/3; 7; 11; 16; 20; 24; 28 and 32 ms, FOV = 4×4 cm, matrix = 256×256, slice thickness = 1 mm, no gap, 7 slices) *; Diffusion-weighted imaging (*TR/TE = 3000/21.50 ms, b-values = 10, 20, 40, 60, 80, 100, 400, 600, 800 et 1000 s/mm2, FOV = 4×4 cm, matrix = 108×96, slice thickness = 1 mm, no gap, 7 slices) *; Flow sensitive alternating recovery-echo planar imaging (FAIR-EPI) perfusion Arterial-spin labelling (ASL) sequence : (inversion time [TI]* = 35, 100, 200, 300, 400, 500, 600, 700, 800, 900, 1000, 1100, 1200, 1300, 1400 and 1600 ms, FOV = 4×4 cm, matrix = 108×96, 1 slice).

Image Processing and Analysis

Signal characteristics, hematoma volume and apparent diffusion coefficient (ADC) values were evaluated serially in the course of the study. At each time point and for each sequence, two areas were manually outlined to define regions of interest (ROIs): (1) periphery of the hematoma and (2) healthy contralateral striatal tissue.

<u>ICH and PHA volume assessment</u>

ICH and PHA volumes were semi-automatically segmented using Mango© software (nom entreprise, ville/état, pays). In Mango©, prior to any segmentation procedures, all T2-axial images underwent brightness/contrast enhancement using a contrast control tool to increase image quality and enhance background separation as much as possible. Thresholding was then applied, the values were automatically set (using the auto-threshold tool) to include only regions having pixels with high intensity levels, that isolated ICH, PHA and normal parenchyma. Ellipsoid region of interest (ROI) was then manually defined. Segmentations were independently performed by two experienced operators (L.P and F.A) with excellent interobserver agreement (r=0.92 and 0.82 for ICH and PHA volumes respectively). To ensure that all rats in the ICH group had a significant lesion, we excluded rats with initial ICH volume < 10 mm^3.

Multimodal PHA characterization

Beyond volumetric analysis, we aimed to investigate the nature of PHA using different sequences. All the parametric maps reconstructions and manual ROIs delineation detail below were performed with ParaVision5.1® (PV5.1) software (Bruker, Biospin, Germany). ROIs representing the PHA were first segmented from axial T2 sequence and were then coregistered onto the other MRI sequences to ensure that the estimates were taken from the same area with some manual adjustment if needed.

As the absolute values differ in each experimental setup, relative values were calculated for each MRI parameter. To do so, a ratio (r) was calculated between the value of the lesion side (ROI 1) and the healthy side of a corresponding mirror ROI (ROI2). For instance, the ratio (rADC) between the ADC value of the lesion side and the healthy side of a corresponding mirror ROI was calculated as rADC = ADC_{roi1}/ ADC_{roi2}).

We investigated five components of the PHA:

Calculation of T2 and T2*: water density and iron accumulation

The T2 relaxation times were calculated by fitting the T2 signal decrease with a monoexponential function. The equation used was as follows:

$$S(TE) = S_0 \times e\text{^}(-TE/T2)$$

Where So is the proton density and TE is the echo time. TE is expressed in milliseconds (ms)

Relaxation rates (R2 and R2*) were expressed in Hz and calculated as follow:

$$R2\ or\ R_2^{\ *} = \frac{1000}{T2\ or\ T2*}$$

We quantified "water density" using R2: rR2 values > 1.1 and < 0.9 indicated an increase and decrease of water density.[27] We quantified iron accumulation using R2*: rR2* > 1 indicated an iron accumulation.[28,29]

Calculation of the Apparent Diffusion Coefficient (ADC): parenchymal water mobility

We used ADC values (mm2/s) from diffusion weighted imaging (DWI) sequence to investigate the water mobility in the brain parenchyma. ADC coefficient were calculated by fitting diffusion signal on monoexponential curve. The exponential function used was the following:

$$S(b) = S_0 \times\ e\text{^}(-b/ADC)$$

Where S0 is the signal measured when b = 0, b is the so-called "b factor" S_0 is the signal measured when b = 0.

Vasogenic and cytotoxic edema were defined as rADC >1.1 and < 0.9 respectively. Based on our preliminary analysis and previous clinical studies,[30] we hypothesized that both cytogenic and vasogenic oedema can occur concomitantly within the PHA. Hence, we used voxel-based approach rather than the absolute values of the ROI. To do so, we used the Paravision 5.1 software to estimate the number of voxels within ROIs and their respective grey level intensity and build a histogram to represent the distribution of grey level. The 95%IC distribution of voxel within the contralateral ROI was consider as the reference. We stratified voxel within PHA into three categories based on grey level distribution: voxels with ADC < 2.5th and > 97.5th percentile of contralateral voxels indicated hypoADC and hyperADC values, whilst voxels within the 95%IC range were considered normal. The percentage of each category was then calculated.

Calculation of the pseudo-diffusion coefficient (D*): microvascular fluid mobility

We used the DWI sequence to assess variations of water mobility in the microvascular compartment within the PHA. At low b values between 0 and 100 s/mm2, the constraints of water molecules in the microvascular compartment can be evaluated quantitatively by calculating the pseudo-diffusive component D*.[31] The D* value was obtained from a bi-exponential equation according to Le Bihan et al.[32] corrected and solved on GraphPad Prism

(version 7.00 for Mac, GraphPad Software, La Jolla, CA, USA), as follows:

$$\frac{S}{S0} = (1-f).e^{-ADC.b} + f.e^{-(ADC\times D^{*}).b}.e^{-\left(\frac{TE}{T2r}\right)}$$

In this formula, b is the diffusion coefficient, S is the signal measured for a value of b, S0 is the signal measured when b = 0, f is the fraction of the circulating blood volume fixed between 0 and 0.05%, and ADC is the apparent diffusion coefficient. TE is the echo time (21.50 ms), and T2r the relaxation of brain tissue without diffusion gradients (b = 0). Indeed, considering the edematous nature of PHA during ICH, relaxation times of brain tissue (T2) may have significant differences. We thus included a correction in the data analysis for low b values, the latter being sensitive to T2r. Relative D* (rD*) values > 1.1 accounted for an increased mobility of water molecules in the microvasculature referring to an increased microvascular patency or blood-brain barrier leakage.[31] In contrast, relative D* values < 0.9 accounted for a decreased mobility of water molecules in microvessels, referring to a decreased microvascular patency.

Calculation of the Cerebral Blood Flow (CBF): brain tissue blood perfusion

The CBF was assessed using the Flow-sensitive Alternating Inversion-Recovery Pulsed Arterial Spin Labelling (FAIR PASL) sequences.[33] ASL uses arterial blood water as an endogenous tracer by inverting the magnetization of the blood using radiofrequency pulses.

After a delay (TI: Inversion Time) allowing to the labelled blood to flow into the brain tissue, “labelled” images are acquired. Separate “control” images are also acquired without prior labelling of arterial spins. The signal difference between “control” and “labelled” images provides a measure of labelled blood from arteries delivered to the tissue by perfusion. CBF calculation was performed using the following formula:

$$CBF = \lambda \times \frac{T1_{\text{"control" images}}}{T1_{blood}} \times \left(\frac{1}{T1_{\text{"labeled" images}}} - \frac{1}{T1_{\text{"Control" images}}}\right)$$

Where λ is the blood-brain partition coefficient. In our experiences T1blood and λ are equal respectively to 2400 ms and 0,9 mL/g. The unit of CBF is mL/100 g/min. Relative rCBF > 1.1 and < 0.9 indicated a hyper and hypo-perfusion. We hypothesized that both hypo- and hyper-perfusion can occur concomitantly within the PHA. Hence, we used voxel-based approach with the same method described for ADC values.

Neurobehavioral Testing

Spontaneous locomotion

Spontaneous locomotor activity was measured using an infrared actimeter (Panlab, Bioseb, Vitrolles, France). The apparatus consisted of a square arena (45 cm in length, 45 cm in width and 35 cm in height) with a black polymethyl methacrylate floor and transparent 34-cm-high polymethyl methacrylate walls. Rats were placed in the center of the arena and allowed to explore freely for 10 min. Activity was recorded by two rows of infrared photocell sensors and processed with Actitrack software (Bioseb). The total distance covered (in cm), the number of rearings (n), the maximum speed recorded (Smax, in cm/second) and the duration of inactivity (resting time, in seconds) were collected at each time-point.

Histopathological correlates: tissue characterisation, neuroinflammation and microvascular changes.

At the end of the protocol, rats were euthanized with an overdose of pentobarbital (200 mg/kg, intraperitoneal). For tissue staining, rats were transcardially perfused with heparinized physiologic saline for 5 min and decapitated. Subsequently, brains were isolated and fixed in methacarn solution (60% methanol-30% chloroform- 10% acetic acid) at 4 °C for 1 day, then in 70% ethanol at 4 °C for 1 day, followed by paraffin embedding. Brains were serially sliced at 5µm thickness. All stainings and immunolabellings were performed on serial-sections of 5µm each. Sections of formalin-fixed paraffin embedded tissue were stained routinely with hematoxylin–eosin (H&E) for the identification of ICH and structural analysis of the tissue. Perls' staining was done to screen for iron deposits using Tissue-Tek Prisma Plus automated Stainer (Sakura). Slides were placed in Potassium Ferricyanide solution (2% Potassium Ferricyanide – 25ml and 2% Hydrochloric acid -25ml) for 20 minutes, and then counterstained in Nuclear fast Red for 5 minutes, rinsed in distilled water, dehydrated and mounted. We used Glial fibrillary acidic protein (GFAP) and ionized calcium-binding adapter molecule 1 (Iba1) immunolabelling to identify neuroinflammatory cells (active astrocytes and microglia respectively) within the PHA. These markers were immunolabelled using a VENTANA BenchMark GX immunohistochemistry automated staining machine (Roche). The primary antibody was a rabbit polyclonal IgG (Ventana-Roche). We used the i-View DAB detection kit® (Ventana Medicals System, Roche Group) as an indirect biotin streptavidin system for the detection of the primary IgG antibody. Tissue sections were counterstained using bluing reagent

solution (Ventana-Roche). The presence of GFAP was assessed by (EP672Y) rabbit monoclonal primary antibody from (Roche). The presence of Iba1 was assessed by a rabbit anti-mouse IgG antibody (1:500, Wako Chemicals USA, Richmond, VA, USA). Nucleated cells were stained green using a Methyl Green solution (H-3402, Vector Laboratories). For each immunostaining, a tissue section was processed identically except that the primary antibody was omitted as a specificity control and revealed no signal. A brightfield slide scanner (Zeiss Axioscan Z1) digitised the whole tissue section at 20-fold magnification after staining. Immunolabelled sections were independently analysed by two experienced operators (L.P and V.B). A staining surface ratio ([stacking surface/whole section surface]*10^3) was calculated with a semi-automated method using ImageJ software in order to quantify the positively stained or labelled surface in the PHA.

The fluorescence-based visualization of brain microvascular patency as well as BBB integrity was enabled by the observation of both distribution and extravasation of fluorescein isothiocyanate (FITC)-Dextran (2000 kDa, 10 mg.mL-1, Sigma-Aldrich, Saint-Quentin Fallavier, France) through patent microvessels. A 500 µL volume of FITC-Dextran in physiologic saline solution was injected into the caudal vein of rats. After 2 min, rats were decapitated. Brains were extracted, frozen in liquid nitrogen and stored at -80°C until use. Thirty micrometer-slices were coronally cut using a cryostat (Leika), and mounted with Vectashield hardset medium with DAPI (Vector Laboratories, Burlingame, CA, USA). The resulting slides were scanned in three dimensions using a slide scanner (Zeiss Axio Scan.Z1, Gena, Germany), and post-processed using a 3D data projection method that projects the voxels of maximum intensity of the different slices into a viewing plane (Maximum Intensity Projection).

Statistical Analysis

Distribution of the data was established using the Kolmogorov-Smirnov test. All data are presented as mean ± SD or median [IQR]. Statistical differences in data with normal distribution were analyzed with Student test, others with Mann-Whitney U test. First, we used linear regression model to assess time-effect on each MRI parameters. We estimated the Pearson coefficients to test correlations between the different MRI parameters. We used log-transformation to ease the correlation between MRI parameters and immunolabelling values. To assess markers associated with PHA progression between D0 and D3, we define a specific

variable as follows: ΔPHA = PHA volume D3-PHA volume D0. We used different multivariate linear regression models (adjusted for sex) to test the relation between PHA progression and other MRI features and to assess the relation between radiological features and locomotor performances with adjustment for sex. All statistical tests were 2-sided and a *p-value* of ≤0.05 was considered as statistically significant.

Results:

Among the 156 ICH animals, 8 died before the first MRI and 19 had a baseline ICH volume < 10 mm^3. Therefore, 74 shams and 129 ICH animals were included in the study.

Temporal assessment of ICH and PHA volumes

The natural history of ICH and PHA volume are reported in Figure 1. In the ICH group, D0 hematoma mean volume was 22.28 ± 9.4 mm^3 (Figure 1A). The volume of ICH was similar between D0 and D3 and decreased significantly at D7 (13.10 ± 6.2 mm^3, p< 0.0001 with D0 as reference). This corresponded to a ≈40% reduction of the ICH volume. In the ICH group, D0 PHA mean volume was 22.92 ± 7.8 mm^3 (Figure 1A). We observed the PHA volume peak at D3 (25.23 ± 10.1 mm^3) and a dramatic decrease at D7 (1.73 ± 1.1 mm^3; p< 0.0001 with D3 as reference).

Figure 1: Temporal course of ICH and PHA volume in the acute phase.

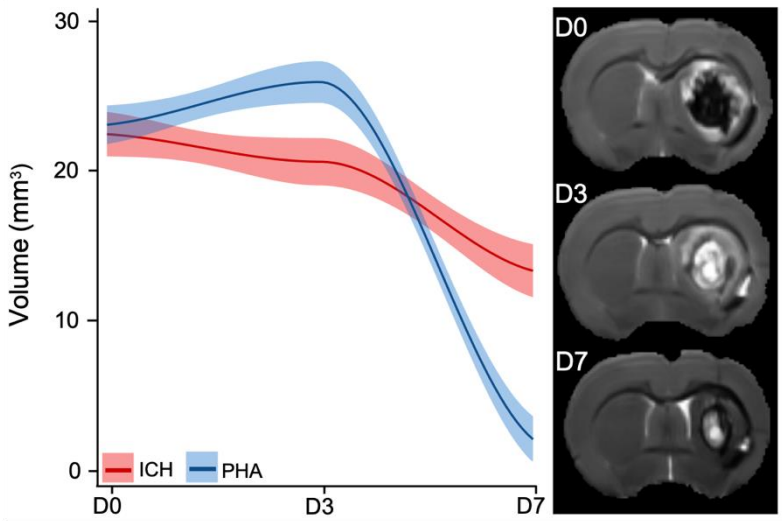

Temporal course of ICH and PHA volumes between day 0 and day 7. On the left, representative brain MRI axial T2 image of an ICH rat. ICH core appears in hyposignal surrounding by a hyperintensity signal (PHA) within the right striatum. The adjacent hypersignal corresponds to the peri-hematomal oedema. ICH = intracerebral haemorrhage, PHA = peri-haematomal area.

Spontaneous locomotor performances

Figure 2 shows the spontaneous locomotion of animals between day 0 and day 7. At day 0, ICH rats showed severe impairment affecting all the parameters of spontaneous locomotion: distance travelled (ICH group *vs* sham group, p-value: 989±376 vs 2946±255 cm, p<0.0001), number of rearing (3[1-8] vs 56[38-67], p<0.0001), maximum speed recorded (24 ±7 vs 36±5 cm/s, p<0.0001) and resting time (432±81 vs 262±88 sec, p< 0.0001). At day 3, we observed a partial recovery in the ICH group that did not reach yet the sham's performances on three out of the four studied parameters: distance travelled (2875±246 vs 3538±176 cm, p= 0.001), number of rearing (31[17-55] vs 64[41-78], p<0.0001) and maximum speed recorded (33 ±6 vs 38±5 cm/s, p<0.0001). At day 7, ICH rats showed complete recovery of locomotor function (all p-value > 0.1 vs. sham). In multivariate regression model adjusted for sex, spontaneous locomotor performances were associated with the peak of PHA volume at D3 (p< 0.05 for each parameter, see Table 1 for statistic details).

<u>Figure 2</u>: Spontaneous locomotion recovery in the acute phase.

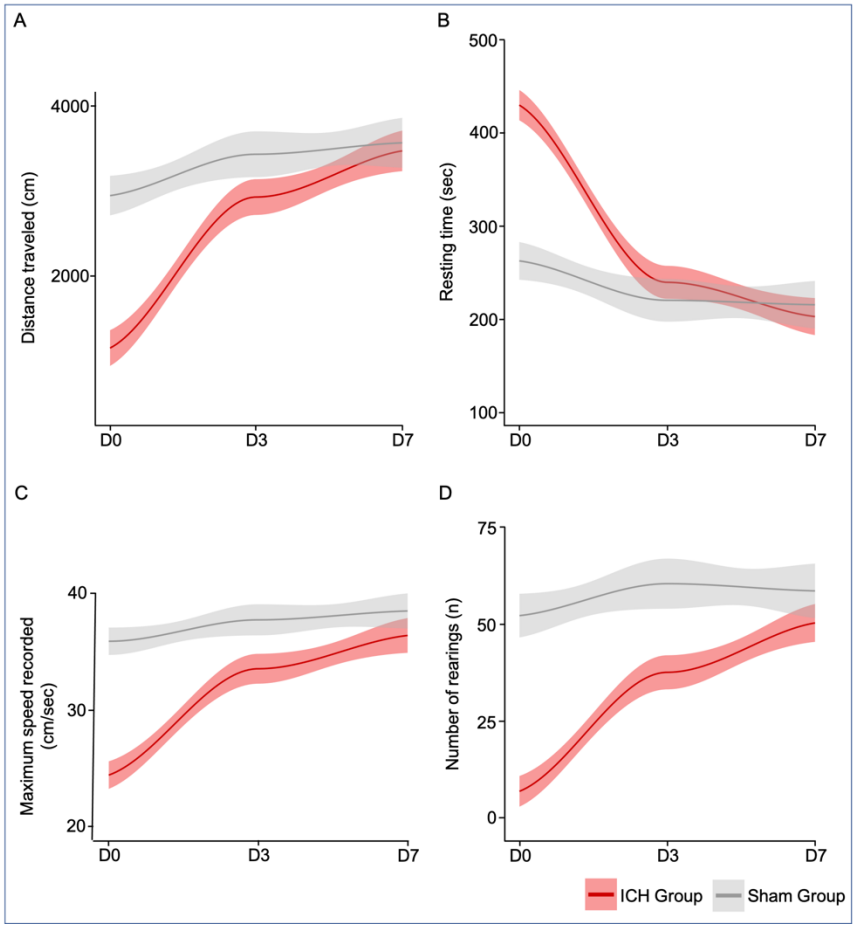

*Traveled distance in cm (A), resting time in seconds (B), (C) maximum speed recorded in cm/seconde an (D) number of rearings. Red and grey lines correspond to the ICH groups and the sham groups performances respectively with mean values (solid lines) and standard error. Measurements were assessed at day 0, day 3 and day 7. Symbols and bars correspond to the mean value and the SD. The p-value came from a t-student test (***p≤0.001, **p≤0.01, *p≤0.05, ns: not significant).*

Table 1. Association between PHA peak and spontaneous locomotion performances

Parameters	Estimates	p-values*
Distance traveled (cm)	-33.69	0.0061
Number of rearing (n)	-0.72	0.0089
Maximum speed (cm/sec)	-0.20	0.0013
Resting time (sec)	+2.66	0.0079

*Legend. The statistical data comes from a multivariate regression model adjusted for sex. The PHA peak estimates suggest that for every 10 mm^3 increase in PHA volume, holding other predictor (sex) constant, one can expect a significant decrease of -34*10 = -340 ; -0.7*10 = -7 and -0.2*10 = -2 in the distance traveled (cm), number of rearings (n) and maximum recorded speed (cm/sec), and an average increase of +2.6*10=26 seconds in the resting time.*

Contribution of multimodal MRI to characterize the PHA

Water content: rR2 was maximal at D0 (1.47 ± 0.24), remained high but slightly decreased at D3 (1.34 ± 0.18) and significantly decreased at D7 (0.86 ± 0.07; $p < 0.0001$ with D3 as reference) (Figure 3A).

Iron Accumulation: rR2* was 1.70 ± 0.34 at D0, 1.45 ± 0.26 at D3 and peaked at D7 (2.11 ± 0.46; $p < 0.0001$ with D3 as reference) (Figure 3A).

<u>Figure 3</u>: Water content, iron accumulation and neuroinflammation within the PHA

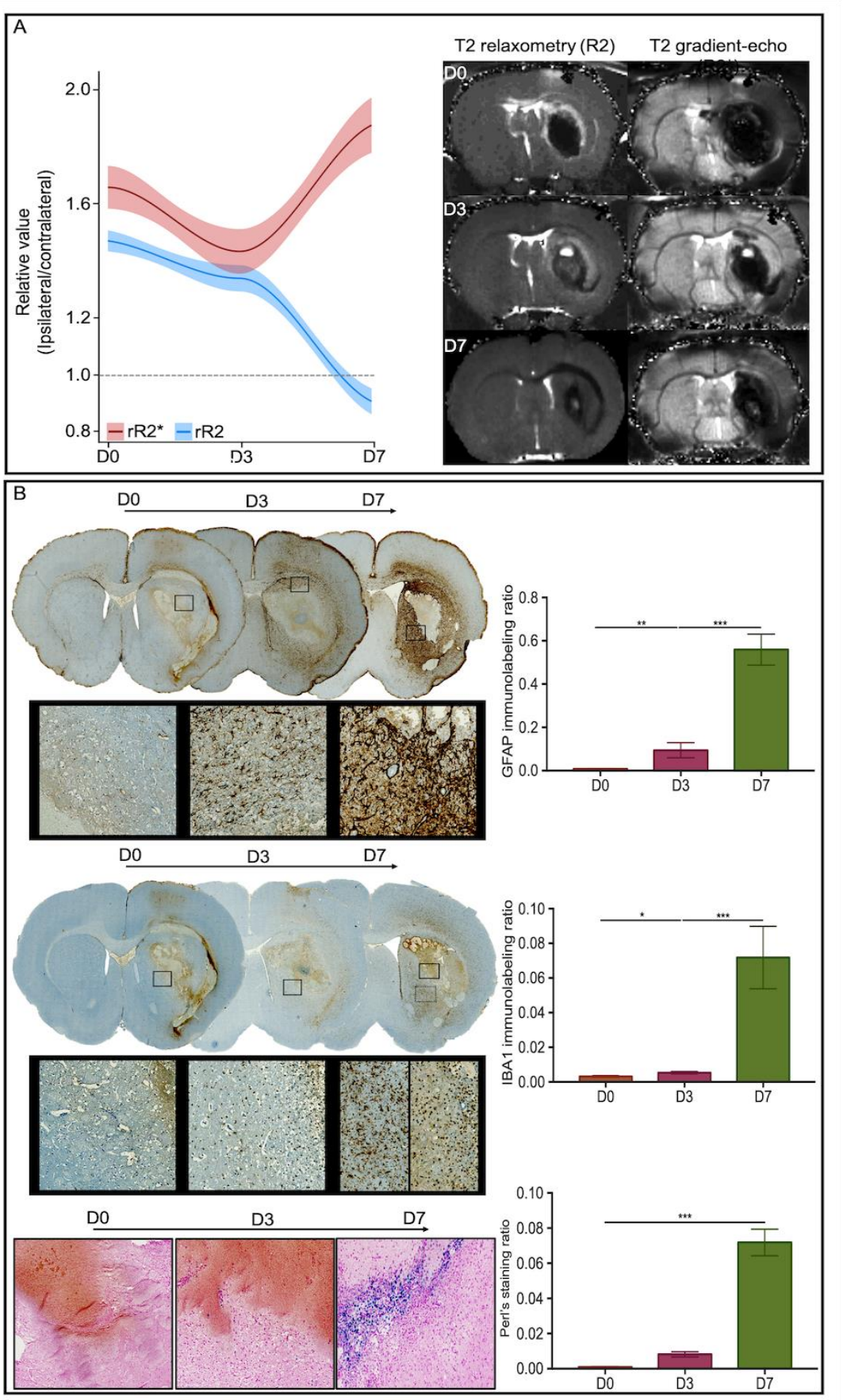

(A) Temporal course of rR2 (blue line), indicating water content, and rR2 (red line) values, indicating of iron load between day 0 and day 7. The dotted grey line indicates a normal ratio value (= 1). On the left, representative MRI sequences for each sequence at each time-point. (B) Brain slices from ICH animals euthanatized at D0, D3 and D7 immunolabelled for GFAP and Iba1 and stained for Perl's reaction indicating reactive astrocytes and microglia and iron deposits within the PHA. At D7, we observed two types of microglia: ramified (remotely from the PHA) and ameboid (at the border of ICH core). The graphs correspond to immunolabelling and staining ratio ([stacking surface/whole section surface]*10^3) of GFAP, Iba1 and iron load within the PHA of n=8 representative ICH rats (sex ratio 1:1). Bars and symbols correspond to the median value and the width of the 95% CI. Ratios were significantly different between time points according to Kruskal-Wallis followed by a Tukey post hoc test (***p≤ 0.00, **p≤ 0.01, *p≤ 0.05). Scale bars = 50 µm.*

Water mobility: rADC was 0.95 ± 0.11, 1.26 ± 0.14 (p< 0.0001 with D0 as reference) and 1.08 ± 0.10 at D0, D3 and D7 respectively (Figure 4A, B). Voxel-based analysis of ADC showed both cytotoxic and vasogenic values at D0 (32% and 29% of cytotoxic and vasogenic voxels). At D3, PHA was mostly vasogenic (77% of voxels) (Figure 4B).

Microvascular Water Mobility Assessment: rD* was 0.69 ± 0.23, 1.16 ± 0.14 (p< 0.0001 with D0 as reference) and 1.11 ± 0.12 at D0, D3 and D7 respectively (Figure 4A).

Tissue perfusion: rCBF was 0.50 ± 0.19, 1.06 ± 0.26 (p< 0.0001 with D0 as reference) and 1.10 ± 0.23 at D0, D3 and D7 respectively (Figure 4A, B). Voxel-based analysis of ADC showed that PHA at D0 was mainly hypoperfused (40% and 3% of hypo and hyper-perfused voxels). We then observed at D3 and D7 a normalisation of CBF within the PHA (>80% of voxels in normal values, with contralateral striatum as reference), even if some animals had a hyperperfused zone within their PHA at D3 (Figure 4B).

Whatever the sequences, we did not find substantial changes in relative values in the sham group over time.

<u>Figure 4</u>: Water mobility, micro-vascular wter mobility and tissular perfusion within the PHA

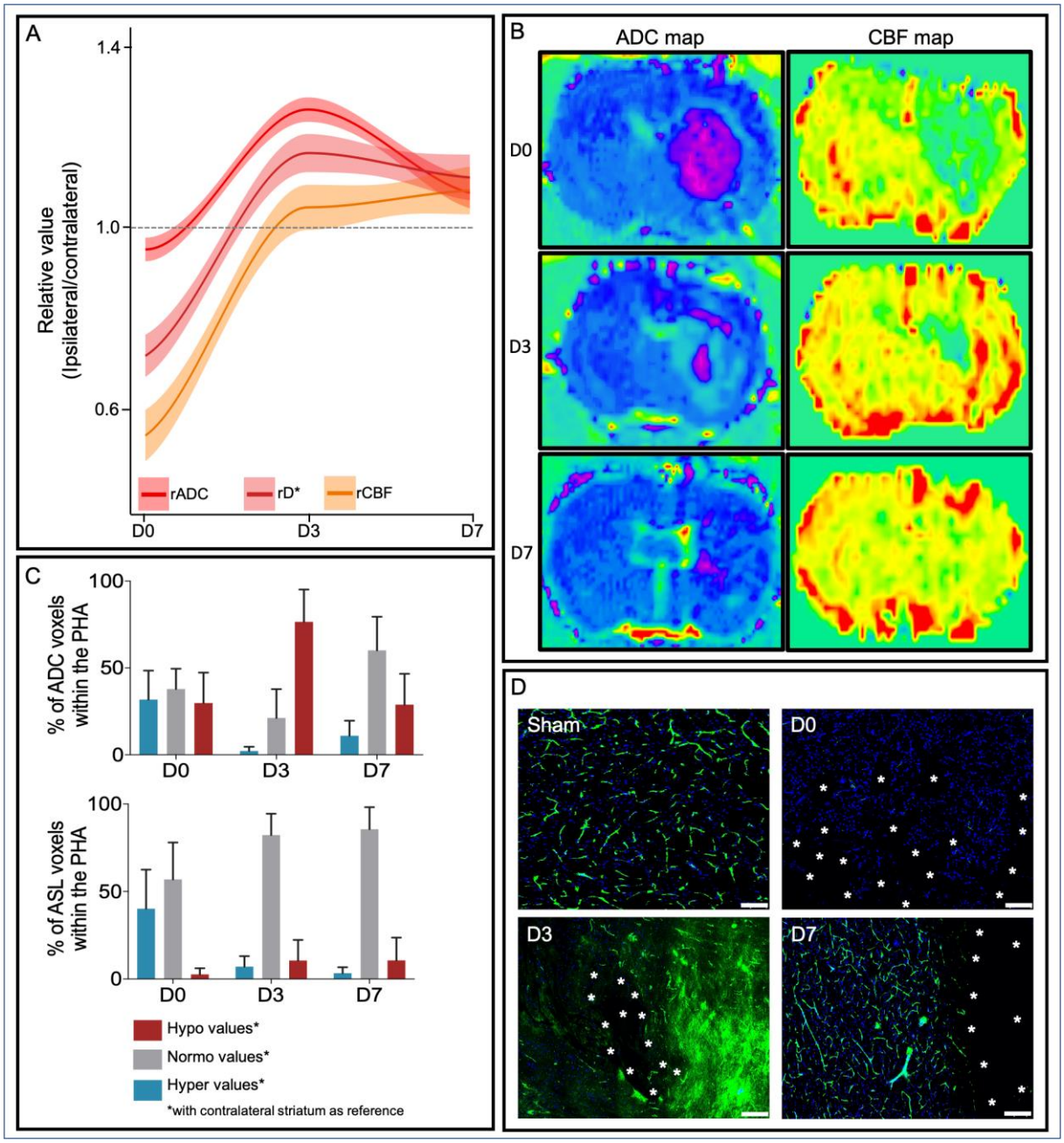

Temporal course between D0 and D7 of rADC (red line), rD (purple-red line) and rCBF (orange line) values that indicate water mobility in brain tissue, water mobility in brain microvessels, and tissue perfusion within the PHA. The dotted grey line indicates a normal ratio value (= 1). (B) Representative brain MRI of ADC and CBF maps from DWI and ASL sequences. (C) Voxel-based analysis of ADC and CBF values within the PHA compared to contralateral striatum as reference. (D) Brain slices from fluorescein isothiocyanate (FITC)-Dextran-infused animals illustrate the different states of microvessel in the PHA. At D0, we observed a dramatic decrease of the microvessel density compared to sham, indicating a drop in microvascular patency at this stage of ICH. At D3, we observed an abundant leakage of the the tracer resulting in an intense fluorescence signal. At D7, we observed a normalization of vascular integrity although some leaky capillaries were still sparsely found in the PHA. Asterisks indicate ICH area. Scale bars = 50 µm. ICH = intracerebral haemorrhage. PHA = peri-haematomal area.*

Relevant correlation between MRI features and predictors of PHA growth

We found a positive correlation between rASL and rADC values at each time point but especially at D0 ($r=0.47$, $p<0.0001$ for relative values and $r=0.62$, $p<0.0001$ for number of voxels in hypo ADC and ASL values). Relative ADC values were positively correlated to PHA volume at D3 ($r=0.73$, $p<0.0001$). The rR2* at D7 was positively correlated to ICH and PHA volumes at D0 ($r=0.66$ and 0.53 respectively, all p-values < 0.001).
In linear regression models adjusted for sex, we identified several parameters associated with PHA growth at D3: the proportion of voxels in hypoADC and hypoASL values at D0 (Estimates + 0.16 per-voxel, $p=0.003$ for hypoADC values and Estimates +0.12 per-voxel, $p=0.035$ for hypoASL values). Edema growth was also associated with the proportion of hyperASL values at D3 (Estimates +0.25 per-voxel, $p=0.005$) and hyperADC values (Estimates +0.24 per-voxel, $p< 0.0001$).

Histopathological correlates

Tissue characterisation with H&E and MSB stainings confirmed the presence of blood within the right striatum of ICH rats. The PHA was characterized by tissue pallor, that was maximal at D3. At D0, we did not observe any activated astrocytes (positive for GFAP) nor microglia (positive for Iba-1) within the PHA (all p=ns vs. sham, Figure 3B). The expression of GFAP and Iba1 slightly increased from D3 (all $p< 0.01$ vs. D0 as reference, Figure 3B) and reached the peak at D7 (all $p< 0.0001$ vs. D0 as reference, Figure 3B). Perls' staining (indicative of iron deposition) showed large numbers of iron-positive cells along the inner border of the haematoma from D3 but mostly at D7 (Figure 3B). The sham animals did not exhibit significant astrocytes nor microglia activation.

The expression level of GFAP and IBA1 were negatively correlated with rR2 values ($r= -0.95$ and -0.83, all p-value < 0.0001). The rR2* values were positively correlated with iron deposition from D3 to D7 ($r= 0.82$, p-value < 0.0001).

FITC-Dextran was used as a fluorescent tracer for assessing microvascular patency and integrity within the PHA (Figure 4D). At DO, we observed a dramatic decrease of the microvessel density compared to sham, indicating a drop in microvascular patency at this stage of ICH. In contrast, at D3, the tracer was kept in the lumen of tight capillaries, revealing the vascular segments, but diffused out of the leaky capillaries, which were then surrounded by a blurred signal alongside the vascular segments, resulting in an intense fluorescence signal. At

D7, we observed a normalization of vascular integrity although some leaky capillaries were still sparsely found in the PHA.

Discussion

Our study based on longitudinal multimodal MR imaging and behavioral and histological correlates in a large cohort of healthy male and female rats offered novel insight on kinetics of natural perihaematomal injuries and repair following ICH.

We first observed that even if all rats exhibited an initial sizable ICH lesion and were severely injured, they had a spontaneous blood resorption (≈ 40% of the initial lesion) and a complete locomotion recovery at D7. This favorable natural evolution demonstrates that spontaneous clearance processes are triggered after ICH. All rats exhibited PHA changes as early as the first four hours, that peaked three days after ICH induction and almost disappeared at D7. Our volumetric measurements of PHA (peak at D3) are consistent with literature in the field that is mainly based on the dry/wet method that require the euthanasia of animals.[34] The peak of PHA volume was predictive for spontaneous locomotor performances at D3 without sex-effect in adjusted analysis.

Beyond volumetric data, we aimed to characterize the longitudinal changes that occur within the PHA using various MRI parameters. The PHA is usually termed "peri-haematomal edema" in the literature this term did not reflect the full extent of phenomena occurring within the PHA.[2,34] Based on our multimodal MRI and histological correlates, we found four distinct components, that contribute to the genesis of peri-ICH tissue injuries: (1) tissular water infiltration; (2) (micro-)vascular changes; (3) neuroinflammatory cells infiltration and (4) iron deposits. They have their own intervention kinetics and we identified three critical phases of ICH natural history that can serve as endpoints for future experimental therapeutic studies: a hyperacute phase of tissular crush and mass-effect (4 hours); a pro-inflammatory induction phase (D3) and a subacute phase of resorption (D7).
We observed that the rR2 value, indicative for water content, peaked as early as four hours after ICH. This early and massive water entry in the ICH surrounding tissue is mainly related to clot formation and extravasation of plasma proteins secondary to clot retraction.[35,36] All these parameters precipitate the early formation of vasogenic edema. We observed the peak of PHA volume at D3 while the excess in water content tended to decrease. This confirms that water content is not the only component of PHA injury. Interestingly, the rR2 value appeared to be

negatively correlated to neuroinflammatory cells activation within the PHA over time: At D0, we observed a ≈ 50% (vs. sham) increase of water content without evidence for significant cellular infiltration. By contrast, at D7, we found a ≈ 20% (vs. sham) decrease of water content with a concurrent overexpression of both activated astrocytes and microglia. Haematoma resolution gradually occurs in the first few days after ICH and might contribute to the recovery of neurological function. Microglia and blood-derived macrophages participate in the clearance of apoptotic, dislocated, and damaged cells through phagocytosis.[37] These results suggest that, beyond water content assessment, rR2 might be a reliable *in vivo* marker of inflammatory cellular activation and infiltration in brain tissue after ICH.

We then assessed water mobility and microvascular changes over time. The mean rADC value at D0 was neither obviously increased nor decreased. Our voxel-based analysis approach showed that both cytotoxic and vasogenic ADC values co-exist within the PHA during the hyperacute phase of ICH. This emphasizes the heterogeneous nature of PHA and decrease the value of overall mean ADC values that is usually used in the current literature. Histological examination confirms the presence of swelling cells, the hallmark of cytotoxic process. The role of this cytotoxic edema in the acute phase after ICH remains unclear in humans[38–40] and whether ischemia occurs in ICH pathophysiology has been a matter of some controversy.[41] Our findings suggested the presence of early hypoperfusion (hypoCBF and cytotoxic ADC on voxel-based analysis) in the few hours following ICH induction. The low values of D* coefficient at D0 indicated that this hypoperfusion occurs at the microvessel level. We suggest that this reversible hypoperfusion is related to the mass effect of clot formation collapsing the microvessels in the vicinity of ICH. Those findings were supported by FITC-Dextran examination that showed a reduced detection of the flurorescent signal in microvessels, evidencing a drop in the patency of the latter. Importantly, longitudinal assessment showed a critical signal inversion of both rADC (almost 80% of voxel in vasogenic values), rCBF and rD* values at D3 with concurrent blood-brain barrier leakage observed on FITC sections. This confirms that the observed hypoperfusion at D0 does not reach the threshold of ischemia and is reversible.[42,43] This also confims that the disruption of the blood–brain barrier occurs after ICH and contributes to PHA formation. Our histologic data showed that microglia and astrocytes activation started at D3 when the ADC signal reached its peak. This suggested that suggested that the high ADC signal observed at edema edge (D3) is related to blood brain barrier disruption and activation of an exacerbated inflammatory process.

Clot-derived factors, including haemoglobin and iron, have been implicated in having a major role in secondary injury. We used R2* map to quantify iron concentration which is a well-

admitted robust method.[44] The massive entry of fresh blood was responsible for a diffuse blooming effect that artificially increased the rR2* value within the PHA at D0. One can not rule out that this increase was related to the spread of red blood cells. We did not find any iron deposits at D0. From D3 to D7, we found a strong correlation between rR2* values and histological peri-haematomal iron concentrations.
Most of current experimental studies investigate the PHA with methods that require animal euthanasia and so exclude follow-up behavioral or tissular injuries measurements in the same subject. Ongoing research in ICH and the prospects of therapy have raised the need for a noninvasive method to investigate ICH in rodent models. Whatever the sequence studied, we found throughout our results low standard deviations. The consistent patterns of changes in these parameters and their correlation with terminal histological measures and behaviour promote the use of *in vivo* markers in experimental models. Longitudinal studies using advanced MRI methods for assessing microvessel injury, BBB disruption, neuroinflammation or iron deposits as presented in this study could be essential for assessing the efficacy of treatments targeting these parameters. Monitoring these *in vivo* parameters after ICH may be useful for evaluating potential experimental therapies with longitudinal design. Importantly, all the MRI sequences described in this study are already used in human which facilitate the translational pipeline.

Our study has some limits. Although the experimental ICH model used in these studies may not exactly mimic the clinical presentation of ICH, given it does not reproduce the vessel rupture. Indeed, the primary damage observed might have been under-estimated, but allowed the secondary damage to be observed without extended contribution of the primary damage. It thus provides a reproducible tool for tracking and characterizing ICH-induced tissue changes that may be useful for testing potential therapeutic interventions targeting secondary injury.

Our study has also strengths including the longitudinal design, the large sample size, the inclusion of both male and female rats. To minimize measurement bias and subjectivity of scales, we used fully automated method to assess spontaneous locomotion. Our MRI multimodal approach was strengthened by the use of semi-automated method for volume segmentation and the use voxel-based approach to better reflect the true nature of PHA. Finally, we included both males and females, so our design was consistent with the 'Sex and Gender Equity in Research' guidelines.[45]

Conclusion:

Our current study shows that multimodal MRI is a reliable tool to track the dynamic progression of peri-haematomal injuries (water content, microvascular changes, neuroinflammatory cells infiltration and iron deposition) that could be widely uses to monitor therapeutic interventions in preclinical ICH models.

References

1. Recommendations for Clinical Trials in ICH: The Second Hemorrhagic Stroke Academia Industry Roundtable. *Stroke*. 2020;51:1333–1338.

2. Keep RF, Hua Y, Xi G. Intracerebral haemorrhage: mechanisms of injury and therapeutic targets. *Lancet Neurol*. 2012;11:720–731.

3. Ironside N, Chen C-J, Ding D, Mayer SA, Connolly ESJ. Perihematomal Edema After Spontaneous Intracerebral Hemorrhage. *Stroke*. 2019;50:1626–1633.

4. Li M, Akhavan-Sharif RM, Friedlander RM, Du R, Thiex R. What sequences on high-field MR best depict temporal resolution of experimental ICH and edema formation in mice? *J Biomed Biotechnol*. 2012;2012:961461.

5. Wang J, Wang G, Yi J, Xu Y, Duan S, Li T, Sun X-G, Dong L. The effect of monascin on hematoma clearance and edema after intracerebral hemorrhage in rats. *Brain Res Bull*. 2017;134:24–29.

6. Jin H, Wu G, Hu S, Hua Y, Keep RF, Wu J, Xi G. T2 and T2* magnetic resonance imaging sequences predict brain injury after intracerebral hemorrhage in rats. *Acta Neurochir Suppl*. 2013;118:151–155.

7. Bobinger T, Manaenko A, Burkardt P, Beuscher V, Sprügel MI, Roeder SS, Bäuerle T, Seyler L, Nagel AM, Linker RA, et al. Siponimod (BAF-312) Attenuates Perihemorrhagic Edema And Improves Survival in Experimental Intracerebral Hemorrhage. *Stroke*. 2019;50:3246–3254.

8. Sun Z, Zhao Z, Zhao S, Sheng Y, Zhao Z, Gao C, Li J, Liu X. Recombinant hirudin treatment modulates aquaporin-4 and aquaporin-9 expression after intracerebral hemorrhage in vivo. *Mol Biol Rep*. 2009;36:1119–1127.

9. Wang G, Li T, Duan S-N, Dong L, Sun X-G, Xue F. PPAR-γ Promotes Hematoma Clearance through Haptoglobin-Hemoglobin-CD163 in a Rat Model of Intracerebral Hemorrhage. *Behav Neurol*. 2018;2018:7646104.

10. Goulay R, Naveau M, Gaberel T, Vivien D, Parcq J. Optimized tPA: A non-neurotoxic fibrinolytic agent for the drainage of intracerebral hemorrhages. *J Cereb Blood Flow Metab*. 2018;38:1180–1189.

11. Guan J, Zhang B, Zhang J, Ding W, Xiao Z, Zhu Z, Han Q, Wu C, Sun Y, Tong W, et al. Nerve regeneration and functional recovery by collagen-binding brain-derived

neurotrophic factor in an intracerebral hemorrhage model. *Tissue Eng Part A*. 2015;21:62–74.

12. Strbian D, Tatlisumak T, Ramadan UA, Lindsberg PJ. Mast cell blocking reduces brain edema and hematoma volume and improves outcome after experimental intracerebral hemorrhage. *J Cereb Blood Flow Metab*. 2007;27:795–802.

13. Li M, Li Z, Ren H, Jin W-N, Wood K, Liu Q, Sheth KN, Shi F-D. Colony stimulating factor 1 receptor inhibition eliminates microglia and attenuates brain injury after intracerebral hemorrhage. *J Cereb Blood Flow Metab*. 2017;37:2383–2395.

14. Yang J-T, Lee T-H, Lee I-N, Chung C-Y, Kuo C-H, Weng H-H. Dexamethasone inhibits ICAM-1 and MMP-9 expression and reduces brain edema in intracerebral hemorrhagic rats. *Acta Neurochir (Wien)*. 2011;153:2197–2203.

15. Abbas M, Haddad E, Hamer M, Nowrangi D, Zhang J, Pearce WJ, Tang J, Obenaus A. Acute Treatment With Gleevec Does Not Promote Early Vascular Recovery Following Intracerebral Hemorrhage in Adult Male Rats. *Front Neurosci*. 2020;14:46.

16. Qureshi AI, Wilson DA, Hanley DF, Traystman RJ. No evidence for an ischemic penumbra in massive experimental intracerebral hemorrhage. *Neurology*. 1999;52:266–272.

17. Orakcioglu B, Becker K, Sakowitz OW, Unterberg A, Schellinger PD. Serial diffusion and perfusion MRI analysis of the perihemorrhagic zone in a rat ICH model. *Acta Neurochir Suppl*. 2008;103:15–18.

18. Orakcioglu B, Fiebach JB, Steiner T, Kollmar R, Jüttler E, Becker K, Schwab S, Heiland S, Meyding-Lamadé UK, Schellinger PD. Evolution of early perihemorrhagic changes--ischemia vs. edema: an MRI study in rats. *Exp Neurol*. 2005;193:369–376.

19. Knight RA, Han Y, Nagaraja TN, Whitton P, Ding J, Chopp M, Seyfried DM. Temporal MRI assessment of intracerebral hemorrhage in rats. *Stroke*. 2008;39:2596–2602.

20. Huang L-C, Liew H-K, Cheng H-Y, Kuo J-S, Hsu W-L, Pang C-Y. Brain Magnetic Resonance Imaging of Intracerebral Hemorrhagic Rats after Alcohol Consumption. *J Stroke Cerebrovasc Dis*. 2018;27:3493–3502.

21. Yang D, Knight RA, Han Y, Karki K, Zhang J, Chopp M, Seyfried DM. Statins Protect the Blood Brain Barrier Acutely after Experimental Intracerebral Hemorrhage. *J Behav Brain Sci*. 2013;3:100–106.

22. Liew H-K, Huang L-C, Yang H-I, Peng H-F, Li K-W, Tsai AP-Y, Chen S-Y, Kuo J-S, Pang C-Y. Therapeutic effects of human urocortin-1, -2 and -3 in intracerebral hemorrhage of rats. *Neuropeptides*. 2015;52:89–96.

23. Yang D, Knight RA, Han Y, Karki K, Zhang J, Ding C, Chopp M, Seyfried DM. Vascular recovery promoted by atorvastatin and simvastatin after experimental intracerebral hemorrhage: magnetic resonance imaging and histological study. *J Neurosurg*. 2011;114:1135–1142.

24. MacLellan CL, Silasi G, Poon CC, Edmundson CL, Buist R, Peeling J, Colbourne F. Intracerebral hemorrhage models in rat: comparing collagenase to blood infusion. *J Cereb Blood Flow Metab*. 2008;28:516–525.

25. Belayev L, Saul I, Curbelo K, Busto R, Belayev A, Zhang Y, Riyamongkol P, Zhao W, Ginsberg MD. Experimental intracerebral hemorrhage in the mouse: histological, behavioral, and hemodynamic characterization of a double-injection model. *Stroke*. 2003;34:2221–2227.

26. Deinsberger W, Vogel J, Kuschinsky W, Auer LM, Böker DK. Experimental intracerebral hemorrhage: description of a double injection model in rats. *Neurol Res*. 1996;18:475–477.

27. Cheng H-LM, Stikov N, Ghugre NR, Wright GA. Practical medical applications of quantitative MR relaxometry. *J Magn Reson Imaging*. 2012;36:805–824.

28. Haque ME, Gabr RE, Zhao X, Hasan KM, Valenzuela A, Narayana PA, Ting S-M, Sun G, Savitz SI, Aronowski J. Serial quantitative neuroimaging of iron in the intracerebral hemorrhage pig model. *J Cereb Blood Flow Metab*. 2018;38:375–381.

29. Wei J, Novakovic N, Chenevert TL, Xi G, Keep RF, Pandey AS, Chaudhary N. Perihematomal brain tissue iron concentration measurement by MRI in patients with intracerebral hemorrhage. *CNS Neurosci Ther*. 2020;26:896–901.

30. Tsai Y-H, Hsu L-M, Weng H-H, Lee M-H, Yang J-T, Lin C-P. Voxel-based analysis of apparent diffusion coefficient in perihaematomal oedema: associated factors and outcome predictive value for intracerebral haemorrhage. *BMJ Open*. 2011;1:e000230.

31. Kuntz M, Mysiorek C, Pétrault O, Pétrault M, Uzbekov R, Bordet R, Fenart L, Cecchelli R, Bérézowski V. Stroke-induced brain parenchymal injury drives blood-brain barrier early leakage kinetics: a combined in vivo/in vitro study. *J Cereb Blood Flow Metab*. 2014;34:95–107.

32. Le Bihan D. The “wet mind”: water and functional neuroimaging. *Phys Med Biol*. 2007;52:R57-90.

33. Wang DJJ, Alger JR, Qiao JX, Hao Q, Hou S, Fiaz R, Gunther M, Pope WB, Saver JL, Salamon N, et al. The value of arterial spin-labeled perfusion imaging in acute ischemic stroke: comparison with dynamic susceptibility contrast-enhanced MRI. *Stroke*. 2012;43:1018–1024.

34. Zheng H, Chen C, Zhang J, Hu Z. Mechanism and Therapy of Brain Edema after Intracerebral Hemorrhage. *Cerebrovasc Dis*. 2016;42:155–169.

35. Xi G, Wagner KR, Keep RF, Hua Y, de Courten-Myers GM, Broderick JP, Brott TG, Hoff JT. Role of blood clot formation on early edema development after experimental intracerebral hemorrhage. *Stroke*. 1998;29:2580–2586.

36. Wagner KR, Xi G, Hua Y, Kleinholz M, de Courten-Myers GM, Myers RE, Broderick JP, Brott TG. Lobar intracerebral hemorrhage model in pigs: rapid edema development in perihematomal white matter. *Stroke*. 1996;27:490–497.

37. Garton T, Keep RF, Hua Y, Xi G. CD163, a Hemoglobin/Haptoglobin Scavenger Receptor, After Intracerebral Hemorrhage: Functions in Microglia/Macrophages Versus Neurons. *Transl Stroke Res*. 2017;8:612–616.

38. Pascual AM, López-Mut JV, Benlloch V, Chamarro R, Soler J, Láinez MJA. Perfusion-weighted magnetic resonance imaging in acute intracerebral hemorrhage at baseline and during the 1st and 2nd week: a longitudinal study. *Cerebrovasc Dis*. 2007;23:6–13.

39. Stösser S, Neugebauer H, Althaus K, Ludolph AC, Kassubek J, Schocke M. Perihematomal Diffusion Restriction in Intracerebral Hemorrhage Depends on Hematoma Volume, But Does Not Predict Outcome. *Cerebrovasc Dis*. 2016;42:280–287.

40. Olivot J-M, Mlynash M, Kleinman JT, Straka M, Venkatasubramanian C, Bammer R, Moseley ME, Albers GW, Wijman CAC. MRI profile of the perihematomal region in acute intracerebral hemorrhage. *Stroke*. 2010;41:2681–2683.

41. Gass A. Is there a penumbra surrounding intracerebral hemorrhage? *Cerebrovasc Dis*. 2007;23:4–5.

42. Powers WJ, Zazulia AR, Videen TO, Adams RE, Yundt KD, Aiyagari V, Grubb RLJ, Diringer MN. Autoregulation of cerebral blood flow surrounding acute (6 to 22 hours) intracerebral hemorrhage. *Neurology*. 2001;57:18–24.

43. Zazulia AR, Diringer MN, Videen TO, Adams RE, Yundt K, Aiyagari V, Grubb RLJ, Powers WJ. Hypoperfusion without ischemia surrounding acute intracerebral hemorrhage. *J Cereb Blood Flow Metab*. 2001;21:804–810.

44. Chaudhary N, Pandey AS, Griauzde J, Gemmete JJ, Chenevert TL, Keep RF, Xi G. Brain tissue iron quantification by MRI in intracerebral hemorrhage: Current translational evidence and pitfalls. *J Cereb Blood Flow Metab*. 2019;39:562–564.

45. Heidari S, Babor TF, De Castro P, Tort S, Curno M. Sex and Gender Equity in Research: rationale for the SAGER guidelines and recommended use. *Research Integrity and Peer Review*. 2016;1:2.

Travail numéro 2

Deep Intracerebral Haemorrhage Induces Long-Term Cognitive Impairment and Diffuse Atrophy and Hypometabolism in the Rat Brain.

Authors: Laurent Puy; Clémence Leboullenger; Florent Auger; Régis Bordet; Charlotte Cordonnier and Vincent Bérézowski.

Status: Under review

Abstract

The mechanisms underlying intracerebral haemorrhage (ICH) -related cognitive impairment (CI) remain unclear. We aimed to investigate the long-term cognitive effect of ICH induction in rats. We concurrently studied the long-term structural and functional changes that occur in the rat brain. We led a prospective study with 114 healthy male and female Wistar rats. We induced ICH using the double autologous blood injection method. After surgery, each rat underwent short-term (onset, 3 and 7 days) and long-term (3 and 6 months) radiological assessment and behavioral tests exploring spontaneous locomotion, anxiety-like behavior and working, spatial recognition and visual recognition memories. We used 7T-MRI and [18F] FDG PET to semi-automatically segment ICH volumes and study long-term cerebral atrophy and metabolism. Mean initial hematoma volume was 23.35 ± 9.50 mm^3. We found early spontaneous locomotor recovery and significant spontaneous blood resorption (≈ 40% of the initial lesion) from day 0 to day 7. At 3 and 6 months, the ICH group exhibited CI in several domains as compared to the sham group (working memory: 58.1±1.2 vs 70.7±1.2 %, $p< 0.001$; spatial recognition memory: 48.7±1.9 vs 64±1.8 %, $p< 0.001$ and visual recognition memory: 0.14± 0.05 vs 0.33± 0.04, $p= 0.013$, in female only). Concomitantly, ICH rats had a diffuse cerebral atrophy and hypometabolism of ipsilateral striatum, thalamus, limbic system and cortical areas (temporal and parietal lobes). This work demonstrates that a deep ICH provokes long term cognitive impairment and distant cortical atrophy and hypometabolism in a young and disease-free rat brain.

Key words: Stroke; Experimental ICH; cognitive impairment; MRI; Positron Emission Tomography

Introduction

Spontaneous intracerebral hemorrhage (ICH) is among the most severe forms of stroke, accounting for almost half of stroke-related morbidity and mortality (Poon et al., 2014). Despite a slight improvement in inhospital mortality, disability among ICH survivors remains significant, including one third of them with new onset dementia in the ensuing years (Moulin et al., 2016). Recent data offered a better characterization of cognitive impairment (CI) that affected several cognitive domains, such as language, memory, executive functions, processing speed and and visuo-spatial abilities (Donnellan and Werring, 2020). Understanding the underlying mechanism of ICH-related CI is the next step to improve the prevention and treatment of long-term ICH complications. In clinical setting, disentangling the sole effect of bleeding from the coexisting presence neurodegenerative and/or small vessel diseases (such as cerebral amyloid angiopathy) is impossible (Donnellan and Werring, 2020; Pasi et al., 2021). Experimental ICH models may therefore be useful but few data on long-term cognition are currently available in the literature (Hietamies et al., 2018).

We aimed to investigate the long-term hippocampal and non hippocampal cognitive effect of ICH in healthy male and female rats, devoided of underlying cerebrovascular disease. To deepen our understanding of ICH-related CI, we concurrently studied the long-term structural (7T-MRI and automated brain atrophy segmentation) and functional ([18F] FDG PET) changes that occur in the rat brain.

Methods

Ethical aspects

All experiments were approved by the national Ethical Committee in Animal Experimentation (CEEA, Comité d'Ethique en Experimentation Animale), from the French Ministry for Education and Research (agreement number: APAFIS#14066-2018031312529642v3) and were performed in strict compliance with the European Union Directive 2010/63/EU. Experiments were reported in accordance with the ARRIVE guidelines for reporting experiments involving animals.

Animals and study design

We used 12-week-old Wistar rats and included both males (280 g to 350 g) and females (220 g to 300 g). We prospectively studied 114 male and female rats: 74 in the ICH group (sex ratio 1:1) and 40 in the sham group (sex ratio 1:1). After surgery, each rat underwent short-term (day 0, 3 and 7) and long-term (3 and 6 months) behavioral and radiological assessments. Details of the study design are reported in Figure 1.

Figure 1: Design of the study

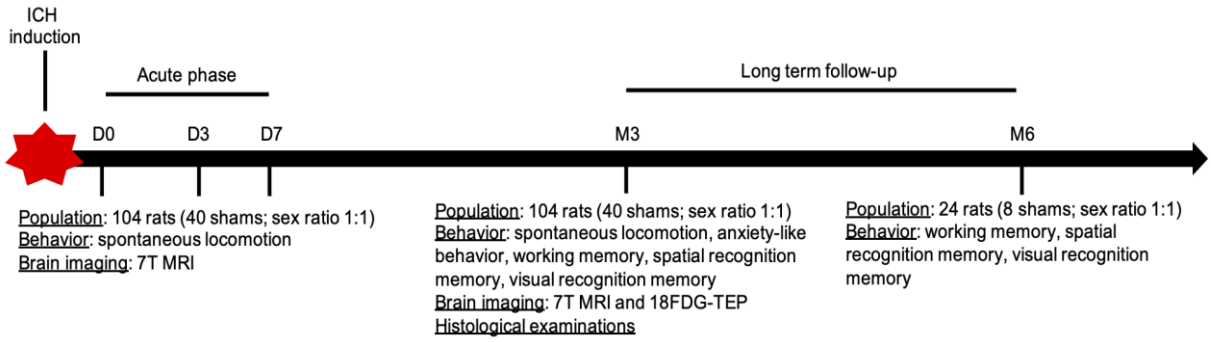

ICH = intracerebral haemorrhage.

Intracerebral haemorrhage induction

Animals were anesthetized with isoflurane (1.5% to 2%) through spontaneous respiration and core temperature was maintained at 36°c to 37°c throughout all surgical procedures. A stereotaxic apparatus was used to position the tip of the needle (26 gauge) at coordinates 0.4 mm anterior, 3.2 mm lateral, and 5.8 mm deep relative to bregma through a 1-mm craniotomy. ICH was produced by injection of 50 µL of fresh (nonheparinized) autologous whole blood into the right striatum at a constant rate of 8 µL/min. After a 10-minute break, other 50 µL of blood were infused at the same rate for a total of 100 µL. The needle was left in place for 10 minutes after the infusion and was then withdrawn and the incision closed with sutures. Rats were randomly assigned to the sham or ICH group. Sham operation was restricted to needle insertion.

Behavioral Testing

Spontaneous locomotion

Spontaneous locomotor activity was measured using an infrared actimeter (Panlab, Bioseb, Vitrolles, France). The apparatus consisted of a square arena (45 cm in length, 45 cm in width and 35 cm in height) with a black polymethyl methacrylate floor and transparent 34-cm-high polymethyl methacrylate walls. Rats were placed in the center of the arena and allowed to explore freely for 10 min. Activity was recorded by two rows of infrared photocell sensors and processed with Actitrack software (Bioseb). The total distance covered (in cm), the duration of inactivity (resting time, in seconds) and the number of rearings were collected.

Anxiety-like behavior

To check whether ICH did not cause alterations in anxiety like behevior, animals were tested using a modified version of the elevated plus maze (Pellow et al., 1985). The apparatus consisted of two open arms (40 cm 20 cm) alternating at right angles with two arms enclosed by 40 cm high walls. The four arms delimited a central area of 20 cm2. The whole apparatus was placed 70 cm above the floor. Rats were placed in the center of the elevated plus maze, facing a closed arm, and were allowed to freely explore the maze for 10 minutes. the percentage of time spent in the open arms were measured.

Working memory

The spontaneous alternation test was performed using a Y-maze (made of black wood) and a closed-circuit video camera (Ethovision XT, Noldus, Wageningen, The Netherlands). The three arms were of the same size (50*15*32 cm) and were oriented at an angle of 120° to each other. The Y-maze was placed in a room with no environmental cues. The rat was placed at the end of one arm and was allowed to move freely between the maze's three arms for 8 min. A visit to an arm was scored when all four of the rat's paws were within the arm area. The sequence of the arm visits was recorded, and an alternation response was scored when the animal entered the least recently visited arm. The alternation score was calculated as the ratio between actual alternations and possible alternations (defined as the total number of arm visits minus 2), multiplied by 100. This calculation was only performed for rats making more than fifteen arm visits (Hidaka et al., 2008).

Spatial recognition memory

Discrimination of novelty versus familiarity can be studied by comparing exploring behavior in the three arms of Y-maze test. Each of the three arms was 35 cm long, 8 cm wide and 15 cm high. To differentiate the arms, three distal cues were placed on the walls around the Y-maze in the testing room and were kept in place throughout the behavioral testing period. Spatial memory was evaluated in a two-trial procedure with an inter-trial interval of one hour. Three arms were designated: the starting arm, in which the rat started to explore (always open), the novel arm (which was closed in the first trial but open in the second trial) and the other arm (always open). The first trial (training session) lasted 10 min and enabled the rat to explore two arms of the maze (the start arm and the other arm). After a 1 h inter-trial interval, the second trial (test session) was performed; the rat was placed in the Y-maze in the same starting arm, with free access to all three arms for 5 min. Behavior was recorded with a video tracking system (Ethovision Noldus, The Netherlands) designed to automate testing in behavior experiments. The tendency to ignore the novel arm was determined by the percentage of time spent in the novel arm over those values in the two other arms during 2nd trial of the Y-maze test. A spontaneous tendency of animals to explore a novel environment as determined by the Y-maze test is generally regarded as a measure of spatial memory (Dellu et al., 1992).

Visual recognition memory

The novel object recognition test is based on the tendency of rats to explore a novel object rather than a familiar one. Rat were habituated to a square arena (50*50*25 cm) for 10 min on the first day. On day 2, rats were exposed to the arena containing two identical objects. On day 3, rats were exposed, in a first phase ("sample phase"), to two novel and identical objects for 15 min. After a 1 h resting time in their cage, they were placed back in the testing arena for 5 min ("test phase"), but a novel object had previously replaced one of the familiar objects. Performance of the rat was video recorded (Ethovision XT, Noldus, Wageningen, The Netherlands). Exploratory behevior was defined as the animal directing its nose toward the object at a distance below 2 cm. Any subject that failed to complete a minimum of 10 s of exploration during the sample phase was excluded from the analysis. The discernment index was calculated as the subtraction of the time spent exploring the novel object and the familiar object divided by the total time exploring either object (Antunes and Biala, 2012).

In Vivo brain MRI

Image Acquisition

All rats underwent a 7-Tesla micro-MRI (7-Tesla; BioSpec 70/ 20, Bruker, Ettlingen, Germany) at day 0, day 3, day 7 and 3 months after ICH induction. Animals were anesthetized with isoflurane (1.5% to 2%) through spontaneous respiration and core temperature was maintained at 36°C to 37°C throughout all surgical and MRI procedures. A cylindrical emitter antenna with a diameter of 72 mm and a cerebral receiving surface antenna both allow data recording. A birdcage radiofrequency coil and a surface coil were used for radiofrequency transmission and reception, respectively. Ear bars and a nose cone, through which the anesthetic gas mixture was supplied, were used to minimize head movement during MRI measurements. A 3-plane scout imaging sequence was obtained at the start of each MRI session to reproducibly position the animal in the magnet. For the current study, we used axial and coronal T2-weighted sequences (repetition time/echo time [TR/TE] = 5000/77 ms, field of view [FOV] = 4*4 cm, matrix = 256*256, slice thickness = 1 mm, no gap, 20 slices).

Image Processing and Analysis: initial ICH volume and cerebral atrophy assessment

We used MRI data obtained at day 0, day 3 and day 7 to quantify ICH volume. To do so, ICH was semi-automatically segmented using Mango© software. In Mango©, prior to any segmentation procedures, all T2-axial images underwent brightness/contrast enhancement using a contrast control tool to increase image quality and enhance background separation as much as possible. Thresholding was then applied, the values were automatically set (using the auto-threshold tool) to include only regions having pixels with high intensity levels, that isolated ICH, edema and normal parenchyma. Region of interest (ROI) was then manually defined. Segmentations were independently analyzed by two experienced operators (L.P and F.A) with excellent interobserver agreement (r=0.92). To ensure that all rats in the ICH group had a significant lesion, we excluded rats with initial ICH volume < 10 mm^3.

To study striatal and cerebral atrophy at 3 months, we proceeded as follows. First, bias field inhomogeneity was corrected from T2-weighted images using N4 algorithm.(Tustison et al., 2010) Then, images were denoised with a multiresolution non-local means filter.(Coupé et al., 2012) Brain mask and label segmentation were automatically extracted with ANTS (Advanced Normalization Tools package) and from Cermep atlas.(Lancelot et al., 2014) All MRI were visually checked and manually corrected when appropriate by two experienced operators (L.P and C.L). We first checked that there was no difference between Sham and ICH in the

contralateral areas (see Figure 1 in supplementary material). The measurement was expressed as a ratio of the ispilateral volumes divided by the contralateral volumes for each ROI.

Supplementary material – Figure 1: Comparison between sham and ICH group regarding the volume of contralateral areas.

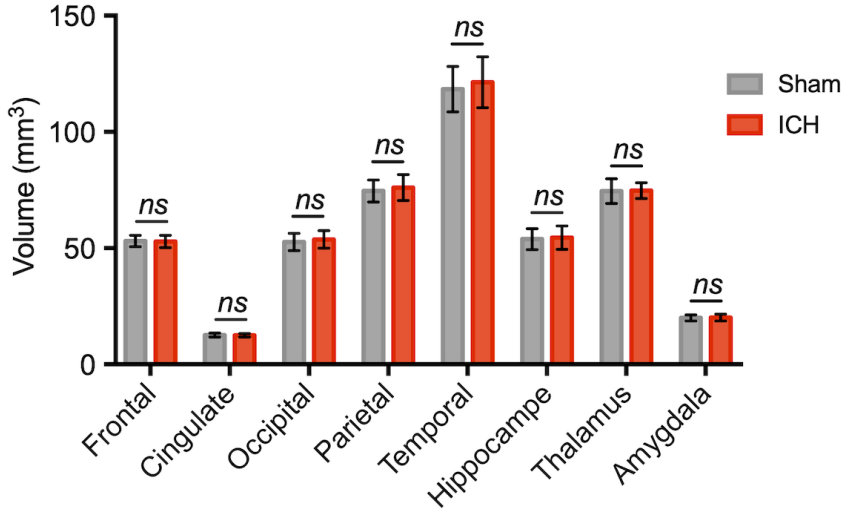

Fluorodeoxyglucose – Positron Emission Tomography.

Three months after surgery, cerebral metabolism was studied by performing a microPET scan (Inveon, Siemens) with an intraveinous injection of fluorinated analog of glucose, the fluorodeoxyglucose ([18F] FDG) (34.76±6.50 MBq; 300µl in volume, IBA-CisBio, Saclay, France) in a sample of 12 representative animals. A 15-min PET scan was initiated 30 minutes after radiotracer injection. To assess changes in metabolism in the regions of interest (striatum, thalamus and hypothalamus, cortex and hippocampus), data from the scanner were formatted into three frames of 5 minutes. Those 3 frames were averaged and registered with SPM 12 (Welcome Department of Cognitive Neurology, London, UK; http://www.fil.ion.ucl.ac.uk/spm/). PET and CT images were rigidly co-registered with SPM 12. All CT scans were registered to an in-house CT template and brain masks were extracted and applied to PET images with ANTS (Advanced Normalization Tools package). PET images were registered with ANTS to their own T2-weighted image which were registered to Cermep rat atlas (Lancelot et al., 2014). FDG brain uptake values were expressed as Standardized Uptake Values (SUV) normalized to the average signal of the whole brain (SUVw). SUVw images were smoothed using an isotropic Gaussian filter [0.8x0.8x0.8mm]. Voxel-based

analysis with Statistical Parametric Mapping (SPM) was performed using SPM12 (Welcome Department of Imaging Neuroscience, London, UK) and the SAMIT toolbox (Vállez Garcia et al., 2015). For each voxel, two-sample t-tests were performed to compare ICH *vs* sham animals. The a-priori hypothesis was that the focal induction of ICH induces a diffuse reduction of cerebral metabolism (decreased cerebral [18F]FDG uptake) compared with the Sham group. The images generated by this post-treatment are statistical T-maps. They show the significant differences (expressed as T-values) between the two groups (ICH vs sham) for each voxel registered onto a MRI rat brain template (Cermep). T-map data were thresholded at $p<0.05$ (uncorrected) and an extent threshold of 200 voxels. Clusters with $p<0.05$ corrected for family-wise error (FWE) were considered significant.

Histopathological correlates

At the end of the protocol (i.e. 3 months or 6 months for the sub-group with extended follow-up), rats were euthanized with an overdose of pentobarbital (200 mg/kg, intraperitoneal). For tissue staining procedure, rats were transcardially perfused with heparinized physiologic saline for 5 min and decapitated. Subsequently, brains were isolated and fixed in methacarn solution (60% methanol-30% chloroform- 10% acetic acid) at 4 °C for 1 day, then in 70% ethanol at 4 °C for 1-3 days, followed by paraffin embedding. Brains were serially sliced at 5 µm thickness. Sections of formalin-fixed paraffin embedded tissue were stained routinely with hematoxylin–eosin (H&E) for the identification of ICH and structural analysis of the tissue. Perls' staining was done to screen for iron deposits using Tissue-Tek Prisma Plus automated Stainer (Sakura). Slides were placed in Potassium Ferricyanide solution (2% Potassium Ferricyanide – 25ml and 2% Hydrochloric acid -25ml) for 20 minutes, and then counterstained in Nuclear fast Red for 5 minutes, rinsed in distilled water, dehydrated and mounted.

Statistical analysis

Distribution of the data was established using the Kolmogorov-Smirnov test. All data are presented as mean ± SD or median [IQR] as appropriate. Statistical differences in data with normal distribution were analyzed with Student test, others with Mann-Whitney U test. First, statistical analyses were performed on total population (ICH versus sham) and then in sex-subgroup. All statistical tests were 2-sided and a *p-value* of <0.05 was considered as statistically significant.

Results

ICH characteristics and locomotor function at the acute phase

Among the 114 ICH animals, 3 died before the first MRI and 7 had a baseline ICH volume < 10 mm^3. Therefore, 104 animals (53 males, 64 ICH) were included in the study. In the ICH group, initial mean hematoma volume was 23.35 ± 9.50 mm^3 (Figure 1A). We did not find significant differences between males and females (24.03 ± 9.82 mm^3 versus 22.60 ± 9.23 mm^3 respectively, p= 0.43) (Figure 2A). The ICH volumes were similar at day 0 and day 3 and decreased significantly at day 7 (13.91 ± 0.9 mm^3, p< 0.0001 with day 0 as reference). The same temporal course was found for both males and females (Figure 2B).

Figure 2: Temporal course of intracerebral haemorrhage volume in the acute phase.

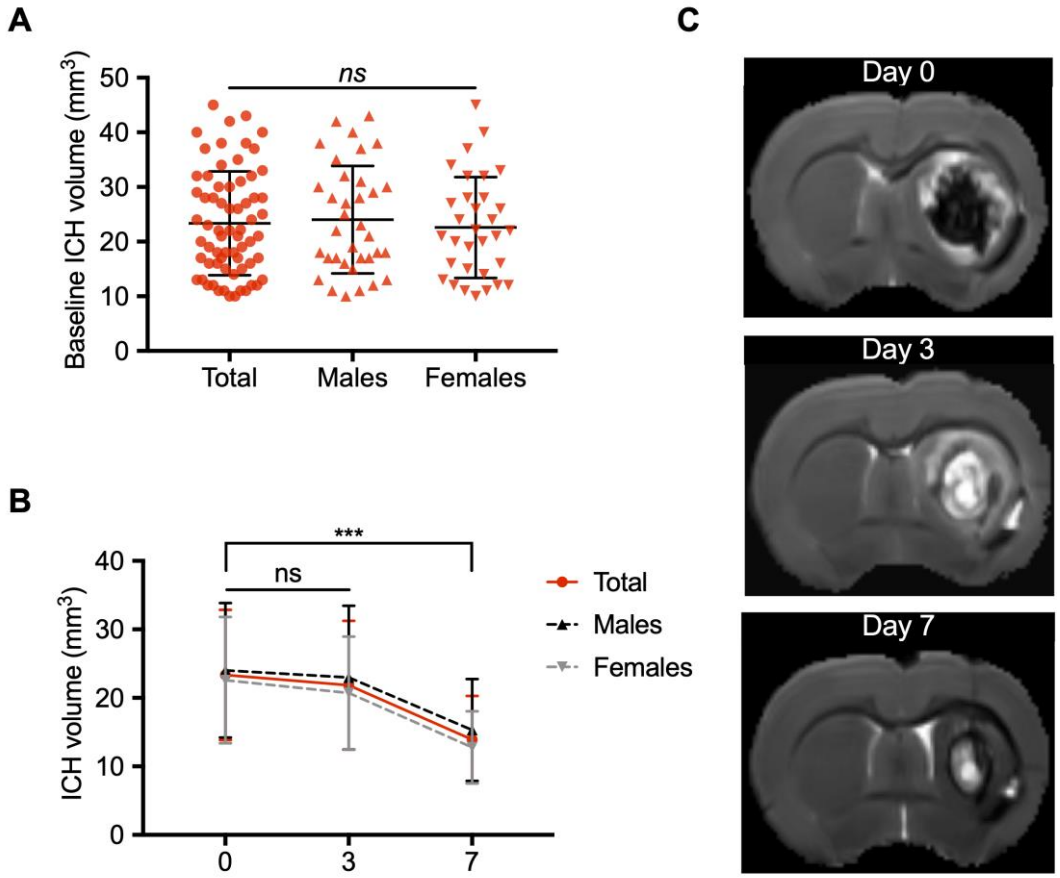

(A) Distribution of the ICH volume at day 0 in the total study population including male and female rats. Magnetic resonance imaging (MRI) was performed at 4±1 hours following ICH induction. (B) Temporal course of haematoma volume between day 0 and day 7. (C) Representative brain MRI axial T2 image of a female rat. Baseline ICH volume was 32 cm^3. Intracerebral haemorrhage core appears in hyposignal within the right striatum. The adjacent hypersignal corresponds to the peri-hematomal oedema. ICH = intracerebral haemorrhage.

Figure 3 shows the spontaneous locomotion of animals (total population and sex-subgroups) between day 0 and day 7. At day 0, ICH rats showed severe locomotor impairment with a significant decrease in the traveled distance (ICH group *vs* sham group, p-value: 961±69 vs 3168±156 cm, p<0.0001), a lower number of rearings (6.7±1.2 vs 57.3±3.1, p<0.0001) and a longer resting time (430±9.3 vs 250±13 sec, p< 0.0001). At day 3, ICH rats showed a partial recovery but were still significantly impaired. We observed a lower traveled distance (ICH group vs sham group, p-value: 3069±131 vs 3548±158 cm, p= 0.024), a lower number of rearings (46.1±3.6 vs 60.9±4.7, p= 0.016) and a still longer resting time: 253±11 vs 222±12 sec, p= 0.07). At day 7, ICH rats showed complete recovery of locomotor function (traveled distance: 3662±123 vs 3844±121 cm, p= 0.42 / number of rearings: 56±3.6 vs 59±3.6, p= 0.58 / resting time: 215±9 vs 226±11 sec, p=0.46). In sex sub-group analysis, males and females were equally injured at day 0. The females tended to recover faster than the males, with spontaneous locomotor performances comparable to their sham group from day 3 (traveled distance and resting time, p<0.05).

<u>Figure 3</u>: Spontaneous locomotion recovery in the acute phase.

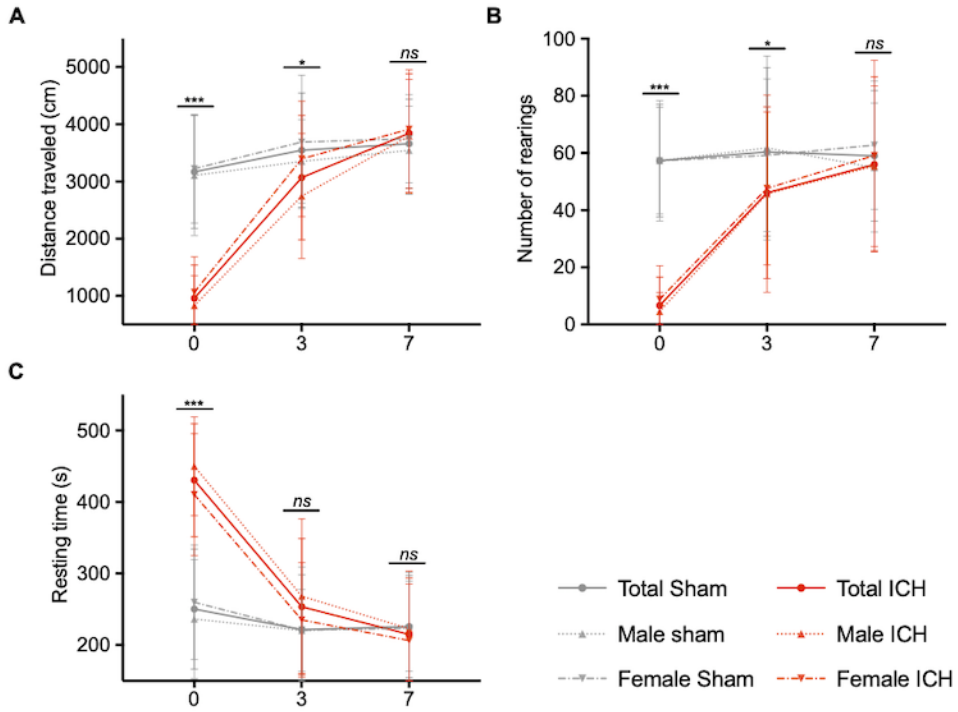

*Traveled distance in cm (A), number of rearings (B), and resting time in seconds (C). Red and grey lines correspond to the ICH groups and the sham groups performances respectively. Solid, dotted and hashed lines correspond to total population, male and female rats respectively. Measurements were assessed at day 0, day 3 and day 7. Symbols and bars correspond to the mean value and the SD. The p-value came from a t-student test (***p≤0.001, **p≤0.01, *p≤0.05, ns: not significant).*

ICH induces long-term cognitive impairment

None of the included animals died between ICH induction and the follow-up assessments. At three months, ICH rats had similar spontaneous locomotor performances compared to the Sham rats (ICH group *vs* sham group, difference between means, p-value; distance traveled: 3646±155 vs 3393±146 cm, 253±228, p= 0.27 / number of rearings: 76.9±3.7 vs 68.4±3.9, 8.5±5.7, p= 0.13 / resting time: 209±8 vs 230±11 sec, -22±13, p= 0.10) (Figure 4A-C). They also did not exhibit more anxiety-like behavior (% of the time spent in open arm: 13.2±0.8 vs 15.0±1 %, -1.8±1.2, p= 0.14) (Figure 4D). Results were similar in both males and females in sex-subgroup analysis.

<u>Figure 4</u>: Long-term spontaneous locomotion and anxiety-like behavior.

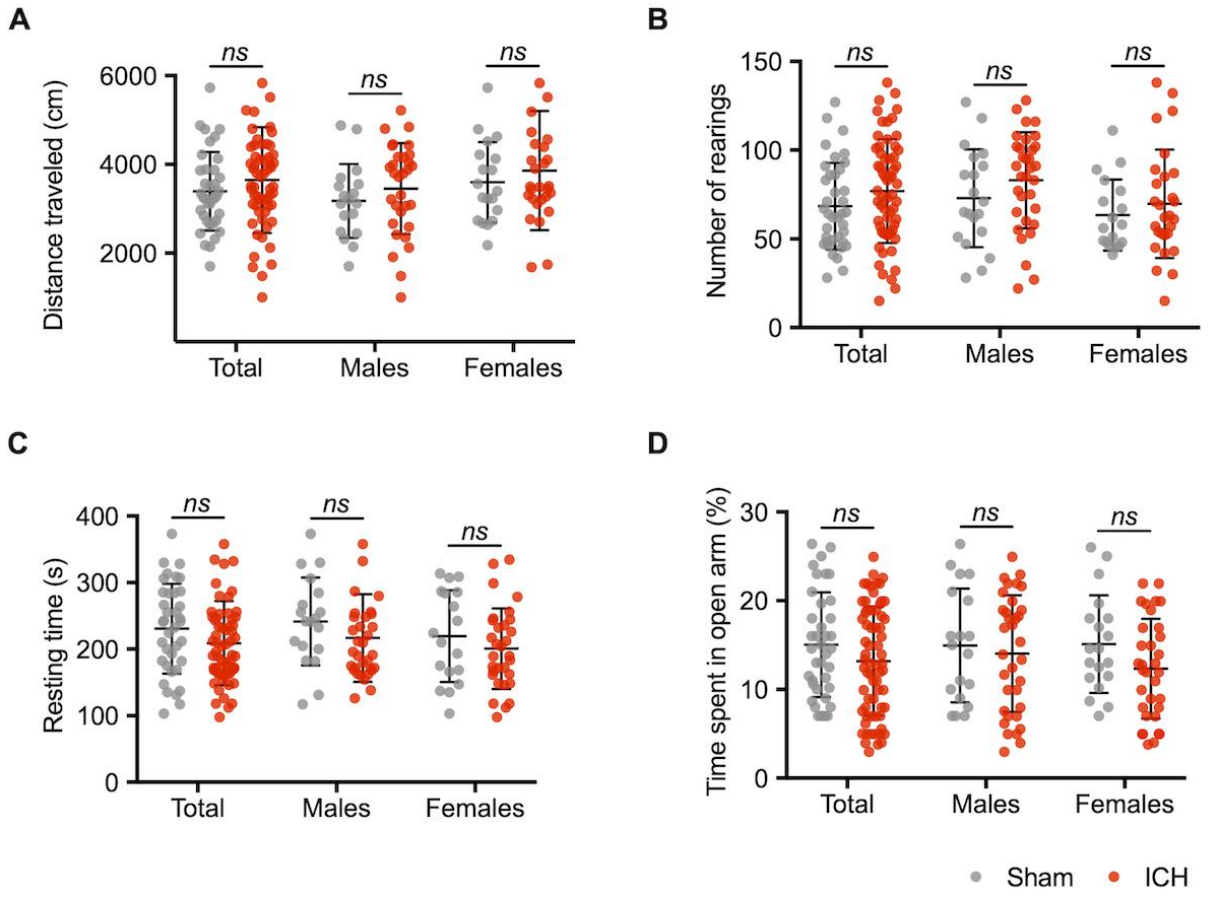

Traveled distance in cm (A), number of rearings (B), and resting time in seconds (C). Anxiety-like behavior (D), values correspond to the time spent in the novel arm, expressed in %. Grey and red symbols corespond to sham and ICH rats respectively. Black bars correspond to the mean value and the SD. The p-value came from a t-student test (ns = non significant).

Figure 5 (A,C and E) shows the cognitive impairment at three months (total population and sex-subgroups). The ICH group exhibited a cognitive impairment in several domains. An alteration of the working memory was observed (% of spontaneous alternation: 58.1±1.2 vs 70.7±1.2 %, -12.6±1.8, p< 0.001). Spatial recognition memory was also altered (% of time spent in the novel arm: 48.7±1.9 vs 64±1.8 %, -15.3±2.9, p< 0.001). We did not find any sex effect regarding the working and spatial recognition memory. Regarding visual recognition memory, ICH female rats showed a deficit in visual recognition memory (discrimination index: 0.14± 0.05 vs 0.33± 0.04, -0.19±0.07, p= 0.013). In the subgroup of 24 animals followed up to 6 months, spontaneous alternation test and the Y-maze spatial test were still impaired compared to the 3-months assessment (Figure 5 B, D and F).

<u>Figure 5</u>: Long-term cognitive impairment after intracerebral haemorrhage induction.

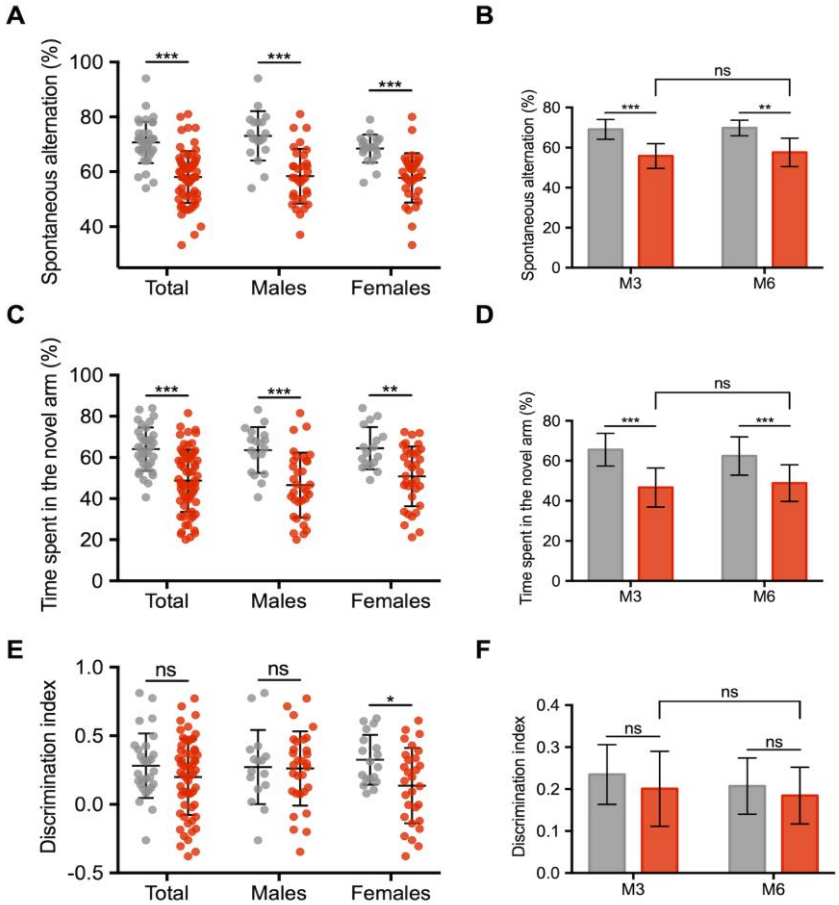

*(A) Assessment of the working memory, expressed in % of spontaneous alternation. (C) Assessment of the spatial and hippocampal memory. Values correspond to the time spent in the novel arm, expressed in %. (E) Assessment of the visual recognition memory. (B, D and F) Comparison of cognitive performances between 3 months and 6 months in a subgroup analysis of 24 animals (10 sham rats, sex ratio 1:1). Grey and red barplots correspond to sham and ICH rats respectively. Black bars correspond to the mean value and the SD. The p-value came from a t-student test (***p≤0.001, **p≤0.01, *p≤0.05), ns: not significant).*

ICH induces long-term structural and metabolic alterations

The ICH group showed a severe ipsilateral atrophy as compared to the sham group (mean index ratio 0.66±0.05 and 0.97±0.02 for ICH and sham group respectively, $p < 0.001$) (Figure 6A). Striatal atrophy was observed in both males and females without sex effect ($p<0.001$). Histological examination of ICH rats confirmed the severe atrophy of the ipsilateral striatum characterized by a loss of alveolar architecture of the tissue. Perl's staining showed the presence of numerous iron deposits in and around the ICH site (Figure 6C-E).

Brain labels extracted from Cermep atlas showed that atrophy was not restricted to the striatum (Figure 6F). Limbic system structures (hippocampus and amygdala) and cortical areas (temporal, occipital and parietal) were atrophied. In males, atrophy was observed in areas involved in the limbic system ipsilateral amygdala (mean index ratio 0.94±0.02 and 1.00±0.04 for ICH and sham group respectively), hippocampus (mean index ratio 0.96±0.03 and 1.01±0.03 for ICH and sham group respectively) and temporal lobe (mean index ratio 1.05±0.02 and 1.12±0.02 for ICH and sham group respectively), all p-value < 0.05 compared to sham animals (a trend was observed in the frontal lobe: $p=0.07$). In females, atrophy was observed in temporal (mean index ratio 1.05±0.04 and 1.13 ±0.04 for ICH and sham group respectively), occipital (mean index ratio 0.95±0.03 and 1.00±0.02 for ICH and sham group respectively) and cingulate lobes (mean index ratio 1.08±0.03 and 1.13±0.04 for ICH and sham group respectively), all p-value < 0.05 compared to shams.

<u>Figure 6</u>: Long-term cerebral atrophy and histological correlates after intracerebral haemorrhage.

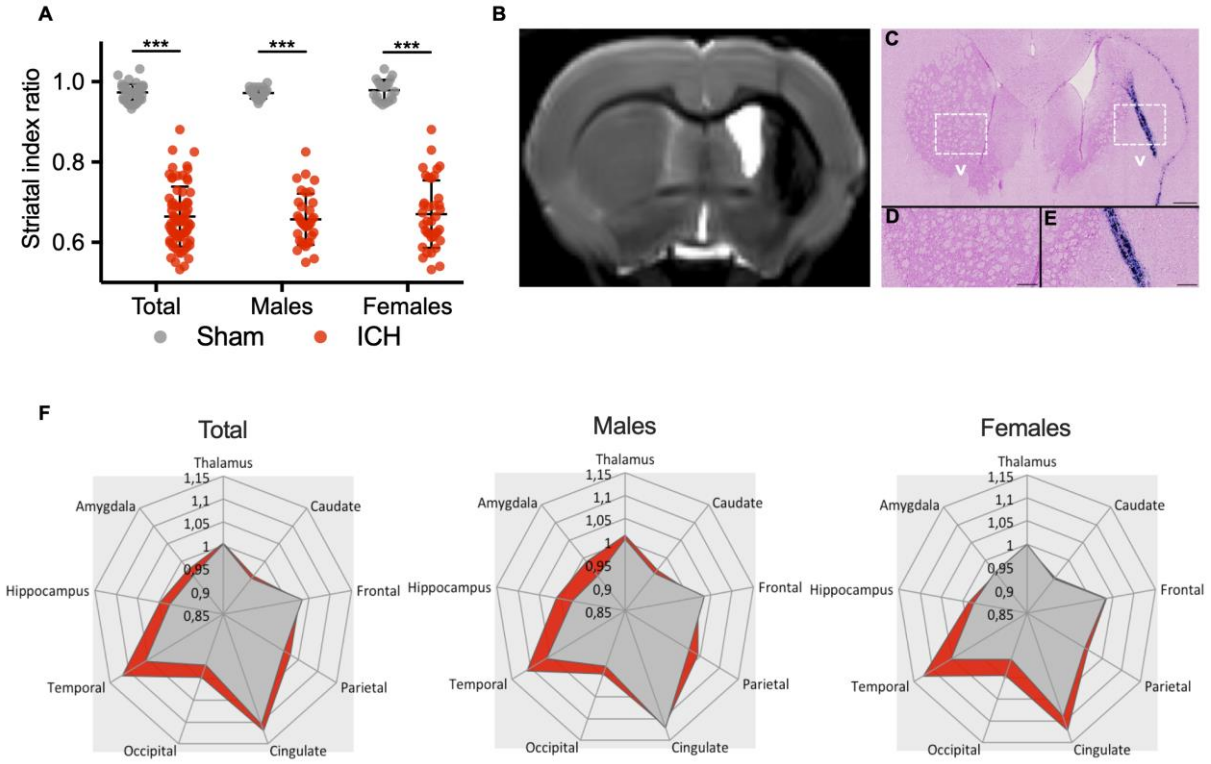

*(A) Striatal index ratio defined as the volume of the ipsilateral striatum / volume of the contralateral striatum. Grey and red symbols correspond to sham and ICH rats respectively. Black bars correspond to the mean value and the SD. The p-value came from a t-student test (***p≤0.001). (B) Representative MRI axial T2 image of the same female rat, as described in Fig.1. One can notice the ICH sequel in the right striatum with an atrophy and hydrocephalus. (C-E) Perl's staining showing iron accumulation within the ICH scar but also within the corpus callosum. One can notice the loss of the alveolar structure of the injuried striatum compared to the contralateral one. Scale bars = 500 µm for C and 100 µm for D and E. ICH = intracerebral haemorrhage. (F) Radar chart of the different brain structures from the Cermep atlas in male and female rats. For each structure, the results are expressed as the ratio of ipsilateral/contralateral. Black and red symbols and lines correspond to sham and ICH rats respectively. Red area highlights the significant differences between ICH and sham animals (all p-value < 0.05 obtained from t-student test).*

Regarding the brain metabolic assessment (Figure 7), ICH (males and females) group exhibited a severe decrease in glucose uptake at the ipsilateral striatum compared to the sham group. In the ICH group, the voxel-based analysis also showed that the hypometabolism was not restricted to striatum. Hypometabolism was also observed in adjacent deep basal ganglia (ipsilateral thalamus, hypothalamus, caudate and putamen) as well as ipsilateral parietal, frontal and temporal lobes. Furthermore, in sex subgroup analysis, male ICH rats exhibited a decrease in glucose uptake in the hippocampus whilst ICH females exhibited a hypometabolism in the ispilateral amygdala (see Figure 7 for statistical details).

<u>Figure 7</u>: Long-term cerebral hypometabolim after intracerebral haemorrhage.

A

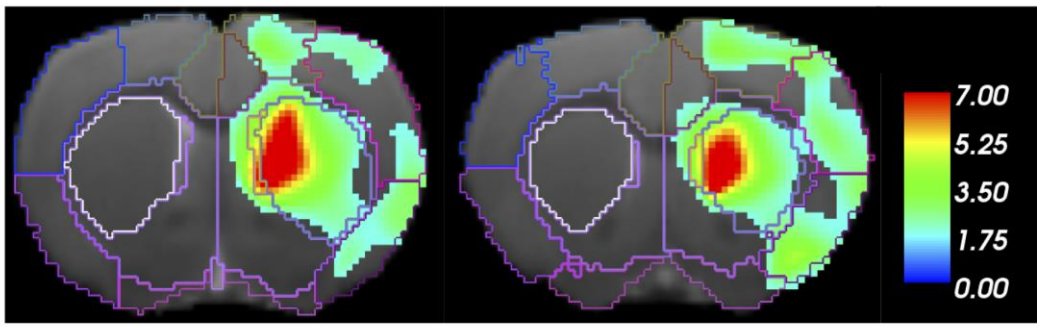

B

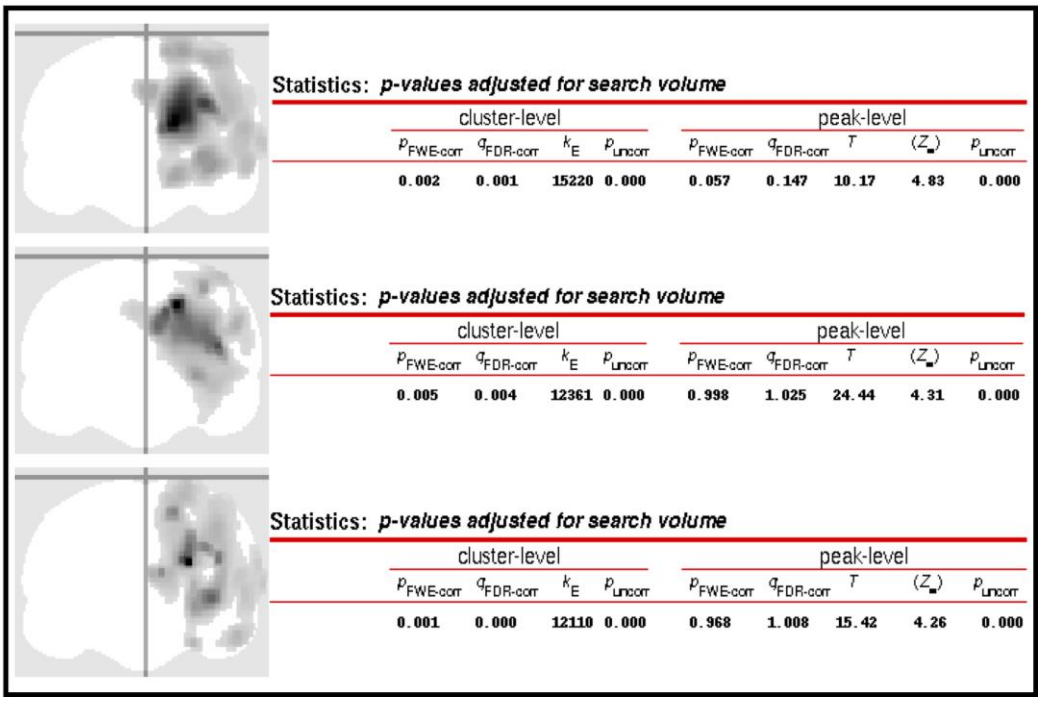

Statistics: *p-values adjusted for search volume*

cluster-level				peak-level				
$p_{FWE-corr}$	$q_{FDR-corr}$	k_E	p_{uncorr}	$p_{FWE-corr}$	$q_{FDR-corr}$	T	$(Z_=)$	p_{uncorr}
0.002	0.001	15220	0.000	0.057	0.147	10.17	4.83	0.000

Statistics: *p-values adjusted for search volume*

cluster-level				peak-level				
$p_{FWE-corr}$	$q_{FDR-corr}$	k_E	p_{uncorr}	$p_{FWE-corr}$	$q_{FDR-corr}$	T	$(Z_=)$	p_{uncorr}
0.005	0.004	12361	0.000	0.998	1.025	24.44	4.31	0.000

Statistics: *p-values adjusted for search volume*

cluster-level				peak-level				
$p_{FWE-corr}$	$q_{FDR-corr}$	k_E	p_{uncorr}	$p_{FWE-corr}$	$q_{FDR-corr}$	T	$(Z_=)$	p_{uncorr}
0.001	0.000	12110	0.000	0.968	1.008	15.42	4.26	0.000

(A) Results of 18-FDG PET voxel-based analysis, overlaid onto Cermep MRI template, comparing ICH and sham rats (males and females). Figure shows clusters (p FWE-corrected < 0.05) of higher [18F]FDG uptake in sham rats compared to ICH rats. ICH = intracerebral haemorrhage. (B) Maximum Intensity Projection (MIP) images and table of voxel-based analysis (at the top: total population, in the middle: females, at the bottom: males).

Discussion

In a large cohort of healthy male and female ICH rats, we show for the first time that: (i) ICH induces long-term cognitive impairment; (ii) a focal striatal lesion induces a long-term diffuse alteration of the brain structure/function network involving the limbic system and cortical areas, and (iii) behavioral and radiological trajectories were similar between males and females despite some sex specificities.

We report for the first time the presence of long-term CI after ICH in rats, including both hippocampal and non-hippocampal aspects of cognition. This point contrasted with both spontaneous early locomotor recovery and significant spontaneous blood resorption (≈ 40% of the initial lesion) during the short-term period (from D0 to D7). Cognitive assessment was not confounded by motor impairment, nor anxiety. In sub-group analyses, we did not observe worsening of cognition between 3 and 6 months after ICH induction. This suggests that, in our model and experimental conditions, ICH itself was responsible for CI, rather than triggering a progressive decline. We aimed to study the specific effect of ICH on cognitive functions. Therefore, we used healthy rats in the young adult stage, devoid of underlying brain parenchymal or small vessel diseases. Future works are needed to determine to what extent the inclusion of disease-relevant comorbidities and risk factors, such as hypertension and aging, can modify the cognitive trajectory after ICH.

To our knowledge, only two studies have assessed the cognitive functions after ICH in rats (Hartman et al., 2009; MacLellan et al., 2009). In the first one, cognitive tests on learning and memory, including spontaneous alternation, elevated plus maze, open-field, Morris water maze, T-maze and the radial arm maze, were cross sectionally conducted 1–7 months after ICH.(MacLellan et al., 2009) In a cohort of 12 rats, no significant learning or memory deficits were observed after ICH. In the second study, investigators found significant learning deficits in a cohort of 17 rats at 2 weeks but not at 8 weeks (Hartman et al., 2009). These results contrast with ours but some limitations hamper to draw solid conclusion, including the inclusion of males only, the small effective size (n=12 and 17 respectively), the small size of ICH lesions (18.24 ± 1.92 mm^3 and 4.02 ± 2.1 mm^3) and heterogeneity in outcome assessment methods. This highlights the need to develop comprehensive and standardized method to assess cognition in experimental stroke models (Hietamies et al., 2018). Our data from brain atrophy and metabolism measurements contribute to deepen our understanding of the mechanisms involved in ICH-related CI: we found a diffuse alteration of both brain structure and function that went beyond the blood injection site. Focal ICH in the striatum induced a loss of one third of the

structure volume, accompanied with severe hypometabolism. Histological examinations showed a loss of volume and architectural integrity of the striatum associated with an abundant sequestration of iron. One can hypothesize a direct involvement of iron neurotoxicity in CI (Salvador et al., 2010). More strikingly, we found that structural and functional consequences of ICH spread beyond the striatum following a network organization: thalamus, the limbic system (amygdala and hippocampus) and cortical areas (especially the temporal, occipital and parietal lobes). These radiological findings are consistent with our behavioral assessments (impairment of working, spatial, hippocampal and, in a lesser extent, visual memory) but also with previous literature on striatum function and its interaction with other cerebral areas (Rolls, 1994; Rektor et al., 2004; Groenewegen and Trimble, 2007; Provost et al., 2015). Taken together, our data confirm that the role of striatum is not limited to motor functions but also plays an integrative role in cognitive processes through extensive connections with key structures involved in the cognitive process.

The design of our study allowed us to study the sex effect. The recent literature on ICH and more generally experimental models reports a sex bias given the under-representation of female animals (Zucker and Beery, 2010; Sugimoto et al., 2019). Even if male and female rats share common outcome trajectories, we observed some differences. First, female rats recovered faster than male rats regarding spontaneous locomotion within the first week following ICH induction. Second, only female rats had alteration of the visual recognition memories. Third, male and female rats share distinct pattern of structural and functional alterations. Indeed, beside the striatum, atrophy and hypometabolism were mostly found in limbic system structures in males and in cortical area in females. To what extent these differences could interfere with the effect of pharmacomodulation is unknown but should be taken into account in preclinical and clinical studies.

Our findings also raise concern regarding assessment of treatments efficacy in ICH models. Indeed, most of stroke model focused on motor functions in the first month following brain injury in rodents (Hietamies et al., 2018). Given that animals showed an early spontaneous motor recovery, the assessment of a potential drug effect solely based on motor function is questionable and CI assessment should be required.

Our study has limitations. Despite a large panel of behavioral assessments, fine motor alterations (e.g. motor coordination, balance and muscle strength) may have been missed. We did not investigate some cognitive domains such as visuospatial memory, cognitive flexibility or learning. Our study has also strengths. We used a large sample size to ensure a reliable

detection of long-term cognitive deficits. The volumes of the ICHs were large enough to mimic bleeding in humans. To minimize measurement bias and subjectivity of scales, we used fully automated method to assess spontaneous locomotion and cognition. We used semi-automated method for volume segmentation and to obtain brain mask atlas. We combined structural and functional data with MRI and 18FDG-TEP to further modelise the structure-function relationship of post-ICH cognitive performance. Finally, to assess sex effect, we included both males and females, so our design was consistent with the 'Sex and Gender Equity in Research' guidelines (Heidari et al., 2016).

Conclusion

We showed that striatal ICH provokes long term cognitive impairment and distant cortical atrophy and hypometabolism in a young and disease-free rat brain. Our results emphasize the need to screen for long-term cognitive performance in ICH rodent model.

References:

Antunes M, Biala G (2012) The novel object recognition memory: neurobiology, test procedure, and its modifications. Cogn Process 13:93–110.

Coupé P, Manjón JV, Robles M, Collins DL (2012) Adaptive multiresolution non-local means filter for three-dimensional magnetic resonance image denoising. IET Image Processing 6:558–568.

Dellu F, Mayo W, Cherkaoui J, Le Moal M, Simon H (1992) A two-trial memory task with automated recording: study in young and aged rats. Brain Res 588:132–139.

Donnellan C, Werring D (2020) Cognitive impairment before and after intracerebral haemorrhage: a systematic review. Neurol Sci 41:509–527.

Groenewegen HJ, Trimble M (2007) The ventral striatum as an interface between the limbic and motor systems. CNS Spectr 12:887–892.

Hartman R, Lekic T, Rojas H, Tang J, Zhang JH (2009) Assessing functional outcomes following intracerebral hemorrhage in rats. Brain Res 1280:148–157.

Heidari S, Babor TF, De Castro P, Tort S, Curno M (2016) Sex and Gender Equity in Research: rationale for the SAGER guidelines and recommended use. Research Integrity and Peer Review 1:2.

Hidaka N, Suemaru K, Li B, Araki H (2008) Effects of repeated electroconvulsive seizures on spontaneous alternation behavior and locomotor activity in rats. Biol Pharm Bull 31:1928–1932.

Hietamies TM, Ostrowski C, Pei Z, Feng L, McCabe C, Work LM, Quinn TJ (2018) Variability of functional outcome measures used in animal models of stroke and vascular cognitive impairment - a review of contemporary studies. J Cereb Blood Flow Metab 38:1872–1884.

Lancelot S, Roche R, Slimen A, Bouillot C, Levigoureux E, Langlois J-B, Zimmer L, Costes N (2014) A multi-atlas based method for automated anatomical rat brain MRI segmentation and extraction of PET activity. PLoS One 9:e109113.

MacLellan CL, Langdon KD, Churchill KP, Granter-Button S, Corbett D (2009) Assessing cognitive function after intracerebral hemorrhage in rats. Behav Brain Res 198:321–328.

Moulin S, Labreuche J, Bombois S, Rossi C, Boulouis G, Hénon H, Duhamel A, Leys D, Cordonnier C (2016) Dementia risk after spontaneous intracerebral haemorrhage: a prospective cohort study. Lancet Neurol 15:820–829.

Pasi M, Sugita L, Xiong L, Charidimou A, Boulouis G, Pongpitakmetha T, Singh S, Kourkoulis C, Schwab K, Greenberg SM, Anderson CD, Gurol ME, Rosand J, Viswanathan A, Biffi A (2021) Association of Cerebral Small Vessel Disease and Cognitive Decline After Intracerebral Hemorrhage. Neurology 96:e182–e192.

Pellow S, Chopin P, File SE, Briley M (1985) Validation of open:closed arm entries in an elevated plus-maze as a measure of anxiety in the rat. J Neurosci Methods 14:149–167.

Poon MTC, Fonville AF, Al-Shahi Salman R (2014) Long-term prognosis after intracerebral haemorrhage: systematic review and meta-analysis. J Neurol Neurosurg Psychiatry 85:660–667.

Provost J-S, Hanganu A, Monchi O (2015) Neuroimaging studies of the striatum in cognition Part I: healthy individuals. Front Syst Neurosci 9:140.

Rektor I, Bares M, Kanovský P, Brázdil M, Klajblová I, Streitová H, Rektorová I, Sochůrková D, Kubová D, Kuba R, Daniel P (2004) Cognitive potentials in the basal ganglia-frontocortical circuits. An intracerebral recording study. Exp Brain Res 158:289–301.

Rolls ET (1994) Neurophysiology and cognitive functions of the striatum. Rev Neurol (Paris) 150:648–660.

Salvador GA, Uranga RM, Giusto NM (2010) Iron and mechanisms of neurotoxicity. Int J Alzheimers Dis 2011:720658.

Sugimoto CR, Ahn Y-Y, Smith E, Macaluso B, Larivière V (2019) Factors affecting sex-related reporting in medical research: a cross-disciplinary bibliometric analysis. Lancet 393:550–559.

Tustison NJ, Avants BB, Cook PA, Zheng Y, Egan A, Yushkevich PA, Gee JC (2010) N4ITK: improved N3 bias correction. IEEE Trans Med Imaging 29:1310–1320.

Vállez Garcia D, Casteels C, Schwarz AJ, Dierckx RAJO, Koole M, Doorduin J (2015) A standardized method for the construction of tracer specific PET and SPECT rat brain templates: validation and implementation of a toolbox. PLoS One 10:e0122363.

Zucker I, Beery AK (2010) Males still dominate animal studies. Nature 465:690.

PARTIE II

ETUDE POST-MORTEM

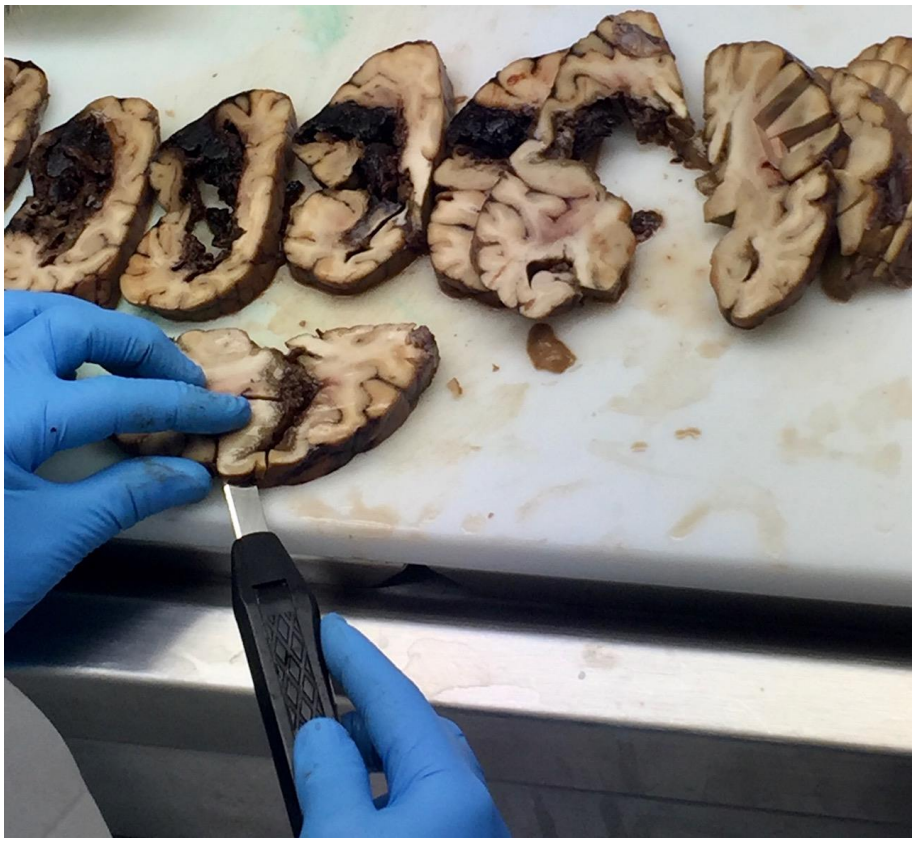

Introduction à l'étude post-mortem

En parallèle de nos travaux sur le modèle animal, nous avons mené une étude post-mortem de patients décédés d'une HIC. Ces échantillons humains sont précieux et offrent de multiples possibilités d'études. Notre constat initial était que la présence de sang libre et en excès dans le parenchyme cérébral devait être toxique pour ce dernier. C'est la raison pour laquelle des thérapies ciblées visant l'évacuation du sang sont développées. La réalité clinique est moins évidente puisque toutes les techniques chirurgicales et pharmacologiques mises au point pour évacuer le sang ne permettent pas d'améliorer le pronostic fonctionnel des patients. A ce jour, ces techniques ne permettent pas une évacuation complète du sang ou au prix de méthodes traumatisantes, mettant elles-mêmes en jeu le pronostic fonctionnel des patients.

Nos travaux de recherche *ex vivo* se sont donc centrés sur la question de la résorption du sang.

1. Un premier travail, s'intéresse à la résorption naturelle, dont l'OPH constitue une interface clef.
2. Un deuxième travail s'est concentré sur les Neutrophiles Extra cellulaires Traps (NETs) qui pourraient être impliqués dans la physiopathologie de l'HIC et des dommages tissulaires péri-hémorragiques

Travail numéro 1

Title: Brain Peri-Hematomal Area, a Strategic Interface for Blood Clearance: a Human Neuropathological and Transcriptomic Study

Authors: Laurent Puy ; Romain Perbet ; Martin Figeac ; Bélinda Duchêne ; Vincent Deramecourt ; Charlotte Cordonnier and Vincent Bérézowski.

Status: Under review

Abstract:

Background and purpose: Enhancing the blood clearance process is a promising therapeutic strategy for ICH. We aimed to investigate the natural kinetic of this process after ICH in human brain tissue with a focus on the monocyte-macrophage scavenger receptor (CD163)/hemoxygenase-1 (HO-1) pathway.

Methods: All ICH patients who came to autopsy after ICH in the Lille Neurobank were included in this post-mortem study. Paraffin-embedded tissue was extracted from four strategic areas: hematoma, peri-hematomal area (PHA), ipsilateral surrounding brain tissue and a control contralateral area. Iba1, CD163 and HO-1 were immunolabelled with an automatised method. RNA extraction was proceeded from the PHA of six representative cases to perform transcriptomic analysis using Nanostring technology.

Results: We included 19 ICH cases (median age: 79 [71-89] years; median delay ICH-death: 13 [5-41] days). The PHA concentrated most of reactive microglia, CD163/HO-1 activities and iron deposits. We found a surge in the blood clearance process from day 7 to day 15 after ICH onset. Transcriptomic analysis showed that HO-1 was the most differentially up-regulated gene (2.81 ± 0.39, adjusted p-value = $1.11x10^{-10}$) and CD163 the sixth (1.49 ± 0.29, adjusted p-value = $1.68x10^{-5}$). We also identified several up-regulated genes that exert a beneficial role aiming at terminating inflammation and enhancing tissue repair.

Conclusion: We provide histological and genomic-based evidence in humans for the predominant expression of CD163/HO-1 pathway in the PHA, with a strategic time-window: from day 7 to day 15 after ICH. An anti-inflammatory environment seems to be suitable to enhance the natural blood clearance process. Our findings contribute to identify innovative therapeutic strategies for ICH.

Key words: ICH ; peri-hematomal area ; CD163 ; hemoxygenase-1 ; post-mortem ; transcriptomic analysis

Introduction

Spontaneous intracerebral hemorrhage (ICH) is a devastating cause of mortality and morbidity devoid of specific treatment.[1] To develop efficient therapeutic strategies for ICH, a deep understanding of its pathophysiology is warranted. The pathological process of ICH includes the primary brain damage resulting from immediate mass effect owing to hematoma formation, and the delayed secondary brain injury occurring in the peri-hematomal area (PHA). In the ensuing days after ICH, the lysis of erythrocytes leads to the release of free hemoglobin (Hb), a major component of these secondary damages.[2] Therefore, the expected benefit of blood evacuation is potentially high. Two therapeutic options to achieve this goal are currently under investigation: a mechanical strategy with minimally invasive surgery,[3] and a pharmacological one, aiming at enhancing the natural clearance of blood.[4,5] The second is of particular interest, but requires a better understanding of the blood clearance process that spontaneously occur in the brain of ICH patients.

One of the primary natural mechanisms protecting the tissue against the deleterious effects of free Hb is ruled by CD163, a monocyte-macrophage scavenger receptor expressed by many cells harboring a phagocytic function such as activated microglia or recruited macrophages.[6] CD163 acts as an endocytic receptor for hemoglobin–haptoglobin (Hb/Hp) complexes and is therefore involved in sequestering toxic hemolysis products.[7,8] After its incorporation, Hb is broken down into Fe2+, CO, and biliverdin via catalysis of heme oxygenase-1 (HO-1),[9] which also has anti-oxydant, anti-inflammatory and anti-apoptotic properties.[10] Therefore, the CD163/HO-1 pathway represents a basic line of defense against Hb neurotoxicity by facilitating its clearance.[11] If it contribution to hematoma clearance is well-established in experimental studies,[12–14] few human data are available.[15–18]

In the current study, we investigated spatial and temporal expression of CD163/HO-1 pathway in human brain tissue from patients deceased of ICH. To do so, we performed both histological and transcriptomic analyses. The latter approach additionally brought an insight to a broader spectrum of potential mechanisms that mediate secondary injury and repair after ICH.

Methods:

Standard protocol approvals, registration, and patient consents.

Human brains were obtained from the Lille Neurobank (CRB/CIC1403 Biobank, BB-0033-00030, agreement DC-2008-642), which fulfils the criteria of the local laws and regulations on biological resources with donor consent, data protection, and ethical committee review.

Human brain sampling

We included all consecutive cases (2005-2019) from the Lille University Hospital brain bank (Lille Neurobank, France) of sICH patients who came to autopsy.[19] Post-morterm examination and brain sampling methods are reported elsewhere.[20] To assess the potential spreading of CD163 and HO-1 expressions within ICH core and surrounding tissue, paraffin-embedded tissue blocks were analysed from four distinct areas: (1) Within the hematoma, (2) within the peri-hematomal area (PHA), (3) next to the PHA within ipsilateral surrounding brain tissue (ISBT). Lastly, a fourth control contralateral area was analysed.

Staining and immunohistochemistry.

Sections of formalin-fixed paraffin embedded (FFPE) tissue were stained with hematoxylin–eosin (H&E) for a global identification and structural analysis of the tissues. To investigate hematoma clearance process, we used ionized calcium-binding adapter molecule 1 (Iba1), CD163 and hemoxygenase-1 (HO-1) immunolabellings to assess microglial activation, scavenging and hemoglobin degradation activities. As a result of hematoma clerance, we used a Perl's staining to quantify iron accumulation.

All stainings (H&E, and Perl's) and all immunolabellings (Iba1, CD163 and HO-1) were performed on serial-sections of 5µm each with an automated method (details are available in supplementary materials). Details of Immunolabellings were performed with a VENTANA BenchMark GX immunohistochemistry automated staining machine (Roche). The primary antibody was a rabbit polyclonal IgG (Ventana-Roche kit for CD163, [1:500, Wako Chemicals USA, Richmond, VA, USA] for Iba1 and [1:400, Merck Millipore, Burlington, Massachusetts, USA] for HO-1). We used the i-View DAB detection kit® (Ventana Medicals System, Roche Group) and nucleated cells stained blue using bluing reagent solution (Ventana-Roche). For each immunolabelling, a tissue section was processed identically except that the primary

antibody was omitted as a specificity control, and revealed no signal. A brightfield slide scanner (Zeiss Axioscan Z1) digitised the whole tissue section at 20-fold magnification after staining. Immunolabelled sections were independently analysed by two experienced operators (L.P and V.B). A staining surface ratio ([stacking surface/whole section surface]) was calculated with a semi-automated method using ImageJ software in order to quantify the positively stained or labelled surface in each area (i.e., hematoma core, PHA, ISBT and control area).

Nanostring and gene identifications

Sample preparation and RNA extraction

FFPE tissue samples were collected from 6 representative patients for RNA extraction. These 6 patients died between day 6 and day 17 after ICH. Two experienced investigators (L.P and R.B) examined the specimen on H&E stained slides and annotated a 0.25cm² area of interest (AOI). The tissue of the AOI was then scraped off on serial slides. For each patient, peri-hematoma tissue and a reference contralateral tissue of the same Brodmann area were selected. RNA was prepared according to the manufacturer's instructions using the Qiagen RNeasy Micro RNA kit (Cat# 74004; Qiagen, Courtaboeuf, France). The purified RNA was eluted in RNase-free water. Quantitation was performed using the NanoDrop 2000c (Thermo Fisher Scientific, Waltham, MA). Quality of RNA was assessed with a bioanalyzer 2100 (Agilent Technologies, Santa Clara, CA).

Gene expression profiling

NanoString nCounter RNA expression profiling was performed according to the manufacturer's instructions with 261 to 526 ng RNA input to adapt to the quality of RNA and using the nCounter® Neuroinflammation Panel (NanoString, Seattle, WA) on 6 relevant cases. Output RCC file and QC was performed using nSolver Analysis Software (version 4.0; NanoString, Seattle, WA) to generate RAW counts data. Further analysis including normalization and differential expression were done with R (https://www.R-project.org) and DESeq2 package.[21] Normalisation was performed using the 13 housekeeping genes included in the commercial design. Differentially expressed gene was define by the association of an adjusted p-value (BH) $< 6x10^{-4}$ (i.e p-value $< 1x10^{-5}$) and Log 2 Fold change > 1 or < -1.

Statistical analysis

Continuous, ordinal and categorical variables were expressed as the mean ± SEM, the median [interquartile range] or the number (percentage), respectively. We first compared the expression levels of Iba1, CD163 and HO-1 between areas of interest (hematoma core, PHA, ISBT versus contralateral area as reference). We then compared expression level between different time-point. To do so, sICH cases were grouped according to the time of death: ≤72 hours (n=2), from day 4 to day 7 (n=4), from day 7 to day 15 (n=5), from day 15 to day 90 (n=4) and >90 days (n=4). We used a Kruskal-Wallis with Tukey *post hoc* tests to compare the different area of interests and timepoints. GraphPad Prism software was used to perform the statistical analysis, with the *p*-value considered as significant when <0.05.

Results

Study population

Between 2005 and 2019, 22 patients with sICH came to autopsy. Among them, three sICH were due to an underlying vascular malformation (arteriovenous malformation, n=2 and cavernous malformation, n=1). Therefore, we included 19 spontaneous ICH cases in this study (median age: 79 [71-89] years, 8 males / 11 females). Median delay between ICH onset and death was 13 days [5-41]. Median sICH volume was 82 [44-112] cm^3, respectively. Characteristics of each case are reported in Table 1.

Table 1. Characteristics of the study population.

Number	Age at ICH onset	Sex	Past history of Hypertension	ICH location	ICH etiology¶	Time from ICH to death (days)	ICH volume (cm^3)
1	84	F	0	Lobar	CAA	1	113
2	65	F	0	Lobar	CAA	2	114
3	84	F	1	Lobar	CAA	4	87
4	76	F	0	Lobar	CAA	5	82
5	89	F	0	Lobar	CAA	5	93
6	86	F	1	Lobar	CAA	6	-
7	89	F	1	Lobar	CAA	8*	53
8	76	M	1	Deep	HTN-SVD	8*	46
9	78	F	1	Lobar	CAA	10*	63
10	76	F	0	Lobar	CAA	13*	42
11	73	M	1	Lobar	CAA	14*	163
12	85	M	1	Lobar	CAA	17*	107
13	78	M	1	Lobar	CAA	27	-
14	71	F	0	Lobar	CAA	30	111
15	76	M	1	Lobar	CAA	41	78
16	82	M	0	Lobar	CAA	90	31
17	73	M	1	Lobar	CAA	135	23
18	84	F	1	Lobar	CAA	240	142
19	72	M	0	Lobar	CAA	1400	12

Legends: ¶ CAA: Neuropathologic diagnosis was confirmed, after Congo Red staining and Amyloid β40 immunolabelling, by an experienced neuropathologist (V.D).
** Cases used for Nanostring transcriptomic analysis.*
sICH: spontaneous intracerebral hemorrhage; F: female; M: male; PHA: peri-hematomal area; CAA: cerebral amyloid angiopathy; HTN- SVD: hypertensive small vessel disease

Spatial distribution of IBA1, CD163 and HO-1 expression

On visual examination of Iba1 immunolabelled sections, microglia was observed in all cases (n=19/19). Iba1 was mainly expressed within the PHA (Figure 1A), and to a lesser extent in the ipsilateral surrounding brain tissue (0.07 ± 0.007 and 0.04 ± 0.004 respectively; p< 0.0001 and p=0.028 vs. control area). Ramified (resting) microglial cells were seen in locations distant from the hematoma while amoeboid (reactive) microglia cells were observed from 24 h post-ICH at the hematoma border. The CD163 expression level was maximal within the PHA (0.12 ± 0.02, p<0.0001 vs. control area) but also significantly observed in ipsilateral surrounding brain tissue (0.05 ± 0.01, p=0.042 vs. control area) (Figure 1B). In these areas, CD163 positive cells were observed at the border of the ICH core and in perivascular spaces of small vessels within the PHA. There was a trend towards increased CD163 expression in the hematoma core (p=0.07 vs. control area). HO-1 expression was exclusively and differentially increased within the PHA (0.016 ± 0.004, p= 0.002 vs. control area) (Figure 1C). Iron deposits were mostly observed within PHA (0.014 ± 0.003, p= 0.0006 vs. control area) and, in a lesser extent, in the hematoma core (0.005 ± 0.001, p= 0.02 vs. control area) (Figure 1D).

Figure 1. Spatial distribution of Iba1, CD163 and HO-1 positive cells.

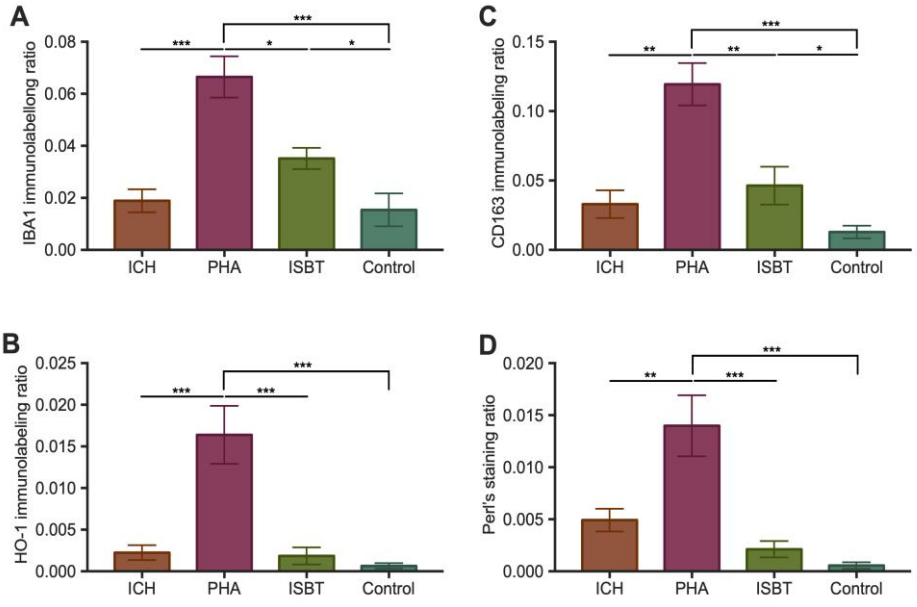

*Immunolabelling ratio ([stacking surface/whole section surface]*10^3) of Iba1 (A), CD163 (B), HO-1 (C) and iron (D) in the brain tissue of 19 patients deceased from spontaneous ICH at different strategic areas: the hematoma (ICH), the peri-hematomal area (PHA), the ipsilateral surrounding brain tissue (ISBT), and the contralateral control area. Bars and symbols correspond to the median value and the width of the 95% CI. Ratios were significantly different between time points according to Kruskal-Wallis followed by a Tukey post hoc test (***p≤0.001, **p≤ 0.01, *p≤ 0.05; ns: not significant).*

Temporal distribution of reactive microglia, CD163/HO-1 expression and iron deposition within the PHA

Iba1 positive cells were observed in the PHA in the early 72 hours (0.038 [0.030-0.056]) with both ramified and ameboid profile. The Iba1 expression increased from day 3 (0.054 [0.028-0.086]) and peaked from day 7 to 15 (0.11 [0.07-0.15], p=0.028 with T1 as reference) with an exclusively ameboid profile. From day 15, we observed a slight decrease (0.07 [0.06-0.11]). From 90 days, there was still a substantial expression of Iba1 (0.045 [0.037-0.062], p= 0.019 with control area as reference) (Figure 2A). We found CD163 positive cells in the early 72 hours (0.021 [0.014-0.028]) but the increase in the expression level was exponential from day 7 onwards (0.15 [0.13-0.21]). CD163 expression level reached a peak from day 15 to 90 (0.17 [0.14-0.24]). Beyond 90 days, the expression level of CD163 did not return to baseline levels (0.11 [0.07-0.13], p< 0.0001 with control area as reference) (Figure 2B). We did not find HO-1 positive cells before day 3, when the expression level slightly increased (0.009 [0.005-0.015]). A surge in HO-1 expression was observed from day 7 (0.023 [0.018-0.036]) while the peak of HO-1 expression was observed from 15 to 90 days (0.030 [0.020-0.048]). Beyond 90 days, the expression level of HO-1 almost returned to baseline (0.005 [0.002-0.008]) (Figure 2C). We did not observe iron deposits before day 7, when they significantly appeared and increased gradually over time with a high gap from day 15 (Figure 2D).

Figure 2. Temporal distribution of Iba1, CD163 and HO-1 positive cells within the PHA

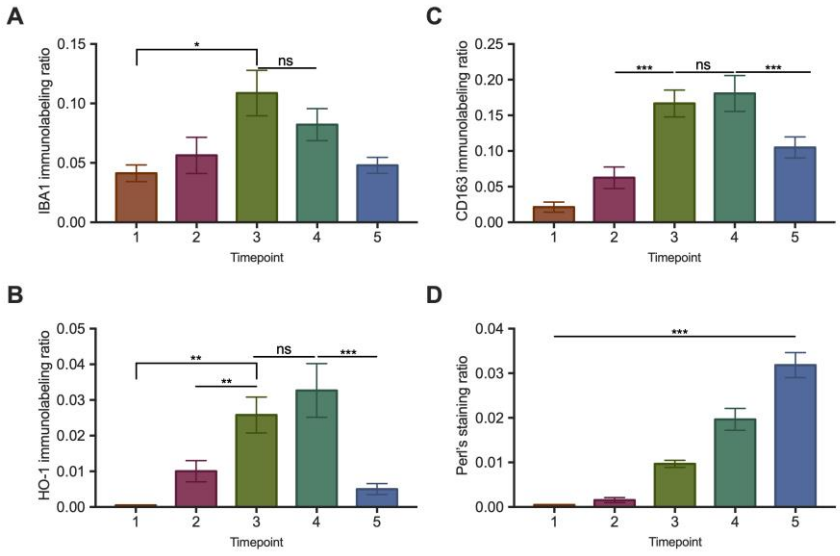

*Immunolabelling and staining ratio ([stacking surface/whole section surface]*10^3) of Iba1 (A), CD163 (B), HO-1 (C) and iron (D) in the brain tissue of 19 patients deceased from spontaneous ICH within the PHA at different time periods after onset (T1: <72 hours, T2: from day 3 to day 7, T3: from day 8 to day 15, T4: from day 16 to day 90 and T5: > day 90). Bars and symbols correspond to the median value and the width of the 95% CI. Ratios were significantly different between time points according to Kruskal-Wallis followed by a Tukey post hoc test (***p≤0.001, **p≤ 0.01, *p≤ 0.05; ns: not significant).*

On visual examinations we observed a specific spatial organization of immunolabelled cells. We reported in the Figures 3 to 7 the serial neuropathological observations for each immunolabelling and Perl's staining at the five different time-points.

Figure 3. Representative histopathological examination of PHA within 72 hours: Activation phase

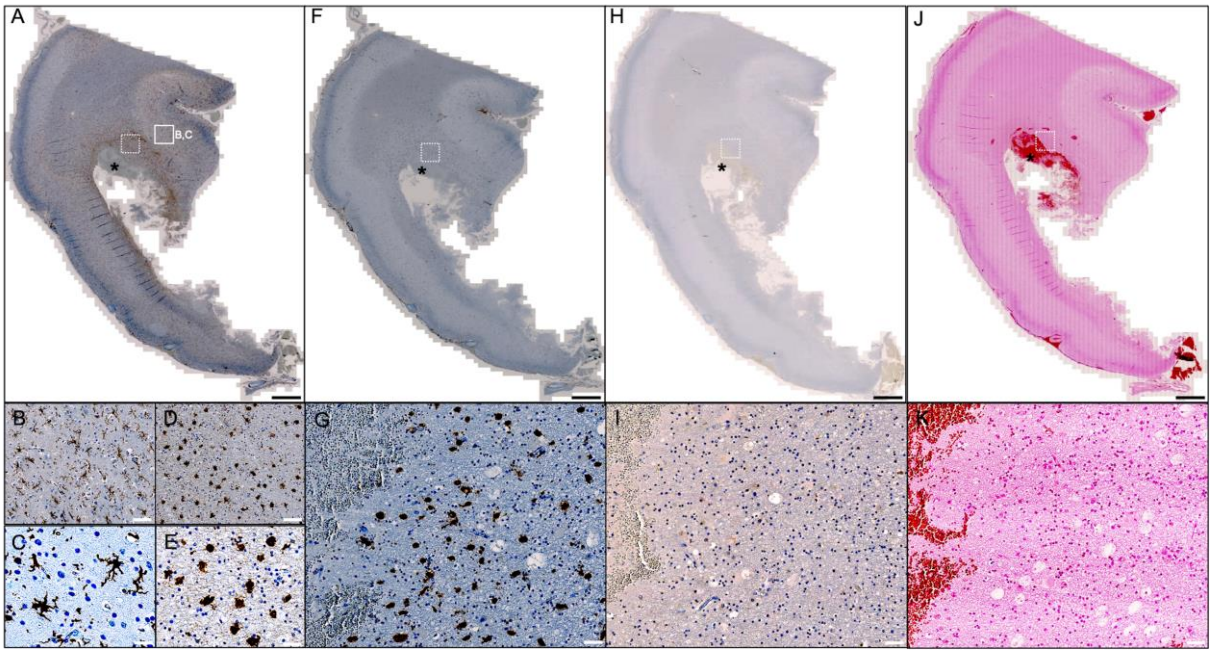

Iba1 (A, B, C, D, E), CD163 (F, G) and HO-1 (H, I) immunolabellings and Perl's staining (J, K) of adjacent slices of representative peri-hemorrhagic area observed in a patient who deceased two days after intracerebral hemorrhage. The asterisk shows the ICH site. We observed numerous ramified (B,C) and ameboid (D, E) microglia. We observed sparse CD-163 positive cells that mainly correspond to brain resident cells (microglia). We did not find any HO-1 positive cell nor iron deposit. Scale bars = 2 cm for A, F, and G; 50 µm for B, C and E; 20 µm for B, C and E.

Figure 4. Representative histopathological examination of PHA from day 3 to day 7: Encircling and induction phase.

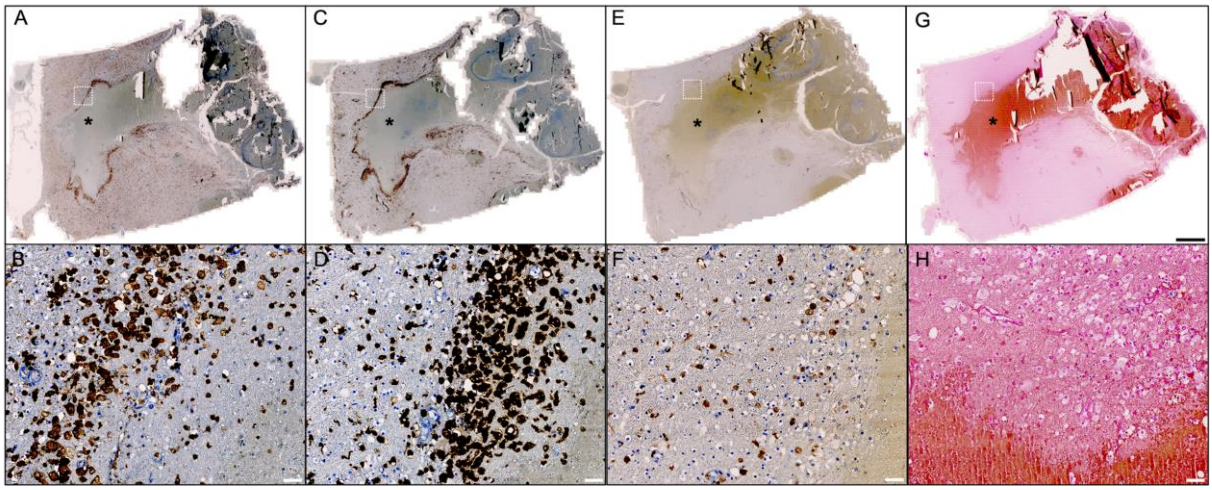

Iba1 (A, B), CD163 (C, D) and HO-1 (E, F) immunolabellings and Perl's staining (G, H) of adjacent slices of representative peri-hemorrhagic area observed in a patient who deceased five days after ICH. The asterisk shows the ICH site. We noted a specific spatial organisation of microglia and monocytes that became more abundant and encircled the ICH core. HO-1 was sparsly observed but no iron deposit was detected. Scale bars = 2 cm for A, D and G; 50 µm for B, C, E, F, H, and I.

Figure 5. Representative histopathological examination of PHA from day 7 to day 15: Amplification phase.

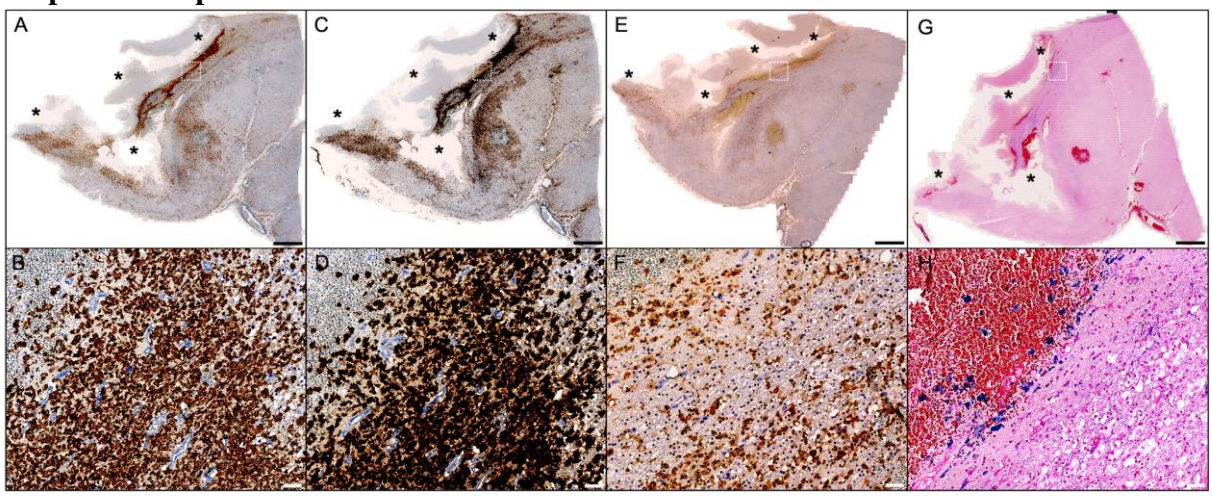

Iba1 (A, B), CD163 (C, D) and HO-1 (E, F) immunolabellings and Perl's staining (G, H) of adjacent slices of representative peri-hemorrhagic area observed in a patient who deceased 13 days after ICH. The asterisks show the ICH site. We observed an abundant amount of ameboid microglia and CD163 positive cells surrounding hematoma core. HO-1 positive cells were also more abundant and first iron desposits appeared (blue). All these substantial changes indicated a surge in the blood clearance process. Scale bars = 2 cm for A, D and G; 50 µm for B, C, E, F, H, and I.

Figure 6. Representative histopathological examination of PHA from day 15 to day 90: Continuation phase.

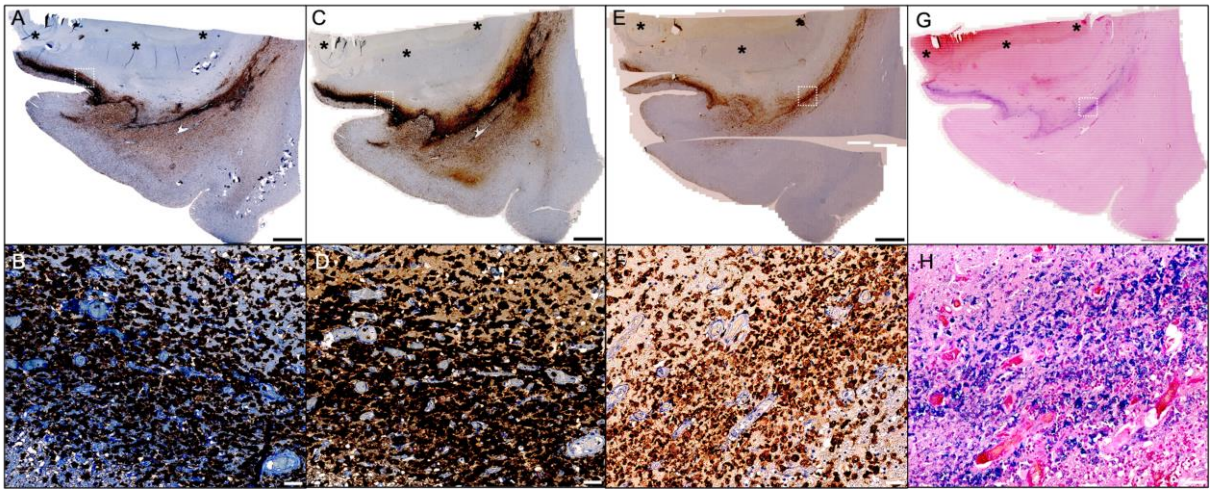

Iba1 (A, B), CD163 (C, D) and HO-1 (E, F) immunolabellings and Perl's staining (G, H) of adjacent slices of representative peri-hemorrhagic area observed in a patient who deceased 30 days after ICH. The asterisks show the ICH site. We noted an increase of microglia/monocytes cells that still encircled the lesion. HO-1 activity was also increased and fitted with iron accumulation (blue). Scale bars = 2 cm for A, D and G; 50 µm for B, C, E, F, H, and I.

Figure 7. Representative histopathological examination of PHA above 90 days: Healing phase

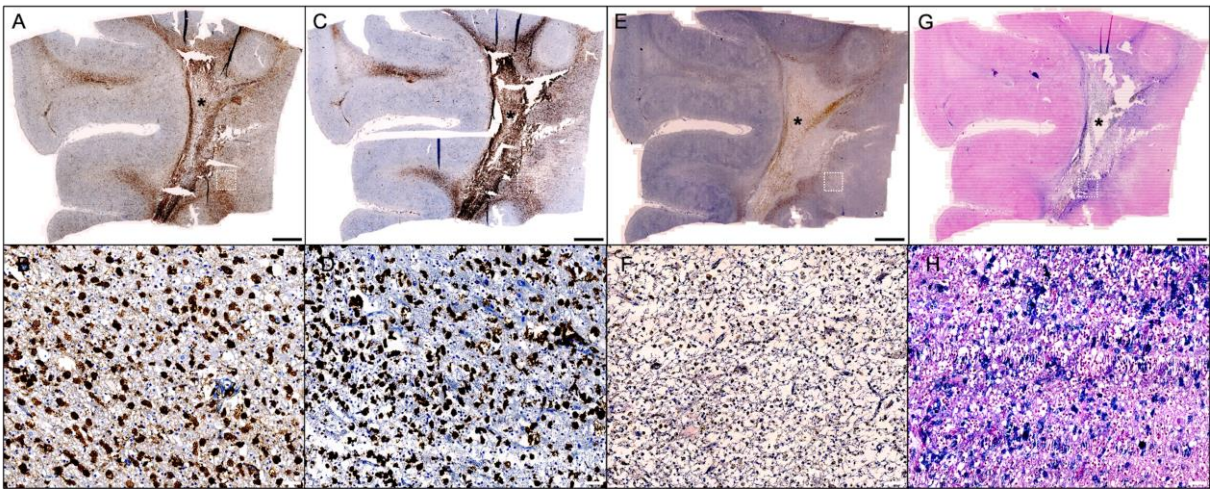

Iba1 (A, B), CD163 (C, D) and HO-1 (E, F) immunolabellings and Perl's staining (G, H) of adjacent slices of representative peri-hemorrhagic area observed in a patient who deceased eight months after ICH. This case illustrated the chronic stage of ICH. The asterisk shows the ICH site. We still observed abundant presence of active microglia and CD163 positive cells although the hematoma was not observed anymore. We observed a reduction of HO-1 activity. The iron load of iron within PHA was high. Scale bars = 2 cm for A, D and G; 50 µm for B, C, E, F, H, and I.

Gene Expression Profile of Human Perihematomal Tissue

The principal component analysis results did not show any bias towards the conditions or the technique given the clear distinction between both regions of interest PHA and control area (Figure 8A). The number of significantly and differentially expressed genes (under- and over-expressed) with FoldChange variations > 1 for p-adjusted < 6.10^{-4} was 13/770. HO-1 was the most differentially up-regulated gene (2.81 ± 0.39, adjusted p-value = $1.11x10^{-10}$). Apart from HO-1, CD163 was the sixth overexpressed gene (1.49 ± 0.29, adjusted p-value = $1.68x10^{-5}$). Among the other up-regulated genes, we found *TNFRSF1b, MMP14, PTX3, IFI30, LAIR1, SERPINE 1,* SPP1 and *SOCS3*. Three genes were differentially down-regulated: *OPALIN, SCL6A1* and *GRIN2A* (Figure 8B). The detailed statistics are provided in Table 2.

Table 2. Main results from Nanostring transcriptomic analysis

Gene	log2FoldChange	lfcSE	Adjusted p-values
Upregulated genes			
HO-1	2.811	0.385	1.11E-10
IFI30	2.494	0.453	4.81E-06
SPP1	2.126	0.454	1.81E-04
MMP14	1.758	0.315	4.73E-06
TNFRSF1B	1.682	0.230	1.11E-10
SERPINE1	1.539	0.313	6.72E-05
CD163	1.491	0.285	1.68E-05
PTX3	1.168	0.211	4.81E-06
SOCS3	1.113	0.251	5.30E-04
LAIR1	1.056	0.212	5.13E-05
Downregulated genes			
GRIN2A	-1.021	0.217	0.0002
OPALIN	-1.637	0.253	2.62E-08
SLC6A1	-1.825	0.348	1.68E-05

Legends: lfsSE, logfoldchange standard error.

A positive and negative log2FoldChange indicates an increase and a decrease gene expression.

Figure 8. Transcriptomic study of PHA

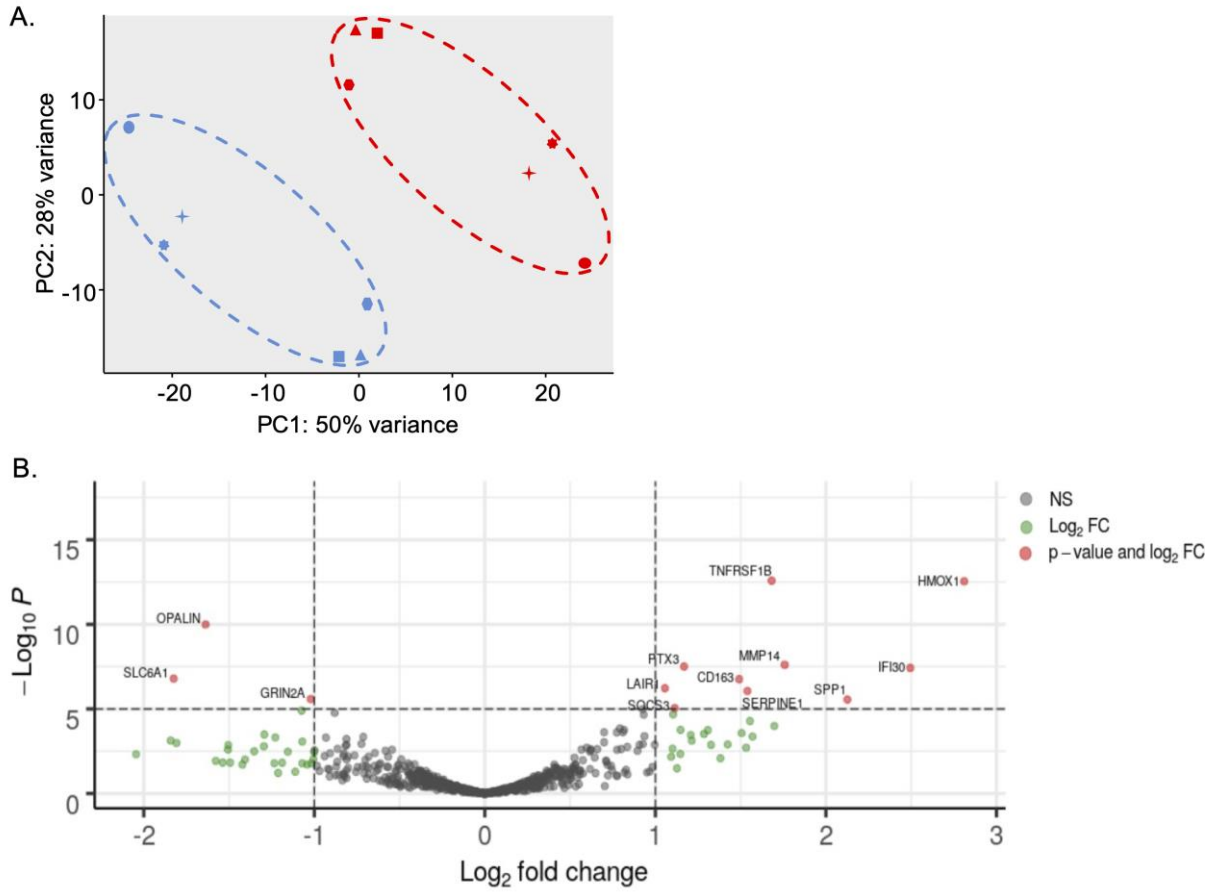

Data provide from 6 patients who deceased from day 6 to day 15 after ICH. We compared PHA to a contralateral area as a reference. (A) PCA based on Variance Stabilizing transformation of molecule counts: Each symbol corresponds to one patient. Localisation is highlighted by a color (Red = PHA, blue = control area). (B) Volcano-plot: Scatter plot of the significance of expression of all genes in perihematomal tissue versus control. Y axis is p-value at log-scale obtained with DEseq2 package. X-axis is the gene expression log Fold Change of PHA versus Control. Red dots are genes that are significantly expressed in PHA versus control area and having an absolute value of log2 Fold Change above or equal 1. Green dots are genes that are not significantly deferentially expressed in perihematomal versus control but having an absolute log2 Fold Change below 1 between both groups.

Discussion

Our study provides novel insights into the natural history of blood clearance after ICH in humans, with a predominant role of CD163/HO-1 pathway.

We first compared the stainings in different strategic areas (ICH core, PHA and ipsilateral surrounding brain tissue) and we observed that PHA concentrates most of the activated microglia, recruited monocytes and Hb-scavenging activities. This confirms that PHA is a key area for neuroinflammation and blood clearance after ICH. On visual examination, we observed amoeboid microglia within the PHA, reflecting increased phagocytic activity to clear the brain from toxic components.[22] In a more distant area (ISBT), we observed resting ramified microglia.[23] Basal CD163 expression was extremely low and restricted to perivascular macrophages in contralateral areas. This shows that microglial cells do not express CD163 under physiologic conditions, until free Hb is released in the tissue.[24] The abundant perivascular CD163 positive cells within the ISBT suggests that this area is a support for monocyte recruitment.

We then characterized the microglial and CD163/HO-1 activities over time within the PHA.

Interestingly, we observed a specific organization of phagocytic cells with distinct steps. Microglia activation (as early as the first 24 hours), encircling of the lesion (from D3), amplification with macrophage recruitment (from D7), continuation and then, resorption. The phase of encircling the lesion suggests a crosstalk between microglia and recruited monocytes to limit the spread of neurotoxic compounds arising from Hb degradation. It also appears to be a critical step in blood clearance process given that we did not find any HO-1 positive cell before this circle formation. The D7-D15 time-window was critical for blood clearance process amplification. HO-1 became therefore much more abundant and was accompagnied by progressive iron accumulation, suggesting the generation of siderophages. Of note, Iba1 and CD163 expression levels remain high several months to years after ICH suggesting a chronic proinflammatory status that might be harmful for the brain tissue.

Since we observed a strategic time-window in blood clearance process, we proceeded to RNA extraction from PHA in patients who deceased around D7 to D15. This transcriptomic analysis confirmed the predominant expression of CD163/HO-1 pathway. To our knowledge, only four studies investigated specifically CD163 and HO-1 expression after ICH in human neuropathological samples. Most of these studies were based on per-operative biopsy and focused on early phase of the disease (< 72h after ICH onset).[15–18] In our study, we also observed

CD163 and HO-1 from 24h and 72h respectively, but their expressions became much more abundant from day 7.

The evidence for CD163/HO-1 implication in ICH human tissue justifies experimental research efforts targeting this pathway. Treatments that enhance the phagocytic function of microglia/macrophages may be promising to reduce the toxicity of blood products. It's also noteworthy that soluble CD163 can be monitored in the plasma of patients to predict their clinical and radiological outcome after ICH.[25] One can hypothesize a future personal based medicine to identify which ICH patients are exposed to CD163/HO-1 overwhelming and may benefit from pharmacomodulation.

Beyond the genomic evidence for CD163/HO-1 overexpression, our transcriptomic analysis provided valuable informations on peri-hematomal tissues changes. PHA has been reported to suffer from edema, apoptosis, necrosis and inflammatory processes, enhancing the so-called "secondary tissue injuries". However, our secondary results also identified several of up-regulated genes that exert a beneficial role aiming at terminating inflammation and enhance tissue repair. *TNFRSF1b* (Tumor necrosis factor receptor superfamily member 1B, also known as *TNFR2*) might regulate inflammation by promoting the expression of anti-inflammatory genes in microglia,[26] protect neurons by preventing apoptosis through antioxidative pathways[27] and repair the ICH-damaged tissue by contributing to remyelination.[28] Other genes play an important role in macrophage and microglia polarization by repressing the M1 pro-inflammatory phenotype: The *LAIR1* gene encoding the leukocyte-associated immunoglobulin-like receptor 1 protein, *SOCS3*, a member of the suppressor of cytokine signaling family and the long pentraxin 3 **(***PTX3***)**, a member of the pentraxin superfamily of prototypic humoral pattern recognition molecules. These genes coordinate the transition from an acute inflammatory phase to a phagocytic phase promoting hematoma resolution or tissue repair.[29–31] Among these three genes, PTX3 is of particular interest. Its up-regulation is induced by thrombin supporting a role in ICH.[32] It also contributes to tissue remodeling and repair, through an interaction with fibrinogen/fibrin, collagen and plasminogen, a group of proteins present in the PHA.[33,34] The membrane-type 14 matrix metalloproteinase (*MMP-14*), expressed by microglia and recruited macrophages, can also act as a negative regulator of inflammation.[35] The *IFI30* gene encodes the gamma-interferon-inducible lysosomal thiol reductase (GILT) enzyme and plays an important role in antigen processing by enhancing the major histocompatibility complex (MHC) class II-restricted presentation.[36] The Secreted Phosphoprotein 1(*Spp1*) gene, which encodes the osteopontin (*OPN*) protein. *OPN* acts as an

immune modulator, regulating the expression of interferon-gamma and interleukin-1, and promotes cell survival by inhibiting apoptosis.[37] These gene over-expression suggest that a transition to an anti-inflammatory phase within the PHA provides a suitable microenvironment for the acquisition of Hb-scavenger properties by microglia and macrophages. This is important information for the therapeutic strategy targeting neuroinflammation that should ensure this transition from a pro-inflammatory to an anti-inflammatory status.

In line with previous work,[38] we found an up-regulation of *SERPINE 1* that may have a deleterious effect in an ICH setting. This gene encodes a member of the serine proteinase inhibitor superfamily, the principal inhibitor of tissue plasminogen activator (*PAI-1*). In addition to its role in the regulation of fibrinolysis, PAI-1 is thought to be a pro-inflammatory mediator.[39] Since triggered by hem accumulation, SERPINE1 might precipitate hem-induced neuronal apoptosis and inflammation in an ICH setting.[40]

Three genes differentially down-regulated indicated tissular injuries. We found a decrease in expression levels of key genes in myelin assembly such as oligodendrocyte myelin paranodal and inner loop protein (*OPALIN*), a marker of mature oligodendrocytes.[41] The down-regulation of *SLC6A1* (encoding γ-aminobutyric acid (GABA) transporter 1 [GAT-1], one of the major GABA transporters in the brain) and *GRIN2A* (encoding the *N*-methyl-D-aspartate receptor (NMDAR) subunit GluN2A) suggests a disturbance in cerebral neurotransmission following ICH.[42] In addition to its role of neurotransmitter and neuronal development, GABA also modulates inflammation and has an inhibitory role in the immune system (decrease of inflammatory cytokine production).[43]

According to a recent meta-analysis, only two studies (one post-mortem and one on per-operative biopsy) used transcriptomic methods to assess gene expression within the PHA.[44] Rosell et al. reported transcriptomic analysis from 4 cases who died within four days after ICH.[38] Interestingly, CD163 expression was among the most differentially up-regulated molecules but authors did not report results on HO-1 expression. Carmichael et al. did not find any up-regulation of HO-1 and did not mention CD163.[45] However, their six samples were obtained within the first 24h after ICH while we mostly observed HO-1 positive cells from day 7.

Our study has some limitations. Our study population included elderly patients and sICH were associated with underlying cerebral amyloid angiopathy (CAA) in 18/19 cases. Therefore, age

and the type of underlying vessel disease may have contributed to our findings. However, the patient with a deep ICH showed similar histological features as lobar ICH cases at similar timepoints. Of note, except from one patient (deceased 8 months after ICH), neither significant neuroinflammation was found in the contralateral hemispheres, suggesting that the changes observed in this latter case were related to the bleeding event and not to the nature of the underlying vasculopathy. Once recruited monocytes differentiate into brain macrophages, they are nearly indistinguishable from reactive microglia and they both express CD163. Therefore, we can not differentiate the contribution of resident microglia from infiltrating macrophages.

Our study also has strengths. Despite the cross-sectional nature of a histopathological study, we obtained several samples at different important timepoints in the natural history of severe sICH. We combined neuropathological and genomic explorations to investigate blood clearance mechanisms. We used an immunohistochemistry automated staining machine and semi-automated technique to quantify immunolabelling of the sections, ensuring reproducibility of our results.

In conclusion, we provide histological and genomic-based evidence in humans for the predominant expression of CD163/HO-1 pathway in the PHA, with a strategic time-window: from day 7 to day 15 after ICH. An anti-inflammatory environment seems to be suitable to enhance the natural blood clearance process. Our findings contribute to identify innovative therapeutic strategies for ICH.

References

1. van Asch CJ, Luitse MJ, Rinkel GJ, van der Tweel I, Algra A, Klijn CJ. Incidence, case fatality, and functional outcome of intracerebral haemorrhage over time, according to age, sex, and ethnic origin: a systematic review and meta-analysis. *Lancet Neurol*. 2010;9:167–176.

2. Aronowski J, Zhao X. Molecular pathophysiology of cerebral hemorrhage: secondary brain injury. *Stroke*. 2011;42:1781–1786.

3. Hanley DF, Thompson RE, Rosenblum M, Yenokyan G, Lane K, McBee N, Mayo SW, Bistran-Hall AJ, Gandhi D, Mould WA, et al. Efficacy and safety of minimally invasive surgery with thrombolysis in intracerebral haemorrhage evacuation (MISTIE III): a randomised, controlled, open-label, blinded endpoint phase 3 trial. *Lancet*.

2019;393:1021–1032.

4. Jing C, Bian L, Wang M, Keep RF, Xi G, Hua Y. Enhancement of Hematoma Clearance With CD47 Blocking Antibody in Experimental Intracerebral Hemorrhage. *Stroke*. 2019;50:1539–1547.

5. Chen-Roetling J, Lu X, Regan RF. Targeting heme oxygenase after intracerebral hemorrhage. *Ther Targets Neurol Dis*. 2015;2.

6. Graversen JH, Moestrup SK. Drug Trafficking into Macrophages via the Endocytotic Receptor CD163. *Membranes (Basel)*. 2015;5:228–252.

7. Kristiansen M, Graversen JH, Jacobsen C, Sonne O, Hoffman HJ, Law SK, Moestrup SK. Identification of the haemoglobin scavenger receptor. *Nature*. 2001;409:198–201.

8. Schaer DJ, Buehler PW, Alayash AI, Belcher JD, Vercellotti GM. Hemolysis and free hemoglobin revisited: exploring hemoglobin and hemin scavengers as a novel class of therapeutic proteins. *Blood*. 2013;121:1276–1284.

9. Dixon SJ, Stockwell BR. The role of iron and reactive oxygen species in cell death. *Nat Chem Biol*. 2014;10:9–17.

10. Campbell NK, Fitzgerald HK, Dunne A. Regulation of inflammation by the antioxidant haem oxygenase 1. *Nat Rev Immunol*. 2021;21:411–425.

11. Thomsen JH, Etzerodt A, Svendsen P, Moestrup SK. The haptoglobin-CD163-heme oxygenase-1 pathway for hemoglobin scavenging. *Oxid Med Cell Longev*. 2013;2013:523652.

12. Leclerc JL, Lampert AS, Loyola Amador C, Schlakman B, Vasilopoulos T, Svendsen P, Moestrup SK, Doré S. The absence of the CD163 receptor has distinct temporal influences on intracerebral hemorrhage outcomes. *J Cereb Blood Flow Metab*. 2018;38:262–273.

13. Liu R, Cao S, Hua Y, Keep RF, Huang Y, Xi G. CD163 Expression in Neurons After Experimental Intracerebral Hemorrhage. *Stroke*. 2017;48:1369–1375.

14. Garton T, Keep RF, Hua Y, Xi G. CD163, a Hemoglobin/Haptoglobin Scavenger Receptor, After Intracerebral Hemorrhage: Functions in Microglia/Macrophages Versus

Neurons. *Transl Stroke Res*. 2017;8:612–616.

15. Zhang XW, Wu Y, Wang DK, Jin X, Li CH. Expression changes of inflammatory cytokines TNF-α, IL-1β and HO-1 in hematoma surrounding brain areas after intracerebral hemorrhage. *J Biol Regul Homeost Agents*. 2019;33:1359–1367.

16. Liu B, Hu B, Shao S, Wu W, Fan L, Bai G, Shang P, Wang X. CD163/Hemoglobin Oxygenase-1 Pathway Regulates Inflammation in Hematoma Surrounding Tissues after Intracerebral Hemorrhage. *J Stroke Cerebrovasc Dis*. 2015;24:2800–2809.

17. Duan S, Wang X, Wang C, Wang D, Qi J, Wang H. [Expressions of heme oxygenase-1 and apoptosis-modulating proteins in peri-hematoma cortex after intracerebral hemorrhage in human being]. *Zhonghua Yi Xue Za Zhi*. 2007;87:1904–1907.

18. Holfelder K, Schittenhelm J, Trautmann K, Haybaeck J, Meyermann R, Beschorner R. De novo expression of the hemoglobin scavenger receptor CD163 by activated microglia is not associated with hemorrhages in human brain lesions. *Histol Histopathol*. 2011;26:1007–1017.

19. Deramecourt V, Slade JY, Oakley AE, Perry RH, Ince PG, Maurage C-A, Kalaria RN. Staging and natural history of cerebrovascular pathology in dementia. *Neurology*. 2012;78:1043–1050.

20. Puy L, Corseaux D, Perbet R, Deramecourt V, Cordonnier C, Bérézowski V. Neutrophil extracellular traps (NETs) infiltrate haematoma and surrounding brain tissue after intracerebral haemorrhage: A post-mortem study. *Neuropathol Appl Neurobiol*. 2021;47:867–877.

21. Love MI, Huber W, Anders S. Moderated estimation of fold change and dispersion for RNA-seq data with DESeq2. *Genome Biol*. 2014;15:550.

22. Shtaya A, Bridges LR, Esiri MM, Lam-Wong J, Nicoll JAR, Boche D, Hainsworth AH. Rapid neuroinflammatory changes in human acute intracerebral hemorrhage. *Ann Clin Transl Neurol*. 2019;6:1465–1479.

23. Davis BM, Salinas-Navarro M, Cordeiro MF, Moons L, De Groef L. Characterizing microglia activation: a spatial statistics approach to maximize information extraction. *Sci*

Rep. 2017;7:1576.

24. Xue M, Del Bigio MR. Intracerebral injection of autologous whole blood in rats: time course of inflammation and cell death. *Neurosci Lett*. 2000;283:230–232.

25. Roy-O'Reilly M, Zhu L, Atadja L, Torres G, Aronowski J, McCullough L, Edwards NJ. Soluble CD163 in intracerebral hemorrhage: biomarker for perihematomal edema. *Ann Clin Transl Neurol*. 2017;4:793–800.

26. Veroni C, Gabriele L, Canini I, Castiello L, Coccia E, Remoli ME, Columba-Cabezas S, Aricò E, Aloisi F, Agresti C. Activation of TNF receptor 2 in microglia promotes induction of anti-inflammatory pathways. *Mol Cell Neurosci*. 2010;45:234–244.

27. Probert L. TNF and its receptors in the CNS: The essential, the desirable and the deleterious effects. *Neuroscience*. 2015;302:2–22.

28. Patel JR, Williams JL, Muccigrosso MM, Liu L, Sun T, Rubin JB, Klein RS. Astrocyte TNFR2 is required for CXCL12-mediated regulation of oligodendrocyte progenitor proliferation and differentiation within the adult CNS. *Acta Neuropathol*. 2012;124:847–860.

29. Qin H, Holdbrooks AT, Liu Y, Reynolds SL, Yanagisawa LL, Benveniste EN. SOCS3 deficiency promotes M1 macrophage polarization and inflammation. *J Immunol*. 2012;189:3439–3448.

30. Carvalheiro T, Garcia S, Pascoal Ramos MI, Giovannone B, Radstake TRDJ, Marut W, Meyaard L. Leukocyte Associated Immunoglobulin Like Receptor 1 Regulation and Function on Monocytes and Dendritic Cells During Inflammation. *Front Immunol*. 2020;11:1793.

31. Jin J, Wang Y, Ma Q, Wang N, Guo W, Jin B, Fang L, Chen L. LAIR-1 activation inhibits inflammatory macrophage phenotype in vitro. *Cell Immunol*. 2018;331:78–84.

32. López ML, Bruges G, Crespo G, Salazar V, Deglesne P-A, Schneider H, Cabrera-Fuentes H, Schmitz ML, Preissner KT. Thrombin selectively induces transcription of genes in human monocytes involved in inflammation and wound healing. *Thromb Haemost*. 2014;112:992–1001.

33. Shiraki A, Kotooka N, Komoda H, Hirase T, Oyama J-I, Node K. Pentraxin-3 regulates the inflammatory activity of macrophages. *Biochem Biophys Rep*. 2016;5:290–295.

34. Doni A, Stravalaci M, Inforzato A, Magrini E, Mantovani A, Garlanda C, Bottazzi B. The Long Pentraxin PTX3 as a Link Between Innate Immunity, Tissue Remodeling, and Cancer. *Front Immunol*. 2019;10:712.

35. Fingleton B. Matrix metalloproteinases as regulators of inflammatory processes. *Biochim Biophys Acta Mol Cell Res*. 2017;1864:2036–2042.

36. Satoh J-I, Kino Y, Yanaizu M, Ishida T, Saito Y. Microglia express gamma-interferon-inducible lysosomal thiol reductase in the brains of Alzheimer's disease and Nasu-Hakola disease. *Intractable Rare Dis Res*. 2018;7:251–257.

37. Rittling SR, Singh R. Osteopontin in Immune-mediated Diseases. *J Dent Res*. 2015;94:1638–1645.

38. Rosell A, Vilalta A, García-Berrocoso T, Fernández-Cadenas I, Domingues-Montanari S, Cuadrado E, Delgado P, Ribó M, Martínez-Sáez E, Ortega-Aznar A, et al. Brain perihematoma genomic profile following spontaneous human intracerebral hemorrhage. *PLoS One*. 2011;6:e16750.

39. Sillen M, Declerck PJ. A Narrative Review on Plasminogen Activator Inhibitor-1 and Its (Patho)Physiological Role: To Target or Not to Target? *Int J Mol Sci*. 2021;22.

40. Wang T, Lu H, Li D, Huang W. TGF-β1-Mediated Activation of SERPINE1 is Involved in Hemin-Induced Apoptotic and Inflammatory Injury in HT22 Cells. *Neuropsychiatr Dis Treat*. 2021;17:423–433.

41. Kippert A, Trajkovic K, Fitzner D, Opitz L, Simons M. Identification of Tmem10/Opalin as a novel marker for oligodendrocytes using gene expression profiling. *BMC Neurosci*. 2008;9:40.

42. Strehlow V, Heyne HO, Vlaskamp DRM, Marwick KFM, Rudolf G, de Bellescize J, Biskup S, Brilstra EH, Brouwer OF, Callenbach PMC, et al. GRIN2A-related disorders: genotype and functional consequence predict phenotype. *Brain*. 2019;142:80–92.

43. Bhat R, Axtell R, Mitra A, Miranda M, Lock C, Tsien RW, Steinman L. Inhibitory role

for GABA in autoimmune inflammation. *Proc Natl Acad Sci U S A*. 2010;107:2580–2585.

44. Loan JJ, Kirby C, Emelianova K, Dando OR, Poon MT, Pimenova L, Hardingham GE, McColl BW, Klijn CJ, Al-Shahi Salman R, et al. Secondary injury and inflammation after intracerebral haemorrhage: a systematic review and meta-analysis of molecular markers in patient brain tissue. *J Neurol Neurosurg Psychiatry*. 2021;

45. Carmichael ST, Vespa PM, Saver JL, Coppola G, Geschwind DH, Starkman S, Miller CM, Kidwell CS, Liebeskind DS, Martin NA. Genomic profiles of damage and protection in human intracerebral hemorrhage. *J Cereb Blood Flow Metab*. 2008;28:1860–1875.

Travail numéro 2

Neutrophil Extracellular Traps (NETs) Infiltrate Haematoma And Surrounding Brain Tissue after Intracerebral Haemorrhage: a Post-Mortem Study.

Running title: NETs in the human sICH brain

Authors: Laurent Puy; Delphine Corseaux; Romain Perbet; Vincent Deramecourt; Charlotte Cordonnier and Vincent Bérézowski

Status: Published in *Neuropathology and Applied Neurobiology* (IF 7.5)

Received: 25 September 2020 | Revised: 31 March 2021 | Accepted: 2 May 2021

DOI: 10.1111/nan.12733

Neuropathology and Applied Neurobiology WILEY

ORIGINAL ARTICLE

Neutrophil extracellular traps (NETs) infiltrate haematoma and surrounding brain tissue after intracerebral haemorrhage: A post-mortem study

Laurent Puy[1] | Delphine Corseaux[2] | Romain Perbet[1,3] | Vincent Deramecourt[1,3] | Charlotte Cordonnier[1] | Vincent Bérézowski[1]

[1]U1172-LilNCog-Lille Neuroscience & Cognition, Univ. Lille, Inserm, CHU Lille, Lille, France

[2]Inserm, CHU Lille, Institut Pasteur de Lille, U1011- EGID, Univ. Lille, Lille, France

[3]Institute of Pathology, Centre de Biologie Pathologie, Lille University Hospital, Lille, France

Correspondence
Charlotte Cordonnier, Univ. Lille, Inserm, CHU Lille, U1172-LilNCog-Lille Neuroscience & Cognition, F-59000 Lille, France.
Email: charlotte.cordonnier@univ-lille.fr

Funding information
This work was supported by the Fondation Recherche sur les Accidents Vasculaires Cérébraux (project FRAVC180713012), the Fondation pour la Recherche Médicale (FDM201806006375, fellowship L.P) and the Fondation I-SITE ULNE (fellowship L.P).

[Correction added on 16 June 2021, after first online publication date: The article title was previously incorrect and has been updated in this current version.]

Abstract

Aims: Because of their prothrombotic and neuroinflammatory effects, neutrophils and neutrophil extracellular traps (NETs) represent interesting therapeutic targets for spontaneous intracerebral haemorrhage (sICH). We investigated the presence, spatial and temporal distribution of NETs in a human sICH post-mortem study.

Methods: From 2005 to 2019, all sICH patients who came to autopsy within the first month after stroke were included and grouped according to the timing of death: 72 h, 4–7 days, 8–15 days and >15 days after ICH onset. Paraffin-embedded tissue was extracted from four strategic areas: haematoma, peri-haematomal area, ipsilateral surrounding brain tissue and a control contralateral area. Myeloperoxidase and histone H3 citrulline were immunolabelled to detect neutrophils and NETs respectively.

Results: Neutrophils were present in the brains of the 14 cases (4 men, median age: 78 years) and NETs were found in 7/14 cases. Both neutrophils and NETs were detected within the haematoma but also in the surrounding tissue. The appearance of neutrophils and NETs was time-dependent, following a two-wave pattern: during the first 72 h and between 8 and 15 days after ICH onset. Qualitative examination showed that neutrophils and NETs were mainly located around dense fibrin fibres within the haematoma.

Conclusions: These observations provide evidence for NETs infiltration in the brain of patients who die from sICH. NETs might interact with early haemostasis within the haematoma core, and with the surrounding neuroinflammatory response. These findings open research perspectives for NETs in the treatment of sICH injuries.

KEYWORDS
Stroke, intracerebral haemorrhage, post-mortem, neutrophils, neutrophil extracellular traps

INTRODUCTION

Spontaneous intracerebral haemorrhage (sICH) is the most feared cerebrovascular event because it is associated with a high rate of mortality and morbidity, and devoid of specific treatmen.[1] Unfortunately to date, interventions to enhance haematoma clearance using recombinant tissue-plasminogen activator (rtPA) infusion have failed, as well as promising experimental neuroprotective treatments to reduce secondary brain tissue damage.[2,3]

Following the rapid accumulation of blood within the brain parenchyma, neutrophils are the first inflammatory cells to reach the haematoma site.[4,5] In addition to the well-established neurotoxicity attributed to their prolonged activation,[4–7] extensive data from ischaemic stroke studies demonstrate a direct action of neutrophils

on clot resistance to rtPA.[7] Furthermore, neutrophils are able to cast out nuclear DNA/histone meshworks, named neutrophil extracellular traps (NETs). The so-called NETosis is a regulated process of neutrophil cell death that contributes to the host defence against various pathogens. NETs correspond to extracellular web-like structures composed of nuclear and/or mitochondrial DNA (decondensed chromatin) and granular contents. Their histopathological identification is based on positive staining for citrullinated histone 3, because histones are the most abundant protein components of NETs.

Upon induction of NETosis, oxidative stress leads to the production of hydrogen peroxide through the NADPH oxidase complex. Hydrogen peroxide is a substrate of myeloperoxidase (MPO) and induces the release of neutrophil elastase (NE) from neutrophil granules. NE subsequently migrates to the nucleus to induce histone degradation, which in turn, leads to DNA decondensation. When the nuclear membrane disintegrates, the decondensed chromatin mixes with cytosolic and granular proteins and the whole complex is then expelled from the neutrophil to form NETs.[8,9]

Data on NETs in the setting of cerebrovascular diseases mainly come from the ischaemic stroke literature: NETosis has been shown to promote resistance to rtPA in the intravascular thrombus[10] and may have an inflammatory-mediated deleterious effect on the brain parenchyma.[11]

As sICH also comprises a neuroinflammatory phase, we hypothesised that NETs might have a key role in the pathophysiology of sICH. Recent experimental data suggested that NETs impaired the efficacy of rtPA-mediated fibrinolysis of the ICH clot in rats.[12] The translation of these data into therapeutic strategies requires the presence of NETs to be demonstrated in human brain tissue after sICH, in relation to the temporal pattern of neutrophil infiltration.

We investigated the histopathologic presence of NETs and describe their spatial and temporal distribution in the core of the haematoma and surrounding brain tissue of sICH patients.

METHODS

Human brain sampling

We included all consecutive cases (2005–2019) from the Lille University Hospital brain bank (Lille Neurobank, France) of sICH patients who came to autopsy within the first month after the onset of a stroke.[13] Patients had been admitted to the Lille University Hospital. Autopsies were performed within 12–36 h after death, and hemispheres were fixed in formalin for 4 to 8 weeks. Data regarding location and dimension of the haematoma were extracted from the standardised post-mortem reports. sICH volume and volume of cerebral oedema were manually segmented using Mango© software from the in-hospital imaging database. The brain sampling comprised relatively large sections (average size 6.5 cm). To assess the potential spreading of neutrophils and NETs within ICH core and surrounding tissue, paraffin-embedded tissue blocks were analysed from four distinct areas (Figure 1): (1) within the haematoma (2–4 blocks per case), (2) within the peri-haematomal area (PHA, 2–4 blocks per case), (3) next to the PHA within ipsilateral surrounding brain tissue (ISBT) (2–3 blocks per case). ISBT was defined as the area adjacent to the PHA where the tissue exhibited normal integrity. Lastly, a fourth control area was analysed (i.e. frontal and/or occipital lobes from the contralateral hemisphere in most of the cases). All post-mortem examinations and neuropathologic diagnosis of the underlying cause of sICH were performed by an experienced neuropathologist (V.D).

Standard protocol approvals, registration and patient consents

Human brains were obtained from the Lille Neurobank (CRB/CIC1403 Biobank, BB-0033–00030, agreement DC-2008–642), which fulfils the criteria of the local laws and regulations on biological

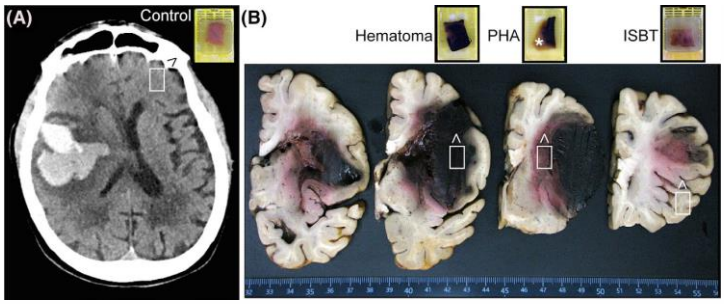

FIGURE 1 Study design. (A) CT scan of a representative patient performed 14 days after symptom onset. Hyperdense lobar intracerebral haemorrhage is shown, surrounded by hypodense peri-haematomal oedema. (B) Formalin-fixed hemispheres of spontaneous intracerebral haemorrhage (sICH) cases were cut into 5-mm-thick blocks taken from 4 specific areas: haematoma, peri-haematomal area (PHA), ipsilateral surrounding brain tissue (ISBT) and contralateral block as reference. Four adjacent 5 μm-thick sections were cut from these blocks and stained with haematoxylin & eosin, Martius Scarlet Blue, and immunolabelled for myeloperoxidase and histone H3 citrulline to detect neutrophil extracellular traps (NETs)

resources with donor consent, data protection and ethical committee review.

Staining and immunohistochemistry

Sections of formalin-fixed paraffin-embedded tissue were stained with haematoxylin–eosin (H&E) for a global identification and structural analysis of the tissues. Martius Scarlet Blue (MSB) staining was then used to identify fibrin (dark pink to red), red blood cells (orange to yellow) and collagen of the vessel wall (blue) to better characterise the areas of bleeding. The MSB staining protocol was as follows: sections were immersed in Bouin's fluid (HT-10132; Sigma-Aldrich) at 60°C for 1 h, after which the sections were washed three times in distilled water and placed in an Autostainer (Leica) for the staining procedure. Sections were immersed in 95% ethanol for 5 min. Sections were then immersed in Naphthol Yellow S (sc215544; Santa Cruz Biotechnology, Heidelberg, Germany) for 2 min followed by five washing steps of 1 min each in distilled water. Subsequently, sections were immersed in Crystal Ponceau 6R (sc214779; Santa Cruz Biotechnology) for 10 min and differentiated in 1% phosphotungstic acid (79690, Sigma-Aldrich) for 10 min to remove all non-specific Crystal Ponceau staining. Finally, sections were immersed in Methyl Blue (M5528; Sigma-Aldrich) for 5 min at room temperature, followed by a washing step in 1% acetic acid and a rapid dehydration by transferring the sections in solutions of increasing ethanol concentration, until 100% ethanol was reached. Next, sections were immersed in a xylene-derivative Sub-X and mounted using Sub-X mounting medium (3801740, Leica).

Myeloperoxidase (MPO) was immunolabelled to identify neutrophils, using a VENTANA BenchMark GX immunohistochemistry automated staining machine (Roche). The primary antibody was a rabbit polyclonal IgG (Ventana-Roche). We used the i-View DAB detection kit® (Ventana Medicals System, Roche Group) as an indirect biotin streptavidin system for the detection of the primary IgG antibody. Tissue sections were counterstained using bluing reagent solution (Ventana-Roche). The presence of NETs was assessed by a rabbit polyclonal primary antibody to histone H3 citrulline (ref ab5103, 0.3 µg/ml, and nucleated cells were stained green using a Methyl Green solution (H-3402, Vector Laboratories). For each immunostain, a tissue section was processed identically except that the primary antibody was omitted as a specificity control and revealed no signal (data not shown). MSB staining, as well as MPO and histone H3 citrulline immunolabelling were performed on serial-sections of 5 µm each. A bright-field slide scanner (Zeiss Axioscan Z1) digitised the whole tissue section at 20-fold magnification after staining. Immunolabelled sections were independently analysed by two experienced operators (L.P and V.B). A staining surface ratio ([stacking surface/whole section surface]*10^3) was calculated with a semi-automated method using ImageJ software in order to quantify the positively stained or labelled surface in each area (i.e. haematoma core, PHA and ISBT).

Statistical analysis

Continuous, ordinal and categorical variables were expressed as the mean ± SD, the median [interquartile range] or the number (percentage) respectively. A first analysis aimed at comparing areas of interest (that encompass haematoma, PHA and ISBT) and the control block from the contralateral hemisphere. To do so, bivariate comparisons were performed using Student's *t* test or Mann–Whitney U test as appropriate. To assess the temporal changes, sICH cases were grouped according to the time of death: 72 h (n = 2), 4–7 days (n = 4), 8–15 days (n = 5) and >15 days (n = 3). We used a Kruskal–Wallis with Tukey *post hoc* tests to compare the different timepoints within the areas of interest. GraphPad Prism software was used to perform the statistical analysis, with the p-value considered as significant when < 0.05.

RESULTS

Study population

Between 2005 and 2019, 22 patients with sICH came to autopsy. Among them, three sICH were due to an underlying vascular malformation (arteriovenous malformation, n = 2 and cavernous malformation, n = 1) and five patients had died more than 1 month after sICH onset. Therefore, we included 14 sICH cases in the present study (median age: 78 [76–85] years, 4 males / 10 females). Median sICH and oedema volumes were 90 [61–112] cm^3 and 74 [68–94] cm^3 respectively. Characteristics of each case are reported in Table 1.

Neutrophils: presence, spatial distribution and temporal pattern

Neutrophils were observed in all cases (n = 14/14). All ipsilateral formalin-fixed paraffin-embedded sections had increased neutrophil counts compared to control contralateral sections in which no neutrophils were observed within the tissue (p < 0.0001). Neutrophil distribution followed a centripetal gradient from the ipsilateral surrounding brain tissue to the haematoma core (0.16 [0.11–0.41] for the ipsilateral surrounding brain tissue; 14.67 [2.4–19.3] for the PHA and 41.5 [11.2–94.9] for the haematoma core, p < 0.0001). Kinetic evolution of neutrophil immunolabelling in each area of interest is reported in Figure 2. Neutrophils labelling varied over time in each area of interest (Kruskal–Wallis test: p = 0.042, 0.038 and 0.034 for haematoma, PHA and ISBT respectively), as detailed below:

Neutrophils within the haematoma

Neutrophils (Figure 2B) were observed within the haematoma as early as the first 24 h (staining surface ratio: 72.14 [62–82]). The MPO-labelled surface decreased by 80% between day 4 and day 7

TABLE 1 Characteristics of the study population

Number	Age	Sex	Past history of Hypertension	Antithrombotic use at the time of ICH onset	ICH location	sICH aetiology¶	ICH volume (cm^3)	Oedema volume (cm^3)	Time from ICH to death (days)
1	84	F	no	yes	Lobar	CAA	113	67	1
2	65	F	no	yes	Lobar	CAA	114	74	2
3	84	F	yes	no	Lobar	CAA	87	105	4
4	76	F	no	yes	Lobar	CAA	82	93	5
5	89	F	no	no	Lobar	CAA	93	102	5
6	86	F	yes	yes	Lobar	CAA	-	-	6
7	89	F	yes	no	Lobar	CAA	53	69	8
8	76	M	yes	no	Deep	HTN-SVD	46	63	8
9	78	F	yes	yes	Lobar	CAA	63	74	10
10	76	F	no	no	Lobar	CAA	42	47	13
11	73	M	yes	no	Lobar	CAA	163	68	14
12	85	M	yes	no	Lobar	CAA	107	96	17
13	78	M	yes	no	Lobar	CAA	-	-	27
14	71	F	no	no	Lobar	CAA	111	78	30

Note: CAA: Neuropathologic diagnosis was confirmed by Red Congo staining and Amyloid β40 immunolabelling by one experienced neuropathologist (V.D). The first evidence for NETs infiltration following intracerebral haemorrhage in the human brain.

Abbreviations: CAA, cerebral amyloid angiopathy; F, female; HTN- SVD, hypertensive small vessel diseaseM, male; PHA, peri-haematomal area; sICH, spontaneous intracerebral haemorrhage.

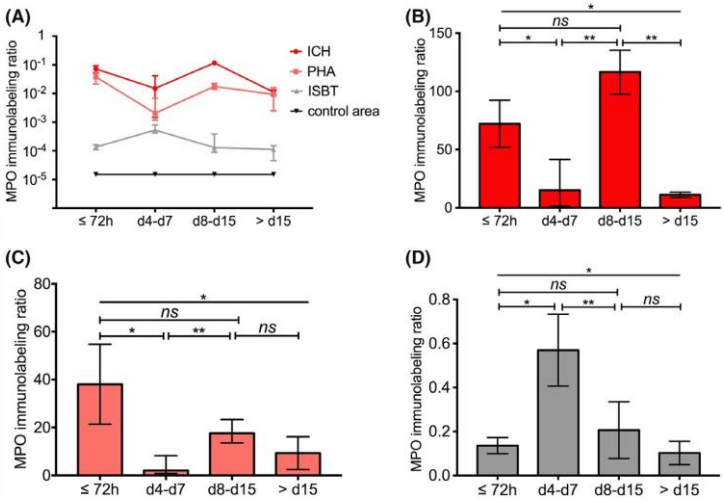

FIGURE 2 Temporal and spatial distribution of neutrophils in the human brain after intracerebral haemorrhage. (A) Immunolabelling ratio ([stacking surface/whole section surface]*10^3) of neutrophil myeloperoxidase (MPO) in the post-mortem brain tissue of 14 patients deceased from spontaneous intracerebral haemorrhage at different time periods after onset (before 72 h, from day 4 to day 7, from day 8 to day 15, above day 15). Curves refer to the ratios calculated in brain areas of interest including the haematoma (ICH), the peri-haematomal area (PHA), the ipsilateral surrounding brain tissue (ISBT), and the contralateral area (control area). Bars and symbols correspond to the median value and the width of the 95% CI. Data were log10-transformed for an easier comparison between ICH, PHA, ISBT and control areas. Raw ratios are presented in histograms for ICH (B), PHA (C) and ISBT (D) areas for statistical analysis. Ratios were significantly different between time points according to Kruskal-Wallis followed by a Tukey *post hoc* test (**$p \leq 0.01$, *$p \leq 0.05$; ns: not significant)

(15.12 [2.3–31], $p = 0.048$). In brains of patients who died between day 8 and day 15 after sICH, we observed a 7.8-fold increase in MPO expression (116.66 [107–126], $p = 0.001$). In the brains of patients who died after day 15, the MPO-labelled surface drastically decreased by 90% (11.18 [10–12], $p = 0.005$). Interestingly, qualitative examination revealed that neutrophils deposited preferentially close to dense fibrin fibres (Figure 3D,E). Spatial distribution of neutrophils within the haematoma also varied over time; within the first 72 h neutrophils were more frequently observed in the periphery (75.40% of immunolabelled surface) than in the core of the haematoma (24.6%). Between day 4 and day 7, the opposite situation was observed, 76.8% in the core *vs* 23.2% in the periphery. Between day 8 to day 15, neutrophil labelling was as frequent in the core (52.2% of immunolabelled surface) as in the periphery (47.8%) of the haematoma. In the brains of patients who died more than 15 days after sICH onset, neutrophils were mostly seen in the haematoma core (76.9%).

Neutrophils within the peri-haematomal area (PHA)

Neutrophils were observed within the PHA (Figures 2C and Figures 4D,E) as early as the first 24 h (38.06 [29–46]). The MPO-labelled surface decreased by 95% in patients who died between day 4 and day 7 (2.06 [1.7–3.7], $p = 0.029$). In those who died between day 8 and day 15, we observed an 8.8-fold increase in MPO expression (17.6 [15–20], $p = 0.002$). In patients who died more than 15 days after sICH onset, the MPO-labelled surface slightly decreased (9.3 [5.9–12.7], $p = 0.173$).

Neutrophils within ipsilateral surrounding brain tissue (ISBT)

The MPO-labelled surface within ISBT (Figures 2D and Figure 4F) was low during the first 72 h (0.14 [0.13–0.15]). The MPO-labelled surface was four times higher between day 4 and day 7 (0.53 [0.48–0.62], $p = 0.025$). After day 7, the MPO-labelled surface significantly decreased (0.13 [0.12–0.30], $p = 0.007$ between day 8 and day 15 and 0.11 [0.08–0.13] after day 15). Qualitative examination showed that neutrophils were mostly perivascular but spread to the surrounding brain tissue (Figure 4F).

Evidence for the presence of NETs within the haematoma core and PHA

NETs were found in 50% (n = 7/14) of our study population. NETs were detected in both of the two patients' brains who died within the first 72 h, in three out of four patients who died between day 4 and day 7, and in two out of five patients who died between day 8 and day 15. No NETs were observed in any of the three patients who died after day 15 ($p = 0.016$). This temporal pattern indicated that the presence of NETs was time dependent. Among the

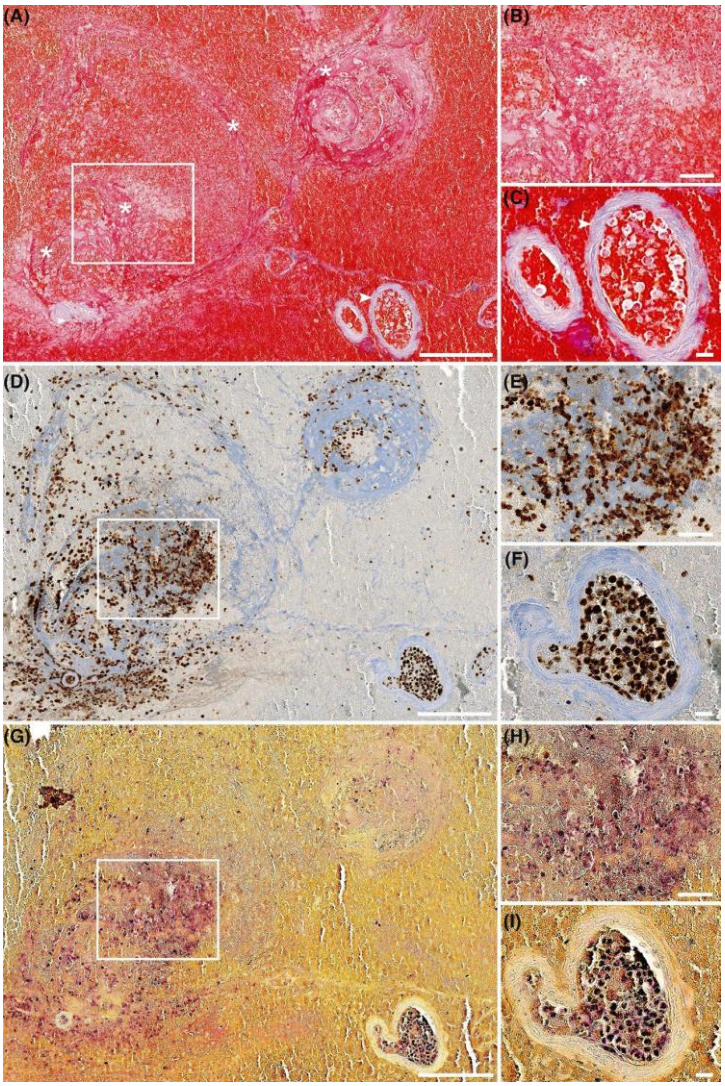

FIGURE 3 Neutrophils and neutrophil extracellular traps are located at dense fibrin fibres within intracerebral haemorrhage. Martius Scarlet Blue (MSB) staining (A, B, C), neutrophil myeloperoxidase (MPO) immunolabelling (D, E, F) and histone H3 citrulline immunolabelling (G, H, I) of adjacent slices of representative haemorrhagic areas observed in a patient who deceased after 13 days post lobar intracerebral haemorrhage (ICH). (A), (D) and (G) correspond to an overview of the examined area. (A) Fibrin fibres (pink to red) are organised into a circular pattern (asterisks), pointing to a bleeding origin at the bottom left vessel, suggestive of significant clot formation. At higher magnification (B), fibrin exhibits a dense fibrillar meshwork (asterisk), and red-stained erythrocytes show typical biconcave morphology and absence of extended haemolysis. Accumulation of non-stained cells in contact with fibrin fibres suggest the presence of leucocyte clusters. In (C), collagen (blue) delineates blood vessel walls (arrowhead) and intravascular erythrocytes and leucocytes. Abundant neutrophils in the extravasated blood are evidenced by MPO (rounded brown stain) close to light-blue fibrillar structures matching with fibrin (D), confirmed at higher magnification (E), as well as in the intravascular compartment (F). Histone H3 citrulline, corresponding to neutrophil extracellular trap (NET) formation, is disclosed both as rounded dark purple dots characteristic of intracellular staining, and as light purple smears, in areas matching with neutrophil clusters in fibrin-rich tissue sites (G), confirmed at higher magnification (H) and inside the vessel lumen (I). Scale bars = 200 μm for A, D and G; 50 μm for B, E and H, and 20 μm for C, F, I

positive cases for NETs, the H3 citrulline-labelled surface within ipsilateral blocks was significantly larger than in control areas in which we did not observe any NETs ($p < 0.0001$). NETs were commonly observed in both haematoma core and PHA (Figures 3G,H and Figures 4D,H) without significant difference between both areas ($p = 0.07$), but no NETs were observed in the ISBT (Figure 4I). The H3 citrulline-labelled surface (Figure 5A) varied with the delay after sICH onset ($p = 0.039$): NETs were observed as early as the

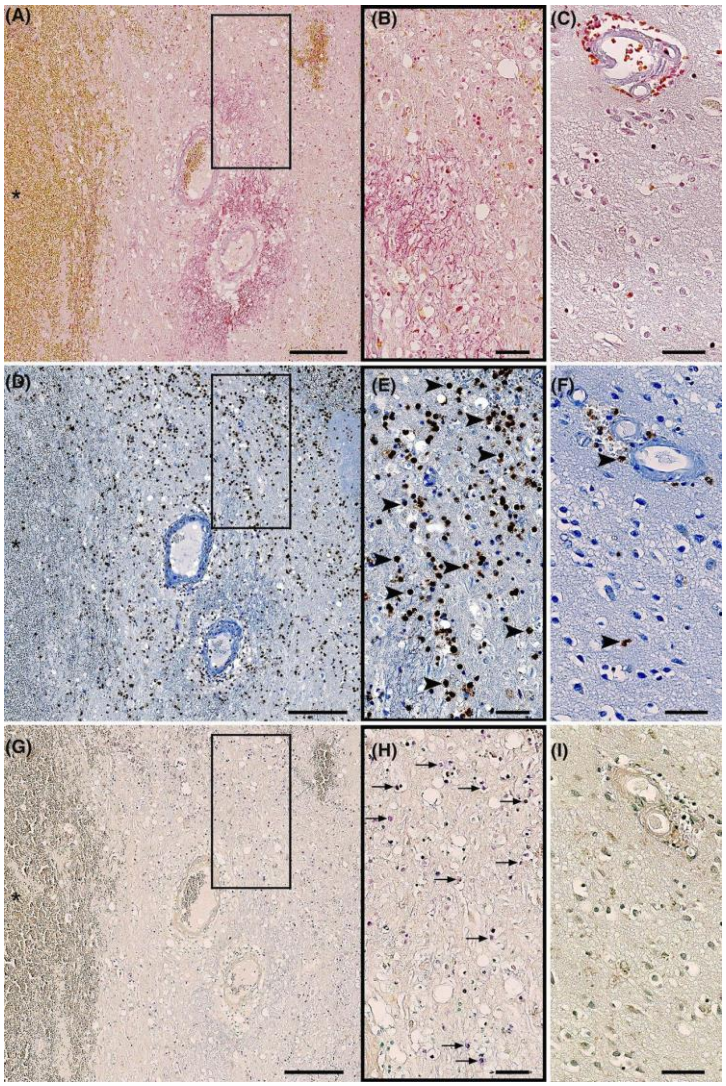

FIGURE 4 Neutrophils and neutrophil extracellular traps infiltrate the surrounding brain tissue after intracerebral haemorrhage. Martius Scarlet Blue (MSB) staining (A, B, C), neutrophil myeloperoxidase (MPO) immunolabelling (D, E, F) and histone H3 citrulline (G, H, I) immunolabelling of adjacent slices of representative peri-haematomal area (PHA) and ipsilateral surrounding brain tissue (ISBT) observed in a patient who deceased 8 days after deep intracerebral haemorrhage (ICH). (A) Blood suffusion (asterisks) at the clot border are observed through yellow-stained erythrocytes. In the PHA, tissue vacuoles and pallor suggest tissue damage and oedema, confirmed at higher magnification (B), and contrary to the ISBT area showing a homogeneous molecular layer between the soma of the more uniformly distributed brain cells (C). Abundant presence of neutrophils is evidenced in the PHA by MPO (rounded brown stain, D), confirmed at higher magnification (E, arrowheads), and contrary to the ISBT area where sparse neutrophils were found, mostly in the perivascular spaces, suggestive of recruitment from the circulation (F, arrowheads). The histone H3 citrulline of neutrophil extracellular traps (NETs) is disclosed mostly as rounded dark purple dots characteristic of intracellular signal in the PHA (G), confirmed at higher magnification (H, arrows), and contrary to the ISBT area where no NETs were found (I). Scale bars = 200 μm for A, D and G; 50 μm for B, C, E, F, H, and I

first 72 h (10.58 [9.7–11.5]). The labelled surface decreased by 74% between day 4 and day 7 (2.75 [2.3–3.4], $p = 0.017$). Between day 8 and day 15, we observed a 3-fold increase in NETs expression (8.61 [8.2–9.0], $p = 0.011$) that declined after 15 days ($p < 0.001$). Qualitative examination showed smears, purple blurred signal both in haematoma core and PHA (Figure 5B,C). Interestingly, haematoma sections showed that NETs tended to agglutinate on dense fibrin fibres (Figure 3G,H).

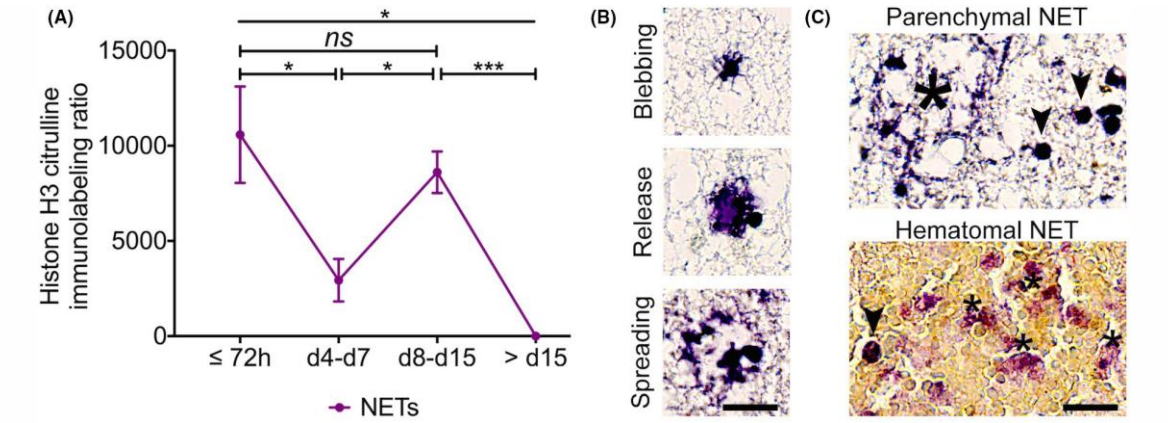

FIGURE 5 Neutrophil extracellular traps are abundant in the human brain after intracerebral haemorrhage. (A) Immunolabelling ratio ([stacking surface/whole section surface]*10^3) of citrullinated histone 3, a hallmark of neutrophil extracellular trap (NET) formation, in the post-mortem brain tissue of 14 patients who died at different time periods after intracerebral haemorrhage (before 72 h, from day 4 to day 7, from day 8 to day 15, above day 15). The curve refers to the ratios calculated in brain areas of interest where NETs were found, including the haematoma and the peri-haematomal area. Bars and symbols correspond to the median value and the width of the 95% CI. Ratios were significantly different between time points according to Kruskal-Wallis followed by a Tukey *post hoc* test (***$p \leq 0.001$, *$p \leq 0.05$; ns: not significant). (B) Representative views of different positive immunolabelling of citrullinated histone 3 (purple), suggestive of different steps of NETosis: membrane blebbing, release of decondensed chromatin to the extracellular space, and spreading of NETs in the surrounding tissue. (C) Representative views of spread NETs in the peri-haematomal area (Parenchymal NETs, large asterisk), or in the haematoma (Haematomal NETs) where multiple smears are observed (small asterisks), next to intracellular NETs (arrowheads). Scale bar = 20 μm for (B) and 50 μm for (C)

DISCUSSION

Four main results emerged from this post-mortem study dedicated to sICH in humans: (1) we have reported for the first time the presence of NETs after sICH in the human brain tissue, (2) NETs were released by two waves of neutrophils: during the first 72 h, and between 8 and 15 days after sICH onset, (3) neutrophils and NETs were abundant within the haematoma and the surrounding brain tissue, and (4) within the haematoma, both neutrophils and NETs were mostly seen around dense fibrin fibres.

We found NETs within the haematoma core and surrounding tissue both as extracellular smears, and more frequently as dense intracellular features. Smears refer to the first mechanism described in 2007 as the 'suicidal NETosis', where DNA/histone meshworks are cast out from the cell to trap pathogens or cell debris, leading to the death of the neutrophil.[14] The intracellular feature might be just the preceding step of suicidal NETosis, or the recently reported 'vital NETosis', where the neutrophil survives since the DNA/histone meshworks are exocytosed upon activation by various stimuli including activated platelets.[15]

NETs are released by neutrophils, which are widely considered to be the earliest leucocytic subtype to infiltrate the haemorrhagic brain tissue. However, our knowledge on the temporal course of neutrophil infiltration in the human brain after sICH remains limited to the hyper-acute phase. Previous data obtained from 33 sICH patients showed that neutrophils infiltrate the PHA within the first 8 h, further increase in 1 day, and disappear around 72 h after sICH onset.[16] In the PHA obtained from 30 sICH patients after craniotomy, neutrophil infiltration further increased 12–24 h after sICH.[17] More recently, Shtaya *et al.* observed infiltration of neutrophils within 2 days of the sICH in most cases and in all cases by 5 days post-ictus. Neutrophils were present up to 12 days.[18] In line with these studies, we observed a first wave of neutrophils and NETs infiltration within the first days (≤72 h), but we also observed a distinct second wave occurring between day 8 and day 15. We observed perivascular neutrophils in the ISBT preceding this second wave (i.e. between day 4 and day 7), suggesting that a recruitment of neutrophils takes place at that time in the direction of PHA and the haematoma. Therefore, we hypothesise that this second wave of recruitment occurred in response to the spread of erythrocytes and possible breakdown products into the brain parenchyma, delaying the development of tissue necrosis.

During this two-wave phenomenon, we observed neutrophils and NETs both in the haematoma core and the surrounding tissue. Within the haematoma, the presence of neutrophils and NETs specifically on dense fibrin fibres was consistent with the preclinical literature. Neutrophils are known to promote clot formation through interaction with platelets, fibrin and coagulation factors.[19–22] NETs comprise prothrombotic molecules that can trigger platelet activation and promote thrombus formation.[23] The thrombogenic potential of NETs is further supported by the experimental finding that DNase inhibits clot formation related to DNA–histone complexes.[12] In addition, the interaction between neutrophils, NETs and fibrin potentiates their respective pro-thrombotic effect [24]. Indeed, by

forming a DNA/plasmin/fibrin complex, the extracellular DNA of NETs pack the fibrin network densely and hinder plasmin-mediated degradation of fibrin clots, leading to clot resistance to fibrinolysis [25,26]. Since haematoma clearance is critical, the issue of fibrinolysis resistance is of importance for sICH management. For instance, fibrinolysis resistance could explain the neutral result of the MISTIE trial since nearly 40% of patients had insufficient blood drainage despite the focal infusion of rtPA.[2,27] Since we observed NETs in abundance within the haematoma core as early as in the first 72 h, we suggest that a pharmacomodulation of NETs activity could facilitate the fibrinolytic effect of rtPA and therefore improve the haematoma clearance. A recent experimental study in rats showed that the disintegration of NETs using DNase I could enhance fibrinolysis and promote haematoma clearance [12], opening a perspective for this treatment strategy in humans.

We observed neutrophils and NETs within the surrounding brain tissue, including the PHA and ISBT. They may contribute to the development of cerebral oedema through a deleterious pro-inflammatory process. Several experimental studies have demonstrated that neutrophils exert deleterious effects upon prolonged activation [7,28], including blood–brain barrier breakdown with ensuing neuronal injury, which can be directly exerted by NETs.[11,29–32] These data were mostly observed in ischaemic stroke [32,33]. Further experimental studies are needed to understand the influence of these NETs and neutrophils in the generation of neuroinflammation, peri-haematomal oedema growth and further necrosis after sICH. Nonetheless, we suggest that targeting neutrophils and NETs recruitment and infiltration within a delayed therapeutic window (between day 3 and day 15) might reduce secondary brain tissue damage. Several experimental treatments targeting neutrophils activation, recruitment and adhesion after ischaemic stroke have been tested but failed to prove benefit.[7] However, our results point to a difference in the role exerted by neutrophils and NETs in the perilesional area between haemorrhagic and ischaemic strokes. Indeed, in a post-mortem study of 25 ischaemic stroke patients, Enzmann *et al.* did not find any significant neutrophil infiltration in the infarcted brain area surrounding the ischaemic core, the vast majority of neutrophils remaining close to the vasculature (intraluminal or perivascular).[34] Since we found neutrophils and NETs within the surrounding brain parenchyma, this therapeutic approach could be more beneficial when applied to sICH as compared to ischaemic stroke.

Finding NETs in sICH makes sense given the presence of haem-related molecules (derived from erythrolysis) has been reported to enhance the release of NETs from neutrophils.[35,36] Recently, it has been demonstrated that haem can activate blood leukocytes and induce NET formation through an increase in intracellular reactive oxygen species (ROS).[37] Therefore, sICH is especially conducive to the formation of haem-induced NETs. Haem concentration following haemorrhage is mainly determined by the excess levels of cell-free haemoglobin release, involving the CD163/ haem oxygenase-1 (HO-1) pathway. CD163 is a monocyte-macrophage scavenger receptor expressed by activated microglia/macrophages. After incorporation of the haptoglobin/haemoglobin complex, haemoglobin is broken down into Fe^{2+} and carbon oxide, and the released haem is catalysed into biliverdin by HO-1.[38,39] Limiting NETs formation through the stimulation of HO-1 could be an interesting therapeutic strategy in ICH but the link between the CD163/HO-1 pathway, haem concentration and NETs formation has yet to be established.

Our study has some limitations. Our study population included elderly patients and sICH were associated with underlying cerebral amyloid angiopathy (CAA) in 13/14 cases. Therefore, age and underlying vessel disease may have contributed to our findings. However, patient 8 with a deep ICH showed similar histological features to lobar ICH cases, especially regarding the spatial distribution of NETs. Of note, neither neutrophil nor NETs infiltration was found in the contralateral hemispheres, suggesting that the changes observed were related to the bleeding event and not to the underlying disease. We did not perform an exhaustive examination or quantification of the entire sICH lesion. However, our assessment of neutrophil and NETs expression was performed on a substantial number of sections (n = 2–4) in strategic areas (ICH, PHA and ISBT). These representative samples provide a good overview of sICH and the surrounding brain damage.

Our study also has strengths. Despite the cross-sectional nature of a histopathological study, we obtained several samples at different important timepoints in the natural history of severe sICH. We used an immunohistochemistry automated staining machine and semi-automated technique to quantify immunolabelling of the sections, ensuring reproducibility of our results.

CONCLUSION

In conclusion, we showed two distinct phases of neutrophil and NETs infiltration in the human sICH brain and how many of these neutrophils entered the brain parenchyma surrounding the haematoma. Our findings provide new insights into the understanding of the mechanisms of sICH-related brain injury. Further efforts are needed to address the issue of whether this infiltration of neutrophils and NETs can lead to novel therapeutic strategies for individuals suffering from sICH.

ACKNOWLEDGMENTS

We warmly thank Marie-Hélène Gevaert, (Department of Histology, Lille), Belinda Duchène (Laboratory of Cancer Heterogeneity, Plasticity and Resistance to Therapies, UMR9020 - UMR-S 1277, Lille) and Eric Boulleaux (Univ. Lille, Inserm, CHU Lille, Institut Pasteur de Lille, U1011- EGID) for their great technical assistance in immunolabelling. We thank Dr Antonino Bongiovani and Dr Meryem Tardivel from the Lille Bioimaging Center for their great technical assistance. Charlotte Cordonnier is a member of the Institut Universitaire de France.

CONFLICT OF INTEREST

The authors declare no conflict of interest.

AUTHORS CONTRIBUTIONS

L.P, V.B and C.C contributed to the conception and design of the study; L.P, V.B, D.C, R.P and V.D contributed to the acquisition and analysis of the data; L.P, V.B and C.C drafted the text and prepared the figures.

ETHICAL APPROVAL

All procedures performed in the study were in accordance with the ethical standards of the Lille University Regional Ethics Committee. Human brains were obtained from the Lille Neurobank (CRB/CIC1403 Biobank, BB-0033–00030, agreement DC-2008–642), which fulfils the criteria of the local laws and regulations on biological resources with donor consent, data protection, and ethical committee review.

PEER REVIEW

The peer review history for this article is available at https://publons.com/publon/10.1111/nan.12733.

DATA AVAILABILITY STATEMENT

All data relevant to the study are included in the article or uploaded as supplementary information. Data are available upon reasonable request.

ORCID

Laurent Puy https://orcid.org/0000-0002-9772-5192
Charlotte Cordonnier https://orcid.org/0000-0002-5697-6892
Vincent Bérézowski https://orcid.org/0000-0002-8915-5513

REFERENCES

1. van Asch CJ, Luitse MJ, Rinkel GJ, van der Tweel I, Algra A, Klijn CJ. Incidence, case fatality, and functional outcome of intracerebral haemorrhage over time, according to age, sex, and ethnic origin: a systematic review and meta-analysis. *Lancet Neurol*. 2010;9:167-176.
2. Hanley DF, Thompson RE, Rosenblum M, et al. Efficacy and safety of minimally invasive surgery with thrombolysis in intracerebral haemorrhage evacuation (MISTIE III): a randomised, controlled, open-label, blinded endpoint phase 3 trial. *Lancet*. 2019;393:1021-1032.
3. Cordonnier C, Demchuk A, Ziai W, Anderson CS. Intracerebral haemorrhage: current approaches to acute management. *Lancet*. 2018;392:1257-1268.
4. Gong C, Hoff JT, Keep RF. Acute inflammatory reaction following experimental intracerebral hemorrhage in rat. *Brain Res*. 2000;871:57-65.
5. Nguyen HX, O'Barr TJ, Anderson AJ. Polymorphonuclear leukocytes promote neurotoxicity through release of matrix metalloproteinases, reactive oxygen species, and TNF-alpha. *J Neurochem*. 2007;102:900-912.
6. Jin R, Yang G, Li G. Inflammatory mechanisms in ischemic stroke: role of inflammatory cells. *J Leukoc Biol*. 2010;87:779-789.
7. Jickling GC, Liu D, Ander BP, Stamova B, Zhan X, Sharp FR. Targeting neutrophils in ischemic stroke: translational insights from experimental studies. *J Cereb Blood Flow Metab*. 2015;35:888-901.
8. Thiam HR, Wong SL, Wagner DD, Waterman CM. Cellular mechanisms of NETosis. *Annu Rev Cell Dev Biol*. 2020;36:191-218.
9. Papayannopoulos V. Neutrophil extracellular traps in immunity and disease. *Nat Rev Immunol*. 2018;18:134-147.
10. Ducroux C, Di Meglio L, Loyau S, et al. Thrombus neutrophil extracellular traps content impair tPA-induced thrombolysis in acute ischemic stroke. *Stroke*. 2018;49:754-757.
11. Manda-Handzlik A, Demkow U. The brain entangled: the contribution of neutrophil extracellular traps to the diseases of the central nervous system. *Cells*. 2019;8(12):1477.
12. Tan Q, Guo P, Zhou J, et al. Targeting neutrophil extracellular traps enhanced tPA fibrinolysis for experimental intracerebral hemorrhage. *Transl Res J Lab Clin Med*. 2019;211:139-146.
13. Deramecourt V, Slade JY, Oakley AE, et al. Staging and natural history of cerebrovascular pathology in dementia. *Neurology*. 2012;78:1043-1050.
14. Fuchs TA, Abed U, Goosmann C, et al. Novel cell death program leads to neutrophil extracellular traps. *J Cell Biol*. 2007;176:231-241.
15. Jorch SK, Kubes P. An emerging role for neutrophil extracellular traps in noninfectious disease. *Nat Med*. 2017;23:279-287.
16. Mackenzie JM, Clayton JA. Early cellular events in the penumbra of human spontaneous intracerebral hemorrhage. *J Stroke Cerebrovasc Dis*. 1999;8:1-8.
17. Guo F, Li X, Chen L, et al. Study of relationship between inflammatory response and apoptosis in perihematoma region in patients with intracerebral hemorrhage. *Zhongguo Wei Zhong Bing Ji Jiu Yi Xue*. 2006;18:290-293.
18. Shtaya A, Bridges LR, Esiri MM, et al. Rapid neuroinflammatory changes in human acute intracerebral hemorrhage. *Ann Clin Transl Neurol*. 2019;6:1465-1479.
19. Ruff CT, Giugliano RP, Braunwald E, et al. Comparison of the efficacy and safety of new oral anticoagulants with warfarin in patients with atrial fibrillation: a meta-analysis of randomised trials. *Lancet*. 2014;383:955-962.
20. Pfeiler S, Stark K, Massberg S, Engelmann B. Propagation of thrombosis by neutrophils and extracellular nucleosome networks. *Haematologica*. 2017;102:206-213.
21. Darbousset R, Thomas GM, Mezouar S, et al. Tissue factor-positive neutrophils bind to injured endothelial wall and initiate thrombus formation. *Blood*. 2012;120:2133-2143.
22. Goel MS, Diamond SL. Neutrophil enhancement of fibrin deposition under flow through platelet-dependent and -independent mechanisms. *Arterioscler Thromb Vasc Biol*. 2001;21:2093-2098.
23. Semeraro F, Ammollo CT, Morrissey JH, et al. Extracellular histones promote thrombin generation through platelet-dependent mechanisms: involvement of platelet TLR2 and TLR4. *Blood*. 2011;118:1952-1961.
24. Varju I, Kolev K. Networks that stop the flow: A fresh look at fibrin and neutrophil extracellular traps. *Thromb Res*. 2019;182:1-11.
25. Longstaff C, Varju I, Sotonyi P, et al. Mechanical stability and fibrinolytic resistance of clots containing fibrin, DNA, and histones. *J Biol Chem*. 2013;288:6946-6956.
26. Staessens S, Denorme F, Francois O, et al. Structural analysis of ischemic stroke thrombi: histological indications for therapy resistance. *Haematologica*. 2020;105:498-507.
27. Hanley DF, Lane K, McBee N, et al. Thrombolytic removal of intraventricular haemorrhage in treatment of severe stroke: results of the randomised, multicentre, multiregion, placebo-controlled CLEAR III trial. *Lancet*. 2017;389:603-611.
28. Segel GB, Halterman MW, Lichtman MA. The paradox of the neutrophil's role in tissue injury. *J Leukoc Biol*. 2011;89:359-372.
29. Kolaczkowska E, Kubes P. Neutrophil recruitment and function in health and inflammation. *Nat Rev Immunol*. 2013;13:159-175.
30. Matsuo Y, Onodera H, Shiga Y, et al. Correlation between myeloperoxidase-quantified neutrophil accumulation and ischemic brain injury in the rat. Effects of neutrophil depletion. *Stroke*. 1994;25:1469-1475.
31. Weston RM, Jones NM, Jarrott B, Callaway JK. Inflammatory cell infiltration after endothelin-1-induced cerebral ischemia:

histochemical and myeloperoxidase correlation with temporal changes in brain injury. *J Cereb Blood Flow Metab*. 2007;27:100-114.
32. Allen C, Thornton P, Denes A, et al. Neutrophil cerebrovascular transmigration triggers rapid neurotoxicity through release of proteases associated with decondensed DNA. *J Immunol*. 2012;189:381-392.
33. Perez-de-Puig I, Miro-Mur F, Ferrer-Ferrer M, et al. Neutrophil recruitment to the brain in mouse and human ischemic stroke. *Acta Neuropathol*. 2015;129:239-257.
34. Enzmann G, Mysiorek C, Gorina R, et al. The neurovascular unit as a selective barrier to polymorphonuclear granulocyte (PMN) infiltration into the brain after ischemic injury. *Acta Neuropathol*. 2013;125:395-412.
35. Kono M, Saigo K, Takagi Y, et al. Heme-related molecules induce rapid production of neutrophil extracellular traps. *Transfusion*. 2014;54:2811-2819.
36. Porto BN, Alves LS, Fernandez PLet al. Heme induces neutrophil migration and reactive oxygen species generation through signaling pathways characteristic of chemotactic receptors. *J Biol Chem*. 2007;282:24430-24436.
37. Chen G, Zhang D, Fuchs TA, Manwani D, Wagner DD, Frenette PS. Heme-induced neutrophil extracellular traps contribute to the pathogenesis of sickle cell disease. *Blood*. 2014;123:3818-3827.
38. Cao S, Zheng M, Hua Y, Chen G, Keep RF, Xi G. Hematoma changes during clot resolution after experimental intracerebral hemorrhage. *Stroke*. 2016;47:1626-1631.
39. Li Q-Q, Li L-J, Wang X-Y, Sun Y-Y, Wu J. Research progress in understanding the relationship between heme oxygenase-1 and intracerebral hemorrhage. *Front Neurol*. 2018;9:682.

How to cite this article: Puy L, Corseaux D, Perbet R, Deramecourt V, Cordonnier C, Bérézowski V. Neutrophil extracellular traps (NETs) infiltrate haematoma and surrounding brain tissue after intracerebral haemorrhage: A post-mortem study. *Neuropathol Appl Neurobiol*. 2021;00:1–11. https://doi.org/10.1111/nan.12733

DISCUSSION GENERALE

Lorsqu'un vaisseau intracérébral se rompt, l'irruption de sang et les lésions tissulaires réactionnelles menacent le pronostic vital et fonctionnel de l'Homme ou de l'animal. L'échec clinique des traitements neuroprotecteurs ou visant à évacuer le sang rend compte de la méconnaissance des mécanismes impliqués dans l'évolution des dommages péri-hémorragiques parenchymateux. Nos travaux s'ancrent dans cette problématique dont les objectifs consistaient à approfondir nos connaissances sur les cascades d'événements qui surviennent dans le parenchyme cérébral en réponse à l'hémorragie et sur ses conséquences. De façon générale, nous avions émis l'hypothèse que des mécanismes de protection naturelle existent mais sont insuffisants pour prévenir le risque vital et fonctionnel.

Dans ce contexte, nous avons dans un premier temps étudié, dans un modèle de rat sain, dépourvu de toute pathologie cérébro-vasculaire, la réaction du cerveau à une entrée massive de sang. Puis, au travers de nos travaux *ex vivo*, nous avons étudié les mécanismes générant l'inflammation et participant à la résorption de l'hémorragie. Notre démarche expérimentale, combinant des approches animales *in vivo* et humaine *ex vivo*, nous a permis de dégager certains concepts pour une meilleure compréhension mécanistique et pour le développement futur de nouvelles stratégies thérapeutiques.

1. Une avancée dans la manière de penser l'OPH

Étudier la dynamique aiguë, subaiguë et chronique des réactions tissulaires survenant autour d'une HIC est un enjeu de taille pour développer une future thérapie ciblée. Ces réactions font l'objet de deux idées reçues : (1) elles sont généralement résumées à un « œdème » et (2), elles sont considérées comme délétères. Nos travaux montrent une réalité plus complexe et participent à la redéfinition de la zone péri-hémorragique.

1.1 Un œdème, des mécanismes

Un « œdème » se définit par un gonflement d'un tissu dû à une accumulation ou un excès intra-tissulaire de liquide dans le milieu interstitiel. Dans l'HIC, ce terme œdème est employé avant tout pour des raisons techniques : les modalités d'imageries utilisées actuellement (essentiellement le scanner cérébral) ne permettent pas d'étudier les mécanismes mais

seulement les conséquences des réaction tissulaires. Cette définition ne rend ainsi pas compte de la complexité des événements survenant dans la zone péri-hémorragique dont les mouvements liquidiens n'en sont que la résultante.

Tout d'abord, nous avons montré qu'il n'existait pas un mais des œdèmes pouvant coexister ensembles avec une composante cytotoxique et vasogénique. La phase hyperaigüe (premières heures) est une phase de sidération, marquée par un phénomène d'écrasement des microvaisseaux et des cellules au contact de la masse hémorragique, responsable d'une hypoperfusion et de nécrose se traduisant par un œdème cytotoxique. Nous avons par ailleurs montré que cette hypoperfusion était transitoire, ne donnant qu'un rôle négligeable à l'ischémie dans la genèse de l'OPH. Dans un second temps (premiers jours), la phase d'activation inflammatoire se caractérise par une importante activation gliale dont le rôle est de contenir la lésion hémorragique et stimuler le recrutement de cellules inflammatoires systémiques (polynucléaires neutrophiles et macrophages) qui infiltrent massivement la zone lésionnelle. Au niveau du micro-vaisseaux, l'écrasement des parois laisse place à une dilatation, une fragilité de la BHE qui devient perméable et fuit. Il en résulte la formation d'un œdème vasogénique. Plus tardivement, nous avons observé que, contrairement à ce que l'on pouvait imaginer, les dépôts de fer siègent préférentiellement dans la zone péri-hémorragique et non pas dans le cœur de l'hémorragie. Nous avons également observé que la zone péri-hémorragique était le siège de lésions micro-vasculaires tels que les microsaignements et microinfarctus (**Figure 7**), qui pourraient contribuer à l'amplification et la diffusion des réactions inflammatoires selon la théorie de l'avalanche de Fisher (Fisher 1971). Cette hypothèse nécessitera la réalisation de travaux dédiés. Enfin, nous avons montré que cette zone péri-hémorragique était une interface indispensable à la résorption de l'hémorragie et à la réparation tissulaire.

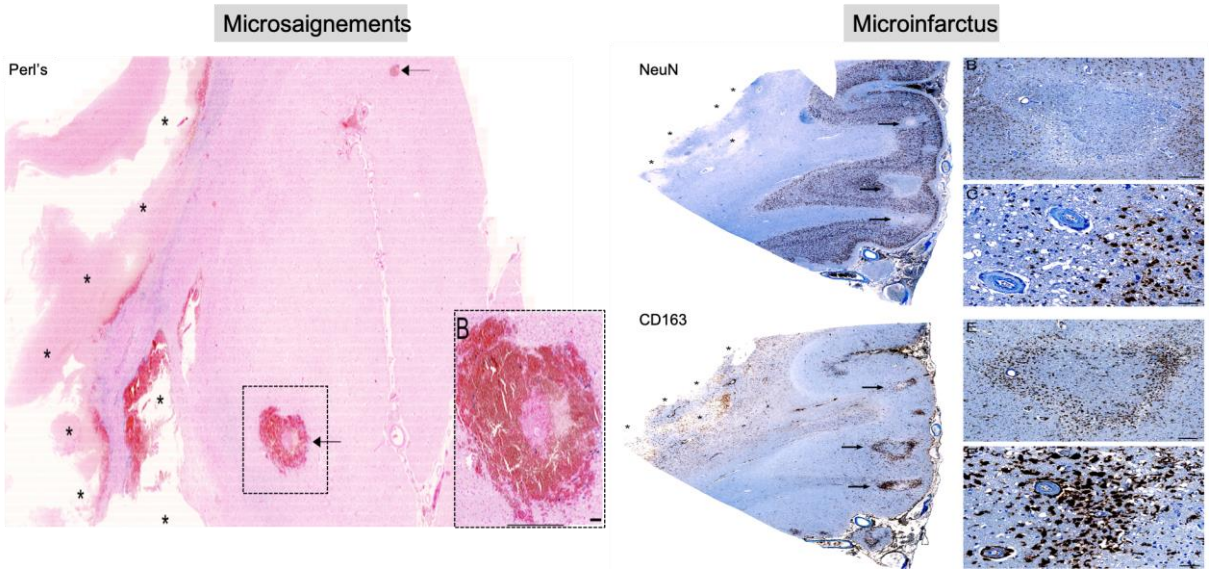

Figure 7. Microsaignements et microinfarctus aigües dans la zone péri-hémorragique observés sur du tissu cérébral humain

Les asterisques indiquent le siège de l'hémorragie. Les flèches noires indiquent la présence de microsaignements et microinfarctus.

1.2 Une manière différente d'appréhender l'inflammation

Lorsqu'une hémorragie cérébrale survient, l'agression tissulaire initiale est telle que la réponse inflammatoire proportionnelle risque de porter préjudice à l'intégrité tissulaire cérébrale. Cette agression est d'autant plus sévère qu'elle survient sur un cerveau vieillissant et exposé à une microangiopathie, deux éléments qui amplifient en intensité et en durée la réponse inflammatoire. C'est pourquoi, pour la majorité des neurologues cliniciens, l'inflammation est perçue comme un phénomène délétère (**Figure 8**). En conséquence, de nombreux travaux à visée thérapeutique ont été menés pour l'interrompre ou en limiter les effets mais les diverses molécules neuroprotectrices prometteuses chez l'animal n'ont pas montré d'efficacité chez l'Homme (Xue et Yong 2020; Mracsko et Veltkamp 2014). Nos observations suggèrent une contribution de l'inflammation plus complexe à la physiopathologie de l'HIC, moins destructrice et plus protectrice que prévue, à l'instar de ce que nombre de travaux en immunologie ont pu démontrer (**Figure 8**). Rappelons qu'en temps normal la réponse inflammatoire a une vertu protectrice. Son rôle est de permettre l'infiltration leucocytaire pour initier les mécanismes immunitaires de défense de l'organisme contre une agression microbienne, ou comme dans notre étude, une lésion. L'oedème provoqué par cette phase inflammatoire est un effet indésirable qui a vocation à rester

transitoire, le temps de la résolution de la lésion.
Au décours d'une HIC, les effets pro/anti-inflammatoires sont principalement orchestrés par les monocytes résidents (microglie) et recrutés (macrophages périphériques). De par leur plasticité phénotypique et fonctionnelle, ils jouent un rôle déterminant dans le signal déclencheur de l'inflammation, puis dans sa terminaison et enfin de la restauration de l'homéostasie tissulaire. Ces phagocytes adaptent leur phénotype au microenvironnement qui contribue à les différencier et à les activer. Une polarisation phénotypique génère principalement des macrophages de type I (M1 pro-inflammatoire) et de type 2 (M2 anti-inflammatoire). Les M1 initient la réponse inflammatoire via l'activation de différentes voies de signalisation (STAT1, NF-κB et MAP kinases), ils activent la production de cytokines pro-inflammatoires (TNF-α, l'IL1-β, et l'IL-6) et sont aussi capables de produire des molécules cytotoxiques comme les ROS (Biswas et Mantovani 2010; Gordon et Martinez 2010). Les M2 sont eux caractérisés par leur capacité à produire des médiateurs anti-inflammatoires, ils déclenchent la terminaison de l'inflammation et préparent la réparation tissulaire. L'un des principaux rôles des M2 est leur contribution à la phagocytose des leucocytes apoptotiques (PNN) après qu'ils aient phagocyté un maximum d'hématies, on parle alors d'efferocytose. Cette dernière inhibe la production de cytokines pro-inflammatoires (Boada-Romero et al. 2020).

Nous avons montré que la zone péri-hémorragique est une interface nécessaire à la résorption de l'hémorragie cérébrale et des processus de réparation tissulaire. Notre étude sur les monocytes de type M2, exprimant le CD163, démontre leurs effets bénéfiques de façon séquentielle. Dans un premier temps ils exercent un effet paracrine visant à l'enkystement de la lésion hémorragique. Ceci permet de contenir la dispersion des hématies dans le parenchyme cérébral. Puis, dans un deuxième temps, par le biais de la voie CD163/HO-1 ils permettent la phagocytose des hématies et donc, la résorption de l'hémorragie ce qui limite la toxicité de ses composants. Par ailleurs, le CD163 induit la sécrétion de cytokines anti-inflammatoires comme l'IL-10. De manière concomitante à l'expression de CD163/HO-1, nous avons identifié plusieurs gènes surexprimés qui exercent un effet anti-inflammatoire tel que *TNFRSF1b* (Tumor necrosis factor receptor superfamily member 1B), *LAIR1* (leukocyte-associated immunoglobulin-like receptor 1 protein), *SOCS3* (suppressor of cytokine signaling family-3) et *PTX3* (Long pentraxin 3). En résumé, le changement phénotypique d'une polarisation M1 vers une polarisation M2 semble être un élément clé de la terminaison inflammatoire et de la résorption de l'hémorragie, qui dépend elle-même du microenvironnement pro- ou anti-inflammatoire local.

Il convient de rappeler que tous les patients inclus dans nos études *ex vivo* sont, par définition, décédés directement ou indirectement de leur HIC. Leurs mécanismes physiologiques de réparation tissulaire ont donc été insuffisants. Et il apparait souhaitable de pouvoir les optimiser pharmacologiquement. Nos travaux suggèrent que plutôt que de limiter le déclenchement et l'intensité de la réaction inflammatoire, mieux vaut stimuler la résolution de cette inflammation en favorisant le passage polarisé d'un état pro- à anti- inflammatoire. Cette approche physiopathologique ouvre de nouvelles perspectives thérapeutiques dont, par exemple, celle de l'activation de facteurs de transcription comme le PPARγ, récepteur nucléaire clef de la différenciation M2 des macrophages (Chawla 2010; Bernardo et Minghetti 2006). Enfin, une autre piste serait d'intervenir sur le microenvironnement des macrophages favorisant cette transition. En effet, le passage d'un état pro à anti-inflammatoire est un processus très actif sous la dépendance de médiateurs lipidiques dérivés des acides gras insaturés membranaires qu'il serait intéressant d'étudier dans l'HIC (Calder et Grimble 2002).

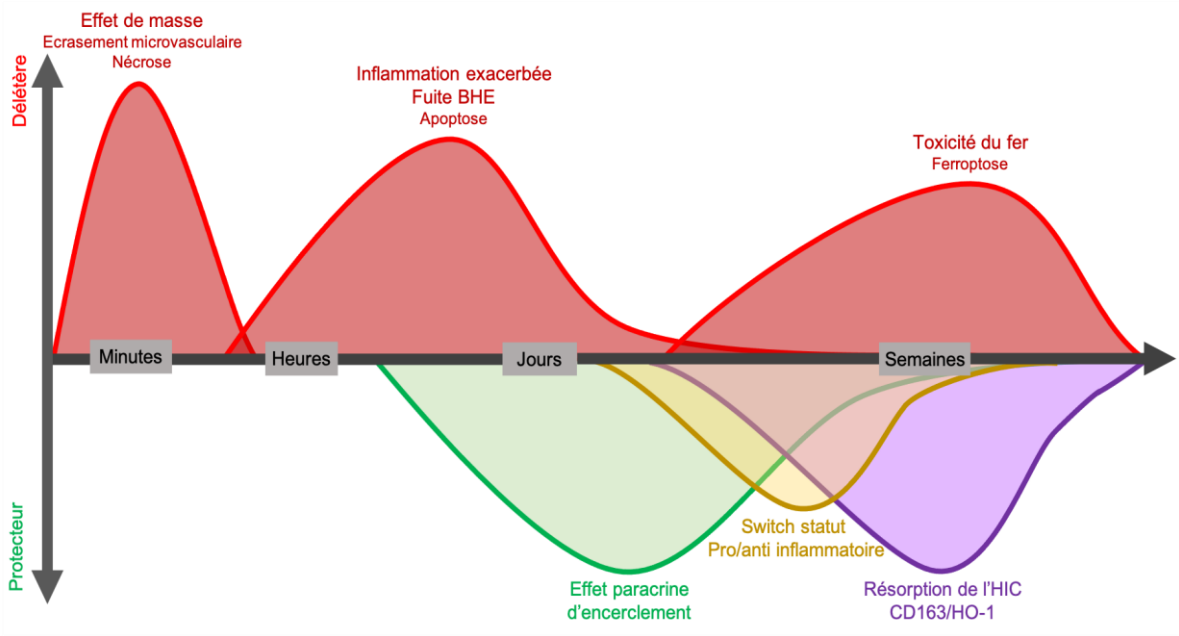

Figure 8. Hypothèses physiopathologiques des mécanismes délétères et protecteurs survenant au sein de la zone péri-hémorragique. Figure inspirée de (Dirnagl, Iadecola, et Moskowitz 1999).

2. Perspectives thérapeutiques

L'ambition première de ce travail de thèse n'était pas de tester une nouvelle thérapie ciblée de l'hémorragie cérébrale. Néanmoins notre caractérisation de l'histoire naturelle de l'HIC et de ses conséquences offre des pistes de réflexions thérapeutiques pour améliorer des stratégies déjà en cours de développement ou pour en penser de nouvelle(s).
Le sang reste le principal responsable des dommages causés dans le cerveau, soit directement par effet d'écrasement, soit indirectement en déclenchant toute une cascade d'événements inflammatoires au sein de la zone péri-hémorragique. L'évacuation du sang est donc légitimement au centre de toutes les intentions et deux options sont alors envisageables : (1) drainer chirurgicalement le sang ou (2) booster les mécanismes naturels de sa résorption.

De manière surprenante, les traitements chirurgicaux de drainage n'ont pas montré d'effet positif sur le devenir des patients. Comment expliquer cela ? Prenons pour exemple, la technique la plus prometteuse qui repose sur la combinaison d'une chirurgie de drainage mini-invasive, combinée à une injection in situ d'Alteplase (rt-PA). Il s'agit d'une technique moins invasive que la craniectomie et qui consiste à insérer un cathéter fin suivi d'une thrombolyse in situ (1 mg, à raison d'une dose toutes les 8 heures jusqu'à 9 doses) pour liquéfier l'hématome et ainsi favoriser son aspiration. Cette technique a fait l'objet d'un essai thérapeutique, MISTIE III (*Minimally Invasive Surgery Plus Alteplase for Intracerebral Hemorrhage Evacuation*) (Hanley et al. 2019). C'est un essai de phase 3, mené en ouvert au sein de 78 hôpitaux répartis en Amérique, au Canada, en Europe, en Australie et en Asie. Les patients inclus devaient être âgés de 18 ans et plus et avoir une HIC supratentorielle non-traumatique spontanée d'au moins 30 mL. Les sujets étaient randomisés dans le groupe MISTIE ou dans le groupe traitement médical standard, avec pour objectif une amélioration du pronostic fonctionnel à un an ainsi qu'une diminution du volume de l'hémorragie d'au moins 15 mL. Au total, 250 sujets assignés au groupe MISTIE et 249 au groupe traitement médical standard ont été inclus. Les analyses n'ont révélé aucune différence significative sur l'indépendance fonctionnelle des individus (critère principal d'évaluation). En effet 45% des patients du groupe MISTIE et 41% du groupe traitement médical standard ont atteint un score de Rankin modifié entre 0-3 à 365 jours, soit

une différence de risque ajustée de 4%, p=0,33. Près d'un patient sur deux (42%) présentaient une évacuation de l'hématome insatisfaisante. L'echec clinique de MISTIE III, peut donc, en partie, s'expliquer par ce drainage insuffisant. Nos travaux de recherche post-mortem ont ici une implication directe pour le clinicien et le patient. En effet, nous avons trouvé, dès les premières 24h de l'hémorragie cérébrale la présence de NETs dans le cœur de l'hémorragie, distribués préférentiellement au contact des fibres de fibrines. Les NETs sont bien connus dans l'AVC ischémique pour leur effet pro-thrombotique et leur capacité de résistance au rt-PA. A la lumière de nos observations, nous pensons qu'une optimisation du rt-PA combinée à une DNase pourrait favoriser la lyse du sang coagulé et ainsi optimiser la procédure MISTIE.

L'optimisation pharmacologique de la voie CD163/HO-1 pourrait être bénéfique en favorisant le drainage du sang intra parenchymateux mais également en exerçant un effet neuroprotecteur. L'optimisation de cette voie a déjà fait l'objet de pharmacomodulation notamment via le facteur nucléaire 2 lié aux érythroïdes (Nrf2) qui est un mécanisme intrinsèque de défense contre le stress oxydant et un anti-apoptotique (Cuadrado et al. 2019). Plusieurs études précliniques ont montré l'efficacité des activateurs de Nrf2 pour améliorer la résolution de l'hématome, ainsi que pour atténuer les dommages oxydatifs et inflammatoires du cerveau, après une HIC (Zhao et al. 2015; G. Wang et al. 2018). La stimulation de l'hème oxygénase 1 (HO-1) par Nrf2 pourrait également avoir des vertus neuroprotectrices de part ces effets anti-oxydants, anti-inflammatoires et anti-apoptotiques (Campbell, Fitzgerald, et Dunne 2021). Nos observations suggèrent que la phase subaiguë (entre J7 et J15 post-HIC) serait propice à une telle pharmacomodulation chez l'Homme.

Le fer est un métabolite indispensable au fonctionnement cérébral, présent sous forme hémique (lié à l'hémoglobine) ou non-hémique (lié à une protéine de transport comme la transferrine, lié à une protéine de stockage comme la ferritine, ou sous forme soluble). En trop grande quantité, le fer soluble devient toxique. Lors d'une hémorragie cérébrale, la lyse des érythrocytes va libérer une importante quantité de fer libre. C'est ce pool de fer libre qui, à trop haute concentration, va devenir toxique pour les cellules cérébrales (Salvador, Uranga, et Giusto 2010). En effet, l'excès de fer en présence d'oxygène est à l'origine d'une production de dérivés réactifs de l'oxygène (DRO) comme les radicaux libres par l'intermédiaire de la réaction d'oxydoréduction de Fenton. Ces DRO favorisent le stress oxydant, endommagent l'ADN mitochondrial et nucléaire et détruisent la membrane lipidique cellulaire par un mécanisme de

peroxydation. Ces éléments aboutissent à la mort cellulaire et illustrent un nouveau concept, la ferroptose, mécanisme de régulation de la mort cellulaire fer- et DRO-dépendant. (Dixon et Stockwell 2014). C'est pourquoi de nombreuses études précliniques ont retrouvé un effet prometteur de la modulation pharmacologique de l'excès de fer dans l'HIC. Cette stratégie neuroprotectrice a récemment été testée chez l'homme. L'essai i-DEF est un essai de phase 2, multicentrique, randomisé, en double aveugle, visant a étudié l'effet d'un chélateur du fer dans l'hémorragie cérébrale : la deferoxamine mesylate (Selim et al. 2019). Cette étude a inclus 294 patients. Les patients ayant reçu le chélateur du fer ne présentaient pas plus de complications sérieuses que le groupe placebo (33% vs 27%, 7% de décès dans chaque groupe). Le traitement n'a pas montré d'efficacité puisque 34% et 33% des patients de chacun des deux groupes présentaient un bon pronostic (mRS 0 à 2) à 3 mois. Les auteurs concluent que bien que Le mésylate de déféroxamine soit sûr, son efficacité clinique médiocre ne justifie pas de mener une étude de phase 3. Les résultats sont donc décevants mais nos observations permettent d'expliquer, au moins en partie, les raisons de cet échec. Si l'on regarde la méthodologie employée, les patients recevaient du mésylate de déféroxamine à raison de 32 mg/kg par jour (jusqu'à une dose maximale de 6000 mg par jour) ou un placebo (solution saline), en perfusion intraveineuse à raison de 7-5 mg/kg par heure pendant 3 jours consécutifs. La première perfusion était réalisée dans les 24 heures suivant l'HIC. Cette fenêtre thérapeutique pose question puisque nous n'avons commencé à observer la présence de fer dans le tissu cérébral humain qu'à partir de J7 avec une augmentation exponentielle au-delà de J15. De même, dans notre modèle expérimental, le fer n'était observé qu'à partir de J3 et plus significativement à J7. Nos observations suggèrent donc que la fenêtre d'administration et la durée de traitement n'étaient pas optimales et expliquent en partie l'échec de cet essai. Cet exemple illustre parfaitement l'importance de vérifier au niveau tissulaire chez l'Homme la cinétique des événements afin d'optimiser le design des interventions thérapeutiques en cours d'évaluation.

3. Comment améliorer le pipeline translationnel de l'animal à l'Homme ?

Malgré des données qui semblaient encourageantes chez l'animal, aucun traitement neuroprotecteur, c'est-à-dire visant à protéger les neurones de la mort cellulaire, n'est recommandé dans la prise en charge de l'HIC. Pourtant, les modèles animaux avaient permis des avancées majeures dans la compréhension des mécanismes physiopathologiques en neurologie-vasculaire ainsi que dans le développement de nouvelles thérapies ciblées.

L'objectif de notre travail n'était pas de pharmacomoduler une nouvelle voie moléculaire. Ce qui constitue une limite à notre travail : nous n'avons donc pas de facteur aggravant ou améliorant la réponse cérébrale à l'entrée massive de sang. Cela constitue également une force puisque nos efforts se sont concentrés sur la caractérisation à court et long terme, des réponses comportementales, radiologiques et histologiques après une HIC induite. Par ailleurs, nous tirons de notre travail des pistes de réflexion pour optimiser le pipeline translationnel :

- ***La résistance des animaux***. Le premier constat que nous avons pu faire au cours de ce travail, est la différence de pronostic vital et fonctionnel entre les animaux et l'homme. La mortalité après une HIC est élevée chez l'Homme, en particulier dans les 48 premières heures (15 %) (Béjot et al. 2017). Or, dans notre étude, aucun rat n'est décédé de mort naturelle au-delà des 24 premières heures (excepté un, qui présentait un syndrome inflammatoire majeur). Tous les décès ont été constatés pendant une phase d'anesthésie (soit pendant la chirurgie, soit pendant la première IRM). Egalement, les rats récupèrent plus vite puisque 7 jours après l'HIC, leurs performances motrices étaient similaires à celle des rats témoins. Ces différences ne peuvent pas être expliquées uniquement par le volume lésionnel puisque les 25 ml moyens de volume lésionnel hémorragique initial représentent environ 50 ml chez l'Homme (Rynkowski et al. 2008)ce qui est bien au-dessus des volumes moyens rapportés dans les différentes études observationnelles. Nous avons observé chez les rats une résolution rapide de l'hémorragie en radiologie et en histologie : sous sept jours, nous observons une résolution quasi-totale de l'oedème et d'environ 40% du sang. Les rats sont donc plus résistants et représentent donc un excellent modèle d'étude des processus de réparation après une HIC. Une des explications à cette résistance est liée au point suivant.
- ***L'âge des animaux***. La plupart des essais thérapeutiques précliniques est menée sur des animaux jeunes et en bonne santé. Dans notre étude, nous avons également fait le choix d'inclure ce type d'animaux afin de mieux caractériser les processus de réaction et de réparation qui surviennent dans le cerveau après une HIC. Nous avons d'ailleurs montré que le pronostic vital et moteur est excellent chez le rongeur, ce qui ne reflète pas du tout la réalité clinique. Chez l'Homme, l'âge, les comorbidités (HTA, diabète) et la microangiopathie fragilisent la BHE et amplifient les réactions inflammatoires (Low et al. 2019). On peut par exemple, émettre l'hypothèse que le switch pro/anti-inflammatoire que nous avons décrit précédemment est moins effectif chez l'Homme âgé que chez le rat jeune. Ainsi, les animaux jeunes sont utiles pour étudier les phénomènes de réparation mais

l'emploi d'animaux plus âgés et comorbides offre un meilleur reflet de la réalité clinique (Withers et al. 2020).

- ***Le sexe des animaux***. L'AVC représente la première cause de mortalité chez la femme. Or, la majorité des études pré-cliniques sont réalisées chez le mâle. La sous-utilisation des femelles repose notamment sur deux dogmes. Le premier consiste à penser que les paramètres fonctionnels étudiés seront inévitablement soumis à variation en fonction des phases de leur cycle œstral. Cependant, une méta-analyse parue en 2014 dans le domaine des neurosciences montrait que l'utilisation de femelles ne nécessitait pas de surveiller leur cycle (Prendergast, Onishi, et Zucker 2014). L'autre raison expliquée par les chercheurs est celui de la duplication des groupes expérimentaux, induisant inévitablement une diminution du rendement, de la productivité scientifique et une augmentation du temps et des moyens financiers utilisés. Ces raisons pratiques ne doivent pas supplanter des rationnels scientifiques. Dans notre étude, bien que mâles et femelles présentaient des trajectoires communes, les femelles semblaient présenter une récupération fonctionnelle motrice plus rapide que les mâles ainsi qu'un taux de croissance d'OPH plus faible dans les trois premiers jours. A plus grande échelle, ces différences pourraient conduire à des ajustements de posologie ou de durée de traitement en fonction du sexe. Dans la perspective d'une médecine personnalisée, nous encourageons donc l'inclusion systématique d'animaux femelles dans les protocoles de recherche préclinique.

- ***Le mode d'évaluation des déficits engendrés.*** L'échec d'adaptation de traitement de l'animal à l'Homme pourrait en partie être expliqué par les différences de méthodes d'évaluation de la récupération après une HIC (Turner, Jickling, et Sharp 2011). En effet, chez l'Homme, le critère de jugement principal est le plus souvent l'évaluation clinique sur le long terme (3 mois à 1 an) puis secondairement, l'évaluation de paramètres radiologiques et/ou biologiques. Dans les études pré-cliniques, l'étude tissulaire *ex vivo* (ou plus rarement en imagerie) relaie au second plan l'étude des effets comportementaux. Par ailleurs, la méthode d'évaluation comportementale pour mesurer l'effet d'un traitement dans la littérature pré-clinique actuelle pose également question. En effet, dans la grande majorité des cas, cette évaluation repose sur des échelles subjectives de motricité (échelle NDS par exemple) (Hietamies et al. 2018). Or chez l'homme, l'évaluation fonctionnelle ne se résume pas aux performances motrices. De plus, nous pouvons nous interroger sur la pertinence de juger de l'efficacité d'un traitement se basant uniquement sur une étude motrice à court terme (généralement au septième jour) puisque nous avons montré dans nos travaux que ce

critère se corrige spontanément et rapidement après l'HIC. Nous avons en revanche montré la présence d'une altération cognitive à long terme qui pourrait constituer un critère de jugement plus pertinent dans les modèles animaux.

- ***La taille des effectifs***. La règle des « 3R » fût élaborée en 1959, elle constitue le fondement de la démarche éthique appliquée à l'expérimentation animale. Cette règle comprend les points suivants : Reduce (Réduire) le nombre d'animaux en expérimentation ; Refine (Raffiner) la méthodologie utilisée ; Replace (Remplacer) les modèles animaux (Hubrecht et Carter 2019). Dans notre étude, l'inclusion d'un grand nombre d'animaux se justifie par l'analyse de différents temps (4), de différentes conditions (inclusion de shams et de femelles) et de différentes fonctions comportementales (motrices et cognitives). C'est grâce à l'importance de notre effectif que nous avons pu mettre en évidence des différences significatives selon les temps, les modes et les conditions d'analyses avec des intervalles de confiance raisonnable. Selon une méta-analyse récente portant sur plus de 2000 études expérimentales sur l'AVC, le nombre d'animaux moyen par groupe expérimental est de huit (Howells, Van der Worp, et Macleod 2009). Ce faible chiffre expose à un risque élevé d'incertitude statistique (Button et al. 2013). Ce constat ne doit pas remettre en cause la règle fondamentale des « 3R » mais doit faire envisager des alternatives. A la lumière de nos travaux, nous proposons par exemple d'adopter systématiquement un design longitudinal avec un monitoring *in vivo* par IRM des réactions tissulaires, permettant ainsi de réduire le nombre d'animaux dédiés à une euthanasie pour des fins histologiques.

- ***L'horloge animale n'est pas celle de l'homme***. Dans le domaine de la neurologie vasculaire, l'ischémie cérébrale est le paradigme le plus étudié. Si bien que les chercheurs peuvent être tentés d'appliquer les dogmes de l'ischémie à l'hémorragie cérébrale. Par exemple, il a été montré que l'efficacité thérapeutique de la thrombolyse intraveineuse avait la même fenêtre temporelle chez l'homme que chez les rongeurs dans l'AVC ischémique (Sena et al. 2010). Or, dans l'HIC, nous avons montré que la cinétique des événements chez l'animal ne s'appliquait pas à l'Homme. En exemple, nous pouvons citer la vitesse de résorption de l'hémorragie, qui est beaucoup plus rapide chez le rat que chez l'Homme. En effet, nous avons observé une clairance du sang d'environ 40 % chez les rongeurs sous sept jours, tandis que chez l'Homme, la mise en jeu du système CD163/HO-1 n'intervient qu'à partir de ce septième jour. Nous pensons que lorsque qu'une thérapie prometteuse émerge du modèle animal il convient de vérifier sur du tissu humain que la molécule ciblée est bien exprimée chez l'Homme et dans des cinétiques comparables.

4. De l’expérimental à la clinique : l’étude COPITCH

Pour compléter notre approche translationnelle de l’HIC et de ses conséquences, nous avons mis en place l’étude clinique **CoPITCH** (influence of Cerebral Oedema on the Prognosis of InTraCerebral Haemorrhages). Il s’agit d’une étude prospective multicentrique observationnelle longitudinale. L’objectif principal est d’évaluer l'influence de l’OPH sur le pronostic fonctionnel 3 mois après un HIC. Nos objectifs secondaires sont de caractériser l’histoire naturelle de l’OPH en IRM, d’évaluer son effet sur la mortalité et les performances cognitives post HIC et d’identifier les patients à risque de développer un OPH malin.

Pour cela, tous patients âgés de plus de 18 ans admis dans les 24 heures suivant l’apparition de l’hémorragie cérébrale spontanée (i.e. non malformative, non traumatique) sont éligibles. Les critères d’exclusion sont : hémorragie intraventriculaire isolée, HIC en lien avec une malformation vasculaire ou une thrombose veineuse cérébrale, une transformation hémorragique d’un infarctus cérébral. Les patients transférés d’un autre hôpital (induisant un biais de sévérité) ainsi que les patients ayant un handicap fonctionnel pré-existant (score de Rankin modifié pré-existant de 4 ou 5) sont également exclus. Tous les patients sont évalués sur le plan clinique, biologique et neuroradiologique de manière longitudinale, à quatre temps : admission (24^{ières} heures), 96 heures, 3 mois et 1 an.

Evaluation clinique. Les données cliniques et démographiques des patients sont recueillies prospectivement. Les chiffres tensionnels, le score de Rankin pré-admission et le score NIHSS sont notamment collectés à l’admission. Tous les patients sont revus à trois mois et à un an en consultation avec un neurologue vasculaire spécialisé. Le devenir fonctionnel sera évalué par le score de Rankin modifié. L’efficience cognitive globale sera évaluée en utilisant l'échelle MOCA (Nasreddine et al. 2005). L’existence d’un trouble cognitif mineur ou sévère préalable à l’hémorragie sera évalué à l’admission en utilisant la version courte de l'IQCODE (Donnellan et Werring 2020). Nous recherchons également des troubles du comportement en utilisant l’inventaire neuropsychiatrique réduit (NPI-R) (Kaufer et al. 2000). *Evaluation neuroradiologique.* Une IRM cérébrale est réalisée pour chaque patient à chaque temps, sur la même machine en utilisant un protocole spécifique pré-établi. Une analyse neuroradiologique exhaustive sera réalisée avec une mesure du volume de l’HIC, du volume de l’OPH, du volume lésionnel total (défini par la somme des 2), du volume relatif d’OPH (défini par le ratio volume OPH/volume HIC) ainsi que du taux d’expansion de l’OPH. Nous utiliserons un logiciel dédié afin de quantifier de manière semi-automatique ces volumes

lésionnels. Un neuroradiologue expérimenté procédera à l'évaluation de chaque IRM en aveugle des données cliniques et du temps d'évaluation. *Evaluation biologique*. Des prélèvements sanguins sont réalisés à l'admission, J4 et 3 mois. Ils sont stockés à -80° et analysés en aveugle des données cliniques et du temps d'évaluation. A l'issue du recrutement, nous analyserons un large panel de biomarqueurs notamment de l'inflammation (tel que le ratio neutrophiles/lymphocytes, facteur de von Willebrand, ICAM-1, MMP-9…), nous étudierons également l'influence du phénotype APOε qui pourrait être associé au pronostic des patients avec HIC (Biffi et al. 2011).

En date du 15 Octobre 2021, 15 patients ont été inclus sur les 500 prévus.

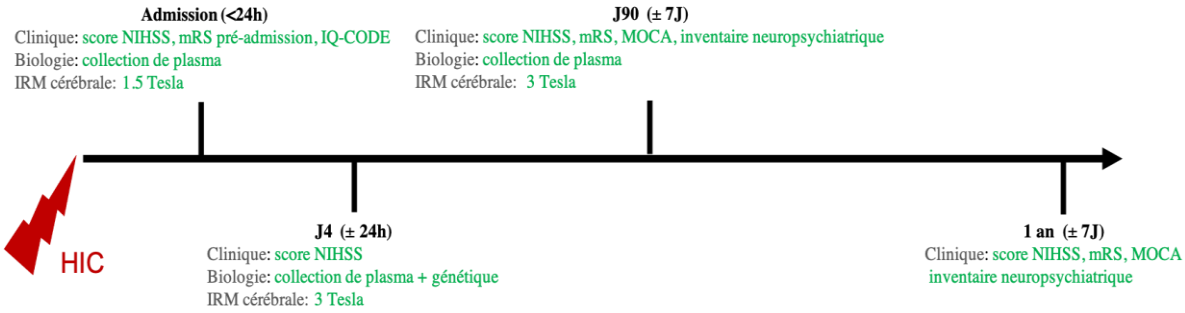

Figure 8. Design de l'étude COPITCH (influence of Cerebral Oedema on the Prognosis of InTraCerebral Haemorrhages).

CONCLUSION :

Basé sur un travail de recherche translationnelle, nos résultats contribuent à affiner notre perception de l'œdème péri-hémorragique, à renforcer les liens entre recherche clinique et pré-clinique, et, nous l'espérons, à identifier des stratégies thérapeutiques innovantes pour l'HIC.

Références

Aguzzi, Adriano, Ben A. Barres, et Mariko L. Bennett. 2013. « Microglia: Scapegoat, Saboteur, or Something Else? » *Science (New York, N.Y.)* 339 (6116): 156-61. https://doi.org/10.1126/science.1227901.

Andaluz, Norberto, Mario Zuccarello, et Kenneth R. Wagner. 2002. « Experimental Animal Models of Intracerebral Hemorrhage. » *Neurosurgery Clinics of North America* 13 (3): 385-93. https://doi.org/10.1016/s1042-3680(02)00006-2.

Appelboom, Geoffrey, Samuel S. Bruce, Zachary L. Hickman, Brad E. Zacharia, Amanda M. Carpenter, Kerry A. Vaughan, Andrew Duren, et al. 2013. « Volume-Dependent Effect of Perihaematomal Oedema on Outcome for Spontaneous Intracerebral Haemorrhages. » *Journal of Neurology, Neurosurgery, and Psychiatry* 84 (5): 488-93. https://doi.org/10.1136/jnnp-2012-303160.

Arima, H., J. G. Wang, Y. Huang, E. Heeley, C. Skulina, M. W. Parsons, B. Peng, et al. 2009. « Significance of Perihematomal Edema in Acute Intracerebral Hemorrhage: The INTERACT Trial. » *Neurology* 73 (23): 1963-68. https://doi.org/10.1212/WNL.0b013e3181c55ed3.

Asch, Charlotte Jj van, Merel Ja Luitse, Gabriël Je Rinkel, Ingeborg van der Tweel, Ale Algra, et Catharina Jm Klijn. 2010. « Incidence, Case Fatality, and Functional Outcome of Intracerebral Haemorrhage over Time, According to Age, Sex, and Ethnic Origin: A Systematic Review and Meta-Analysis. » *The Lancet. Neurology* 9 (2): 167-76. https://doi.org/10.1016/S1474-4422(09)70340-0.

Bai, Qinqin, Jiachen Liu, et Gaiqing Wang. 2020. « Ferroptosis, a Regulated Neuronal Cell Death Type After Intracerebral Hemorrhage. » *Frontiers in Cellular Neuroscience* 14: 591874. https://doi.org/10.3389/fncel.2020.591874.

Bakhshayesh, Babak, Mozaffar Hosseininezhad, Seyedeh Nazanin Seyed Saadat, Malek Moien Ansar, Hamed Ramezani, et Seyed Mohammad Seyed Saadat. 2014. « Iron Overload Is Associated with Perihematoma Edema Growth Following Intracerebral Hemorrhage That May Contribute to In-Hospital Mortality and Long-Term Functional Outcome. » *Current Neurovascular Research* 11 (3): 248-53. https://doi.org/10.2174/1567202611666140530124855.

Beaumont, A., A. Marmarou, K. Hayasaki, P. Barzo, P. Fatouros, F. Corwin, C. Marmarou, et J. Dunbar. 2000. « The Permissive Nature of Blood Brain Barrier (BBB) Opening in Edema

Formation Following Traumatic Brain Injury. » *Acta Neurochirurgica. Supplement* 76: 125-29. https://doi.org/10.1007/978-3-7091-6346-7_26.

Béjot, Yannick, Michael Grelat, Benoit Delpont, Jérôme Durier, Olivier Rouaud, Guy-Victor Osseby, Marie Hervieu-Bègue, Maurice Giroud, et Charlotte Cordonnier. 2017. « Temporal Trends in Early Case-Fatality Rates in Patients with Intracerebral Hemorrhage. » *Neurology* 88 (10): 985-90. https://doi.org/10.1212/WNL.0000000000003681.

Bérézowski, Vincent, Caroline Mysiorek, Mélanie Kuntz, Olivier Pétrault, et Roméo Cecchelli. 2012. « [Dysfunction of the blood-brain barrier during ischaemia: a therapeutic concern]. » *Biologie aujourd'hui* 206 (3): 161-76. https://doi.org/10.1051/jbio/2012020.

Bernardo, Antonietta, et Luisa Minghetti. 2006. « PPAR-Gamma Agonists as Regulators of Microglial Activation and Brain Inflammation. » *Current Pharmaceutical Design* 12 (1): 93-109. https://doi.org/10.2174/138161206780574579.

Biffi, Alessandro, Christopher D. Anderson, Jeremiasz M. Jagiella, Helena Schmidt, Brett Kissela, Björn M. Hansen, Jordi Jimenez-Conde, et al. 2011. « APOE Genotype and Extent of Bleeding and Outcome in Lobar Intracerebral Haemorrhage: A Genetic Association Study. » *The Lancet. Neurology* 10 (8): 702-9. https://doi.org/10.1016/S1474-4422(11)70148-X.

Biswas, Subhra K., et Alberto Mantovani. 2010. « Macrophage Plasticity and Interaction with Lymphocyte Subsets: Cancer as a Paradigm. » *Nature Immunology* 11 (10): 889-96. https://doi.org/10.1038/ni.1937.

Boada-Romero, Emilio, Jennifer Martinez, Bradlee L. Heckmann, et Douglas R. Green. 2020. « The Clearance of Dead Cells by Efferocytosis. » *Nature Reviews. Molecular Cell Biology* 21 (7): 398-414. https://doi.org/10.1038/s41580-020-0232-1.

Bodmer, Daniel, Kerry A. Vaughan, Brad E. Zacharia, Zachary L. Hickman, et E. Sander Connolly. 2012. « The Molecular Mechanisms That Promote Edema After Intracerebral Hemorrhage. » *Translational Stroke Research* 3 (Suppl 1): 52-61. https://doi.org/10.1007/s12975-012-0162-0.

Bullock, R., A. D. Mendelow, G. M. Teasdale, et D. I. Graham. 1984. « Intracranial Haemorrhage Induced at Arterial Pressure in the Rat. Part 1: Description of Technique, ICP Changes and Neuropathological Findings. » *Neurological Research* 6 (4): 184-88. https://doi.org/10.1080/01616412.1984.11739687.

Button, Katherine S., John P. A. Ioannidis, Claire Mokrysz, Brian A. Nosek, Jonathan Flint,

Emma S. J. Robinson, et Marcus R. Munafò. 2013. « Power Failure: Why Small Sample Size Undermines the Reliability of Neuroscience. » *Nature Reviews. Neuroscience* 14 (5): 365-76. https://doi.org/10.1038/nrn3475.

Calder, P. C., et R. F. Grimble. 2002. « Polyunsaturated Fatty Acids, Inflammation and Immunity. » *European Journal of Clinical Nutrition* 56 Suppl 3 (août): S14-19. https://doi.org/10.1038/sj.ejcn.1601478.

Campbell, Nicole K., Hannah K. Fitzgerald, et Aisling Dunne. 2021. « Regulation of Inflammation by the Antioxidant Haem Oxygenase 1. » *Nature Reviews. Immunology* 21 (7): 411-25. https://doi.org/10.1038/s41577-020-00491-x.

Carman, Christopher V. 2009. « Mechanisms for Transcellular Diapedesis: Probing and Pathfinding by "Invadosome-like Protrusions". » *Journal of Cell Science* 122 (Pt 17): 3025-35. https://doi.org/10.1242/jcs.047522.

Carmichael, S. Thomas, Paul M. Vespa, Jeffery L. Saver, Giovanni Coppola, Daniel H. Geschwind, Sidney Starkman, Chad M. Miller, Chelsea S. Kidwell, David S. Liebeskind, et Neil A. Martin. 2008. « Genomic Profiles of Damage and Protection in Human Intracerebral Hemorrhage. » *Journal of Cerebral Blood Flow and Metabolism : Official Journal of the International Society of Cerebral Blood Flow and Metabolism* 28 (11): 1860-75. https://doi.org/10.1038/jcbfm.2008.77.

Chawla, Ajay. 2010. « Control of Macrophage Activation and Function by PPARs. » *Circulation Research* 106 (10): 1559-69. https://doi.org/10.1161/CIRCRESAHA.110.216523.

Cuadrado, Antonio, Ana I. Rojo, Geoffrey Wells, John D. Hayes, Sharon P. Cousin, William L. Rumsey, Otis C. Attucks, et al. 2019. « Therapeutic Targeting of the NRF2 and KEAP1 Partnership in Chronic Diseases. » *Nature Reviews. Drug Discovery* 18 (4): 295-317. https://doi.org/10.1038/s41573-018-0008-x.

Daneman, Richard, et Alexandre Prat. 2015. « The Blood-Brain Barrier. » *Cold Spring Harbor Perspectives in Biology* 7 (1): a020412. https://doi.org/10.1101/cshperspect.a020412.

Deinsberger, W., J. Vogel, W. Kuschinsky, L. M. Auer, et D. K. Böker. 1996. « Experimental Intracerebral Hemorrhage: Description of a Double Injection Model in Rats. » *Neurological Research* 18 (5): 475-77. https://doi.org/10.1080/01616412.1996.11740456.

Dirnagl, U., C. Iadecola, et M. A. Moskowitz. 1999. « Pathobiology of Ischaemic Stroke: An Integrated View. » *Trends in Neurosciences* 22 (9): 391-97. https://doi.org/10.1016/s0166-

2236(99)01401-0.

Dixon, Scott J., Darpan N. Patel, Matthew Welsch, Rachid Skouta, Eric D. Lee, Miki Hayano, Ajit G. Thomas, et al. 2014. « Pharmacological Inhibition of Cystine-Glutamate Exchange Induces Endoplasmic Reticulum Stress and Ferroptosis. » *ELife* 3 (mai): e02523. https://doi.org/10.7554/eLife.02523.

Dixon, Scott J., et Brent R. Stockwell. 2014. « The Role of Iron and Reactive Oxygen Species in Cell Death. » *Nature Chemical Biology* 10 (1): 9-17. https://doi.org/10.1038/nchembio.1416.

Donnellan, Claire, et David Werring. 2020. « Cognitive Impairment before and after Intracerebral Haemorrhage: A Systematic Review. » *Neurological Sciences : Official Journal of the Italian Neurological Society and of the Italian Society of Clinical Neurophysiology* 41 (3): 509-27. https://doi.org/10.1007/s10072-019-04150-5.

Eguchi, Y., S. Shimizu, et Y. Tsujimoto. 1997. « Intracellular ATP Levels Determine Cell Death Fate by Apoptosis or Necrosis. » *Cancer Research* 57 (10): 1835-40.

Elmore, Susan. 2007. « Apoptosis: A Review of Programmed Cell Death. » *Toxicologic Pathology* 35 (4): 495-516. https://doi.org/10.1080/01926230701320337.

Endres, Matthias, Britta Engelhardt, Jari Koistinaho, Olle Lindvall, Stephen Meairs, Jay P. Mohr, Anna Planas, et al. 2008. « Improving Outcome after Stroke: Overcoming the Translational Roadblock. » *Cerebrovascular Diseases (Basel, Switzerland)* 25 (3): 268-78. https://doi.org/10.1159/000118039.

Filley, Christopher M., et R. Douglas Fields. 2016. « White Matter and Cognition: Making the Connection. » *Journal of Neurophysiology* 116 (5): 2093-2104. https://doi.org/10.1152/jn.00221.2016.

Fisher, C. M. 1971. « Pathological Observations in Hypertensive Cerebral Hemorrhage. » *Journal of Neuropathology and Experimental Neurology* 30 (3): 536-50. https://doi.org/10.1097/00005072-197107000-00015.

Fu, Ying, Junwei Hao, Ningnannan Zhang, Li Ren, Na Sun, Yu-Jing Li, Yaping Yan, DeRen Huang, Chunshui Yu, et Fu-Dong Shi. 2014. « Fingolimod for the Treatment of Intracerebral Hemorrhage: A 2-Arm Proof-of-Concept Study. » *JAMA Neurology* 71 (9): 1092-1101. https://doi.org/10.1001/jamaneurol.2014.1065.

Garton, Thomas, Richard F. Keep, Ya Hua, et Guohua Xi. 2017. « CD163, a Hemoglobin/Haptoglobin Scavenger Receptor, After Intracerebral Hemorrhage: Functions in

Microglia/Macrophages Versus Neurons. » *Translational Stroke Research* 8 (6): 612-16. https://doi.org/10.1007/s12975-017-0535-5.

Gebel, James M. Jr, Edward C. Jauch, Thomas G. Brott, Jane Khoury, Laura Sauerbeck, Shelia Salisbury, Judith Spilker, Thomas A. Tomsick, John Duldner, et Joseph P. Broderick. 2002. « Relative Edema Volume Is a Predictor of Outcome in Patients with Hyperacute Spontaneous Intracerebral Hemorrhage. » *Stroke* 33 (11): 2636-41. https://doi.org/10.1161/01.str.0000035283.34109.ea.

Gonzales, Nicole R., Jharna Shah, Navdeep Sangha, Lenis Sosa, Rebecca Martinez, Loren Shen, Mallikarjunarao Kasam, et al. 2013. « Design of a Prospective, Dose-Escalation Study Evaluating the Safety of Pioglitazone for Hematoma Resolution in Intracerebral Hemorrhage (SHRINC). » *International Journal of Stroke : Official Journal of the International Stroke Society* 8 (5): 388-96. https://doi.org/10.1111/j.1747-4949.2011.00761.x.

Gordon, Siamon, et Fernando O. Martinez. 2010. « Alternative Activation of Macrophages: Mechanism and Functions. » *Immunity* 32 (5): 593-604. https://doi.org/10.1016/j.immuni.2010.05.007.

Gould, Douglas B., F. Campbell Phalan, Saskia E. van Mil, John P. Sundberg, Katayoun Vahedi, Pascale Massin, Marie Germaine Bousser, et al. 2006. « Role of COL4A1 in Small-Vessel Disease and Hemorrhagic Stroke. » *The New England Journal of Medicine* 354 (14): 1489-96. https://doi.org/10.1056/NEJMoa053727.

Grunwald, Zachary, Lauren A. Beslow, Sebastian Urday, Anastasia Vashkevich, Alison Ayres, Steven M. Greenberg, Joshua N. Goldstein, et al. 2017. « Perihematomal Edema Expansion Rates and Patient Outcomes in Deep and Lobar Intracerebral Hemorrhage. » *Neurocritical Care* 26 (2): 205-12. https://doi.org/10.1007/s12028-016-0321-3.

Guan, Jing-Xia, Sheng-Gang Sun, Xue-Bing Cao, Zhi-Bin Chen, et E.-Tang Tong. 2004. « Effect of Thrombin on Blood Brain Barrier Permeability and Its Mechanism. » *Chinese Medical Journal* 117 (11): 1677-81.

Gupta, Mani, Rajesh Verma, Anit Parihar, Ravindra K. Garg, Maneesh K. Singh, et Hardeep S. Malhotra. 2014. « Perihematomal Edema as Predictor of Outcome in Spontaneous Intracerebral Hemorrhage. » *Journal of Neurosciences in Rural Practice* 5 (1): 48-54. https://doi.org/10.4103/0976-3147.127873.

Hanley, Daniel F., Richard E. Thompson, Michael Rosenblum, Gayane Yenokyan, Karen Lane,

Nichol McBee, Steven W. Mayo, et al. 2019. « Efficacy and Safety of Minimally Invasive Surgery with Thrombolysis in Intracerebral Haemorrhage Evacuation (MISTIE III): A Randomised, Controlled, Open-Label, Blinded Endpoint Phase 3 Trial. » *Lancet (London, England)* 393 (10175): 1021-32. https://doi.org/10.1016/S0140-6736(19)30195-3.

Hietamies, Tuuli M., Caroline Ostrowski, Zhong Pei, Luyang Feng, Christopher McCabe, Lorraine M. Work, et Terence J. Quinn. 2018. « Variability of Functional Outcome Measures Used in Animal Models of Stroke and Vascular Cognitive Impairment - a Review of Contemporary Studies. » *Journal of Cerebral Blood Flow and Metabolism : Official Journal of the International Society of Cerebral Blood Flow and Metabolism* 38 (11): 1872-84. https://doi.org/10.1177/0271678X18799858.

Howells, D., B. Van der Worp, et M. Macleod. 2009. « CAMARADES (Collaborative Approach to Meta-Analysis and Review of Animal Data from Experimental Stroke): understanding bias and biology in translational medicine: 1A. 3 ». *International Journal of Stroke* 4: 1-2.

Hubrecht, Robert C., et Elizabeth Carter. 2019. « The 3Rs and Humane Experimental Technique: Implementing Change. » *Animals : An Open Access Journal from MDPI* 9 (10). https://doi.org/10.3390/ani9100754.

Ironside, Natasha, Ching-Jen Chen, Simukayi Mutasa, Justin L. Sim, Dale Ding, Saurabh Marfatiah, David Roh, et al. 2020. « Fully Automated Segmentation Algorithm for Perihematomal Edema Volumetry After Spontaneous Intracerebral Hemorrhage. » *Stroke* 51 (3): 815-23. https://doi.org/10.1161/STROKEAHA.119.026764.

Kaufer, D. I., J. L. Cummings, P. Ketchel, V. Smith, A. MacMillan, T. Shelley, O. L. Lopez, et S. T. DeKosky. 2000. « Validation of the NPI-Q, a Brief Clinical Form of the Neuropsychiatric Inventory. » *The Journal of Neuropsychiatry and Clinical Neurosciences* 12 (2): 233-39. https://doi.org/10.1176/jnp.12.2.233.

Keep, R. F., J. Xiang, S. R. Ennis, A. Andjelkovic, Y. Hua, G. Xi, et J. T. Hoff. 2008. « Blood-Brain Barrier Function in Intracerebral Hemorrhage. » *Acta Neurochirurgica. Supplement* 105: 73-77. https://doi.org/10.1007/978-3-211-09469-3_15.

Keep, Richard F., Ya Hua, et Guohua Xi. 2012. « Intracerebral Haemorrhage: Mechanisms of Injury and Therapeutic Targets. » *The Lancet. Neurology* 11 (8): 720-31. https://doi.org/10.1016/S1474-4422(12)70104-7.

Krafft, Paul R., Emma L. Bailey, Tim Lekic, William B. Rolland, Orhan Altay, Jiping Tang, Joanna M. Wardlaw, John H. Zhang, et Cathie L. M. Sudlow. 2012. « Etiology of Stroke and Choice of Models. » *International Journal of Stroke : Official Journal of the International Stroke Society* 7 (5): 398-406. https://doi.org/10.1111/j.1747-4949.2012.00838.x.

Kroemer, G., L. Galluzzi, P. Vandenabeele, J. Abrams, E. S. Alnemri, E. H. Baehrecke, M. V. Blagosklonny, et al. 2009. « Classification of Cell Death: Recommendations of the Nomenclature Committee on Cell Death 2009. » *Cell Death and Differentiation* 16 (1): 3-11. https://doi.org/10.1038/cdd.2008.150.

Lee, S.-H., H.-K. Park, W.-S. Ryu, J.-S. Lee, H.-J. Bae, M.-K. Han, Y.-S. Lee, et al. 2013. « Effects of Celecoxib on Hematoma and Edema Volumes in Primary Intracerebral Hemorrhage: A Multicenter Randomized Controlled Trial. » *European Journal of Neurology* 20 (8): 1161-69. https://doi.org/10.1111/ene.12140.

Levine, Joshua M., Ryan Snider, David Finkelstein, Mahmut E. Gurol, Rishi Chanderraj, Eric E. Smith, Steven M. Greenberg, et Jonathan Rosand. 2007. « Early Edema in Warfarin-Related Intracerebral Hemorrhage. » *Neurocritical Care* 7 (1): 58-63. https://doi.org/10.1007/s12028-007-0039-3.

Li, Na, Yan Fang Liu, Li Ma, Hans Worthmann, Yi Long Wang, Yong Jun Wang, Yi Pei Gao, et al. 2013. « Association of Molecular Markers with Perihematomal Edema and Clinical Outcome in Intracerebral Hemorrhage. » *Stroke* 44 (3): 658-63. https://doi.org/10.1161/STROKEAHA.112.673590.

Li, Na, Hans Worthmann, Meike Heeren, Ramona Schuppner, Milani Deb, Anita B. Tryc, Eva Bueltmann, et al. 2013. « Temporal Pattern of Cytotoxic Edema in the Perihematomal Region after Intracerebral Hemorrhage: A Serial Magnetic Resonance Imaging Study. » *Stroke* 44 (4): 1144-46. https://doi.org/10.1161/STROKEAHA.111.000056.

Li, Qian-Qian, Lan-Jun Li, Xin-Yu Wang, Yu-Ying Sun, et Jun Wu. 2018. « Research Progress in Understanding the Relationship Between Heme Oxygenase-1 and Intracerebral Hemorrhage. » *Frontiers in Neurology* 9: 682. https://doi.org/10.3389/fneur.2018.00682.

Liu, Da-Zhi, Bradley P. Ander, Huichun Xu, Yan Shen, Pali Kaur, Wenbin Deng, et Frank R. Sharp. 2010. « Blood-Brain Barrier Breakdown and Repair by Src after Thrombin-Induced Injury. » *Annals of Neurology* 67 (4): 526-33. https://doi.org/10.1002/ana.21924.

Loan, James Jm, Caoimhe Kirby, Katherine Emelianova, Owen R. Dando, Michael Tc Poon,

Leisan Pimenova, Giles E. Hardingham, et al. 2021. « Secondary Injury and Inflammation after Intracerebral Haemorrhage: A Systematic Review and Meta-Analysis of Molecular Markers in Patient Brain Tissue. » *Journal of Neurology, Neurosurgery, and Psychiatry*, août. https://doi.org/10.1136/jnnp-2021-327098.

López, Mercedes L., Gustavo Bruges, Gustavo Crespo, Victor Salazar, Pierre-Antoine Deglesne, Heike Schneider, Hector Cabrera-Fuentes, M. Lienhard Schmitz, et Klaus T. Preissner. 2014. « Thrombin Selectively Induces Transcription of Genes in Human Monocytes Involved in Inflammation and Wound Healing. » *Thrombosis and Haemostasis* 112 (5): 992-1001. https://doi.org/10.1160/TH14-01-0034.

Low, Audrey, Elijah Mak, James B. Rowe, Hugh S. Markus, et John T. O'Brien. 2019. « Inflammation and Cerebral Small Vessel Disease: A Systematic Review. » *Ageing Research Reviews* 53 (août): 100916. https://doi.org/10.1016/j.arr.2019.100916.

Ma, Qingyi, Nikan H. Khatibi, Hank Chen, Jiping Tang, et John H. Zhang. 2011. « History of Preclinical Models of Intracerebral Hemorrhage. » *Acta Neurochirurgica. Supplement* 111: 3-8. https://doi.org/10.1007/978-3-7091-0693-8_1.

MacLellan, Crystal L., Gergely Silasi, Candice C. Poon, Carmen L. Edmundson, Richard Buist, James Peeling, et Frederick Colbourne. 2008. « Intracerebral Hemorrhage Models in Rat: Comparing Collagenase to Blood Infusion. » *Journal of Cerebral Blood Flow and Metabolism : Official Journal of the International Society of Cerebral Blood Flow and Metabolism* 28 (3): 516-25. https://doi.org/10.1038/sj.jcbfm.9600548.

Mahoney-Sánchez, Laura, Hind Bouchaoui, Scott Ayton, David Devos, James A. Duce, et Jean-Christophe Devedjian. 2021. « Ferroptosis and Its Potential Role in the Physiopathology of Parkinson's Disease. » *Progress in Neurobiology* 196 (janvier): 101890. https://doi.org/10.1016/j.pneurobio.2020.101890.

Manaenko, Anatol, Hank Chen, John H. Zhang, et Jiping Tang. 2011. « Comparison of Different Preclinical Models of Intracerebral Hemorrhage. » *Acta Neurochirurgica. Supplement* 111: 9-14. https://doi.org/10.1007/978-3-7091-0693-8_2.

Maślińska, D., et M. Gajewski. 1998. « Some Aspects of the Inflammatory Process. » *Folia Neuropathologica* 36 (4): 199-204.

McCarron, M. O., K. L. Hoffmann, D. M. DeLong, L. Gray, A. M. Saunders, et M. J. Alberts. 1999. « Intracerebral Hemorrhage Outcome: Apolipoprotein E Genotype, Hematoma, and

Edema Volumes. » *Neurology* 53 (9): 2176-79. https://doi.org/10.1212/wnl.53.9.2176.

Meier, P., A. Finch, et G. Evan. 2000. « Apoptosis in Development. » *Nature* 407 (6805): 796-801. https://doi.org/10.1038/35037734.

Misra, U. K., J. Kalita, P. Ranjan, et S. K. Mandal. 2005. « Mannitol in Intracerebral Hemorrhage: A Randomized Controlled Study. » *Journal of the Neurological Sciences* 234 (1-2): 41-45. https://doi.org/10.1016/j.jns.2005.03.038.

Montfort, I., et R. Pérez-Tamayo. 1975. « The Distribution of Collagenase in Normal Rat Tissues. » *The Journal of Histochemistry and Cytochemistry : Official Journal of the Histochemistry Society* 23 (12): 910-20. https://doi.org/10.1177/23.12.172556.

Moulin, Solène, Julien Labreuche, Stéphanie Bombois, Costanza Rossi, Gregoire Boulouis, Hilde Hénon, Alain Duhamel, Didier Leys, et Charlotte Cordonnier. 2016. « Dementia Risk after Spontaneous Intracerebral Haemorrhage: A Prospective Cohort Study. » *The Lancet. Neurology* 15 (8): 820-29. https://doi.org/10.1016/S1474-4422(16)00130-7.

Moullaali, Tom J., Xia Wang, Reneé H. Martin, Virginia B. Shipes, Thompson G. Robinson, John Chalmers, Jose I. Suarez, Adnan I. Qureshi, Yuko Y. Palesch, et Craig S. Anderson. 2019. « Blood Pressure Control and Clinical Outcomes in Acute Intracerebral Haemorrhage: A Preplanned Pooled Analysis of Individual Participant Data. » *The Lancet. Neurology* 18 (9): 857-64. https://doi.org/10.1016/S1474-4422(19)30196-6.

Mracsko, Eva, et Roland Veltkamp. 2014. « Neuroinflammation after Intracerebral Hemorrhage. » *Frontiers in Cellular Neuroscience* 8: 388. https://doi.org/10.3389/fncel.2014.00388.

Murthy, Santosh B., Sebastian Urday, Lauren A. Beslow, Jesse Dawson, Kennedy Lees, W. Taylor Kimberly, Costantino Iadecola, et al. 2016. « Rate of Perihaematomal Oedema Expansion Is Associated with Poor Clinical Outcomes in Intracerebral Haemorrhage. » *Journal of Neurology, Neurosurgery, and Psychiatry* 87 (11): 1169-73. https://doi.org/10.1136/jnnp-2016-313653.

Nasreddine, Ziad S., Natalie A. Phillips, Valérie Bédirian, Simon Charbonneau, Victor Whitehead, Isabelle Collin, Jeffrey L. Cummings, et Howard Chertkow. 2005. « The Montreal Cognitive Assessment, MoCA: A Brief Screening Tool for Mild Cognitive Impairment. » *Journal of the American Geriatrics Society* 53 (4): 695-99. https://doi.org/10.1111/j.1532-5415.2005.53221.x.

Naval, Neeraj S., Tamer A. Abdelhak, Nathalie Urrunaga, Paloma Zeballos, Marek A. Mirski, et Juan R. Carhuapoma. 2008. « An Association of Prior Statin Use with Decreased Perihematomal Edema. » *Neurocritical Care* 8 (1): 13-18. https://doi.org/10.1007/s12028-007-0081-1.

Negrier, Claude, Midori Shima, et Maureane Hoffman. 2019. « The Central Role of Thrombin in Bleeding Disorders. » *Blood Reviews* 38 (novembre): 100582. https://doi.org/10.1016/j.blre.2019.05.006.

Ozdinc, Serife, Ebru Unlu, Zeynep Karakaya, Ozan Turamanlar, Nurhan Dogan, Yesim Isler, Yucel Gonul, et Mehmet Gazi Boyaci. 2016. « Prognostic Value of Perihematomal Edema Area at the Initial ED Presentation in Patients with Intracranial Hematoma. » *The American Journal of Emergency Medicine* 34 (7): 1241-46. https://doi.org/10.1016/j.ajem.2016.03.048.

Pasi, Marco, Barbara Casolla, Maéva Kyheng, Grégoire Boulouis, Grégory Kuchcinski, Solène Moulin, Julien Labreuche, Hilde Hénon, Charlotte Cordonnier, et Didier Leys. 2021. « Long-Term Mortality in Survivors of Spontaneous Intracerebral Hemorrhage. » *International Journal of Stroke : Official Journal of the International Stroke Society* 16 (4): 448-55. https://doi.org/10.1177/1747493020954946.

Pétrault, Maud, Barbara Casolla, Thavarak Ouk, Charlotte Cordonnier, et Vincent Bérézowski. 2019. « Cerebral Microbleeds: Beyond the Macroscope. » *International Journal of Stroke : Official Journal of the International Stroke Society* 14 (5): 468-75. https://doi.org/10.1177/1747493019830594.

Poon, Michael Tin Chung, Arthur François Fonville, et Rustam Al-Shahi Salman. 2014. « Long-Term Prognosis after Intracerebral Haemorrhage: Systematic Review and Meta-Analysis. » *Journal of Neurology, Neurosurgery, and Psychiatry* 85 (6): 660-67. https://doi.org/10.1136/jnnp-2013-306476.

Prendergast, Brian J., Kenneth G. Onishi, et Irving Zucker. 2014. « Female Mice Liberated for Inclusion in Neuroscience and Biomedical Research. » *Neuroscience and Biobehavioral Reviews* 40 (mars): 1-5. https://doi.org/10.1016/j.neubiorev.2014.01.001.

Pszczolkowski, Stefan, Zhe K. Law, Rebecca G. Gallagher, Dewen Meng, David J. Swienton, Paul S. Morgan, Philip M. Bath, Nikola Sprigg, et Rob A. Dineen. 2019. « Automated Segmentation of Haematoma and Perihaematomal Oedema in MRI of Acute Spontaneous Intracerebral Haemorrhage. » *Computers in Biology and Medicine* 106 (mars): 126-39. https://doi.org/10.1016/j.compbiomed.2019.01.022.

Pun, Pamela B. L., Jia Lu, et Shabbir Moochhala. 2009. « Involvement of ROS in BBB Dysfunction. » *Free Radical Research* 43 (4): 348-64. https://doi.org/10.1080/10715760902751902.

Puy Laurent, Cordonnier Charlotte. 2019. « Accident vasculaire cérébral (AVC) La première cause de handicap acquis de l'adulte ». *Dossier Inserm*, 2019.

Puy, Laurent, et Charlotte Cordonnier. 2019. « [Sporadic cerebral amyloid angiopathy]. » *Geriatrie et psychologie neuropsychiatrie du vieillissement* 17 (1): 73-82. https://doi.org/10.1684/pnv.2018.0776.

Qureshi, A. I., S. Tuhrim, J. P. Broderick, H. H. Batjer, H. Hondo, et D. F. Hanley. 2001. « Spontaneous Intracerebral Hemorrhage. » *The New England Journal of Medicine* 344 (19): 1450-60. https://doi.org/10.1056/NEJM200105103441907.

Raichle, Marcus E., et Debra A. Gusnard. 2002. « Appraising the Brain's Energy Budget. » *Proceedings of the National Academy of Sciences of the United States of America* 99 (16): 10237-39. https://doi.org/10.1073/pnas.172399499.

Rodriguez-Luna, David, Teri Stewart, Dar Dowlatshahi, Jayme C. Kosior, Richard I. Aviv, Carlos A. Molina, Yolanda Silva, et al. 2016. « Perihematomal Edema Is Greater in the Presence of a Spot Sign but Does Not Predict Intracerebral Hematoma Expansion. » *Stroke* 47 (2): 350-55. https://doi.org/10.1161/STROKEAHA.115.011295.

Roh, Jong Seong, et Dong Hyun Sohn. 2018. « Damage-Associated Molecular Patterns in Inflammatory Diseases. » *Immune Network* 18 (4): e27. https://doi.org/10.4110/in.2018.18.e27.

Ropper, A. H., et N. T. Zervas. 1982. « Cerebral Blood Flow after Experimental Basal Ganglia Hemorrhage. » *Annals of Neurology* 11 (3): 266-71. https://doi.org/10.1002/ana.410110306.

Rosell, Anna, Anna Vilalta, Teresa García-Berrocoso, Israel Fernández-Cadenas, Sophie Domingues-Montanari, Eloy Cuadrado, Pilar Delgado, et al. 2011. « Brain Perihematoma Genomic Profile Following Spontaneous Human Intracerebral Hemorrhage. » *PloS One* 6 (2): e16750. https://doi.org/10.1371/journal.pone.0016750.

Rosenberg, G. A., S. Mun-Bryce, M. Wesley, et M. Kornfeld. 1990. « Collagenase-Induced Intracerebral Hemorrhage in Rats. » *Stroke* 21 (5): 801-7. https://doi.org/10.1161/01.str.21.5.801.

Rynkowski, Michal A., Grace H. Kim, Ricardo J. Komotar, Marc L. Otten, Andrew F. Ducruet, Brad E. Zacharia, Christopher P. Kellner, et al. 2008. « A Mouse Model of Intracerebral

Hemorrhage Using Autologous Blood Infusion. » *Nature Protocols* 3 (1): 122-28. https://doi.org/10.1038/nprot.2007.513.

Salvador, Gabriela A., Romina M. Uranga, et Norma M. Giusto. 2010. « Iron and Mechanisms of Neurotoxicity. » *International Journal of Alzheimer's Disease* 2011 (décembre): 720658. https://doi.org/10.4061/2011/720658.

Sansing, L. H., S. R. Messe, B. L. Cucchiara, P. D. Lyden, et S. E. Kasner. 2011. « Anti-Adrenergic Medications and Edema Development after Intracerebral Hemorrhage. » *Neurocritical Care* 14 (3): 395-400. https://doi.org/10.1007/s12028-010-9498-z.

Sansing, Lauren H., Elena A. Kaznatcheeva, Candice J. Perkins, Eugene Komaroff, Frederick B. Gutman, et George C. Newman. 2003. « Edema after Intracerebral Hemorrhage: Correlations with Coagulation Parameters and Treatment. » *Journal of Neurosurgery* 98 (5): 985-92. https://doi.org/10.3171/jns.2003.98.5.0985.

Schlunk, Frieder, et Steven M. Greenberg. 2015. « The Pathophysiology of Intracerebral Hemorrhage Formation and Expansion. » *Translational Stroke Research* 6 (4): 257-63. https://doi.org/10.1007/s12975-015-0410-1.

Selim, Magdy, Lydia D. Foster, Claudia S. Moy, Guohua Xi, Michael D. Hill, Lewis B. Morgenstern, Steven M. Greenberg, et al. 2019. « Deferoxamine Mesylate in Patients with Intracerebral Haemorrhage (i-DEF): A Multicentre, Randomised, Placebo-Controlled, Double-Blind Phase 2 Trial. » *The Lancet. Neurology* 18 (5): 428-38. https://doi.org/10.1016/S1474-4422(19)30069-9.

Sena, Emily S., Catherine L. Briscoe, David W. Howells, Geoffrey A. Donnan, Peter A. G. Sandercock, et Malcolm R. Macleod. 2010. « Factors Affecting the Apparent Efficacy and Safety of Tissue Plasminogen Activator in Thrombotic Occlusion Models of Stroke: Systematic Review and Meta-Analysis. » *Journal of Cerebral Blood Flow and Metabolism : Official Journal of the International Society of Cerebral Blood Flow and Metabolism* 30 (12): 1905-13. https://doi.org/10.1038/jcbfm.2010.116.

Staykov, Dimitre, Ingrid Wagner, Bastian Volbers, Eva-Maria Hauer, Arnd Doerfler, Stefan Schwab, et Juergen Bardutzky. 2011. « Natural Course of Perihemorrhagic Edema after Intracerebral Hemorrhage. » *Stroke* 42 (9): 2625-29. https://doi.org/10.1161/STROKEAHA.111.618611.

Thomsen, Jens Haugbølle, Anders Etzerodt, Pia Svendsen, et Søren K. Moestrup. 2013. « The

Haptoglobin-CD163-Heme Oxygenase-1 Pathway for Hemoglobin Scavenging. » *Oxidative Medicine and Cellular Longevity* 2013: 523652. https://doi.org/10.1155/2013/523652.

Tsai, Yuan-Hsiung, Li-Ming Hsu, Hsu-Huei Weng, Ming-Hsueh Lee, Jen-Tsung Yang, et Ching-Po Lin. 2011. « Voxel-Based Analysis of Apparent Diffusion Coefficient in Perihaematomal Oedema: Associated Factors and Outcome Predictive Value for Intracerebral Haemorrhage. » *BMJ Open* 1 (1): e000230. https://doi.org/10.1136/bmjopen-2011-000230.

Turner, Renée J., Glen C. Jickling, et Frank R. Sharp. 2011. « Are Underlying Assumptions of Current Animal Models of Human Stroke Correct: From STAIRs to High Hurdles? » *Translational Stroke Research* 2 (2): 138-43. https://doi.org/10.1007/s12975-011-0067-3.

Urday, Sebastian, Lauren A. Beslow, Feng Dai, Fan Zhang, Thomas W. K. Battey, Anastasia Vashkevich, Alison M. Ayres, et al. 2016. « Rate of Perihematomal Edema Expansion Predicts Outcome After Intracerebral Hemorrhage. » *Critical Care Medicine* 44 (4): 790-97. https://doi.org/10.1097/CCM.0000000000001553.

Vanden Berghe, Tom, Andreas Linkermann, Sandrine Jouan-Lanhouet, Henning Walczak, et Peter Vandenabeele. 2014. « Regulated Necrosis: The Expanding Network of Non-Apoptotic Cell Death Pathways. » *Nature Reviews. Molecular Cell Biology* 15 (2): 135-47. https://doi.org/10.1038/nrm3737.

Venkatasubramanian, Chitra, Michael Mlynash, Anna Finley-Caulfield, Irina Eyngorn, Rajalakshmi Kalimuthu, R. W. Snider, et Christine Anne Wijman. 2011. « Natural History of Perihematomal Edema after Intracerebral Hemorrhage Measured by Serial Magnetic Resonance Imaging. » *Stroke* 42 (1): 73-80. https://doi.org/10.1161/STROKEAHA.110.590646.

Volbers, Bastian, Antje Giede-Jeppe, Stefan T. Gerner, Jochen A. Sembill, Joji B. Kuramatsu, Stefan Lang, Hannes Lücking, Dimitre Staykov, et Hagen B. Huttner. 2018. « Peak Perihemorrhagic Edema Correlates with Functional Outcome in Intracerebral Hemorrhage. » *Neurology* 90 (12): e1005-12. https://doi.org/10.1212/WNL.0000000000005167.

Volbers, Bastian, Wolfgang Willfarth, Joji B. Kuramatsu, Tobias Struffert, Arnd Dörfler, Hagen B. Huttner, Stefan Schwab, et Dimitre Staykov. 2016. « Impact of Perihemorrhagic Edema on Short-Term Outcome After Intracerebral Hemorrhage. » *Neurocritical Care* 24 (3): 404-12. https://doi.org/10.1007/s12028-015-0185-y.

Wang, Gaiqing, Li Wang, Xin-Gang Sun, et Jiping Tang. 2018. « Haematoma Scavenging in

Intracerebral Haemorrhage: From Mechanisms to the Clinic. » *Journal of Cellular and Molecular Medicine* 22 (2): 768-77. https://doi.org/10.1111/jcmm.13441.

Wang, Yin, Athanasia Metoki, Kylie H. Alm, et Ingrid R. Olson. 2018. « White Matter Pathways and Social Cognition. » *Neuroscience and Biobehavioral Reviews* 90 (juillet): 350-70. https://doi.org/10.1016/j.neubiorev.2018.04.015.

Winkler, D. T., L. Bondolfi, M. C. Herzig, L. Jann, M. E. Calhoun, K. H. Wiederhold, M. Tolnay, M. Staufenbiel, et M. Jucker. 2001. « Spontaneous Hemorrhagic Stroke in a Mouse Model of Cerebral Amyloid Angiopathy. » *The Journal of Neuroscience : The Official Journal of the Society for Neuroscience* 21 (5): 1619-27. https://doi.org/10.1523/JNEUROSCI.21-05-01619.2001.

Withers, Sarah E., Adrian R. Parry-Jones, Stuart M. Allan, et Paul R. Kasher. 2020. « A Multi-Model Pipeline for Translational Intracerebral Haemorrhage Research. » *Translational Stroke Research* 11 (6): 1229-42. https://doi.org/10.1007/s12975-020-00830-z.

Witsch, Jens, Fawaz Al-Mufti, E. Sander Connolly, Sachin Agarwal, Kara Melmed, David J. Roh, Jan Claassen, et Soojin Park. 2019. « Statins and Perihemorrhagic Edema in Patients with Spontaneous Intracerebral Hemorrhage. » *Neurology* 92 (18): e2145-49. https://doi.org/10.1212/WNL.0000000000006931.

Wu, Teddy Y., Gagan Sharma, Daniel Strbian, Jukka Putaala, Patricia M. Desmond, Turgut Tatlisumak, Stephen M. Davis, et Atte Meretoja. 2017. « Natural History of Perihematomal Edema and Impact on Outcome After Intracerebral Hemorrhage. » *Stroke* 48 (4): 873-79. https://doi.org/10.1161/STROKEAHA.116.014416.

Xi, G., K. R. Wagner, R. F. Keep, Y. Hua, G. M. de Courten-Myers, J. P. Broderick, T. G. Brott, et J. T. Hoff. 1998. « Role of Blood Clot Formation on Early Edema Development after Experimental Intracerebral Hemorrhage. » *Stroke* 29 (12): 2580-86. https://doi.org/10.1161/01.str.29.12.2580.

Xue, Mengzhou, et V. Wee Yong. 2020. « Neuroinflammation in Intracerebral Haemorrhage: Immunotherapies with Potential for Translation. » *The Lancet. Neurology* 19 (12): 1023-32. https://doi.org/10.1016/S1474-4422(20)30364-1.

Yang, G. Y., A. L. Betz, et J. T. Hoff. 1994. « The Effects of Blood or Plasma Clot on Brain Edema in the Rat with Intracerebral Hemorrhage. » *Acta Neurochirurgica. Supplementum* 60: 555-57. https://doi.org/10.1007/978-3-7091-9334-1_153.

Yang, Jie, Hisatomi Arima, Guojun Wu, Emma Heeley, Candice Delcourt, Junshan Zhou, Guofang Chen, et al. 2015. « Prognostic Significance of Perihematomal Edema in Acute Intracerebral Hemorrhage: Pooled Analysis from the Intensive Blood Pressure Reduction in Acute Cerebral Hemorrhage Trial Studies. » *Stroke* 46 (4): 1009-13. https://doi.org/10.1161/STROKEAHA.114.007154.

Ye, Fenghui, Hugh J. L. Garton, Ya Hua, Richard F. Keep, et Guohua Xi. 2021. « The Role of Thrombin in Brain Injury After Hemorrhagic and Ischemic Stroke. » *Translational Stroke Research* 12 (3): 496-511. https://doi.org/10.1007/s12975-020-00855-4.

Yu, Y. L., C. R. Kumana, I. J. Lauder, Y. K. Cheung, F. L. Chan, M. Kou, C. M. Chang, R. T. Cheung, et K. Y. Fong. 1992. « Treatment of Acute Cerebral Hemorrhage with Intravenous Glycerol. A Double-Blind, Placebo-Controlled, Randomized Trial. » *Stroke* 23 (7): 967-71. https://doi.org/10.1161/01.str.23.7.967.

Yu, Zhiyuan, Lu Ma, Jun Zheng, et Chao You. 2017. « Prognostic Role of Perihematomal Edema in Intracerebral Hemorrhage: A Systematic Review. » *Turkish Neurosurgery*, janvier. https://doi.org/10.5137/1019-5149.JTN.19659-16.0.

Zazulia, A. R., M. N. Diringer, C. P. Derdeyn, et W. J. Powers. 1999. « Progression of Mass Effect after Intracerebral Hemorrhage. » *Stroke* 30 (6): 1167-73. https://doi.org/10.1161/01.str.30.6.1167.

Zhao, Xiurong, Guanghua Sun, Shun-Ming Ting, Shen Song, Jie Zhang, Nancy J. Edwards, et Jaroslaw Aronowski. 2015. « Cleaning up after ICH: The Role of Nrf2 in Modulating Microglia Function and Hematoma Clearance. » *Journal of Neurochemistry* 133 (1): 144-52. https://doi.org/10.1111/jnc.12974.

Zheng, Haiping, Chunli Chen, Jie Zhang, et Zhiping Hu. 2016. « Mechanism and Therapy of Brain Edema after Intracerebral Hemorrhage. » *Cerebrovascular Diseases (Basel, Switzerland)* 42 (3-4): 155-69. https://doi.org/10.1159/000445170.

Zubkov, Alexander Y., Jayawant N. Mandrekar, Daniel O. Claassen, Edward M. Manno, Eelco F. M. Wijdicks, et Alejandro A. Rabinstein. 2008. « Predictors of Outcome in Warfarin-Related Intracerebral Hemorrhage. » *Archives of Neurology* 65 (10): 1320-25. https://doi.org/10.1001/archneur.65.10.1320.